CHARACTERIZATION OF THE EPIKARST OVER THE HUNTON ANTICLINE, ARBUCKLE-SIMPSON AQUIFER, OKLAHOMA

By

MICHAEL ANDREW SAMPLE

Bachelor of Science in Geology

Oklahoma State University

Stillwater, Oklahoma

2005

Submitted to the Faculty of the
Graduate College of the
Oklahoma State University
in partial fulfillment of
the requirements for
the Degree of
MASTER OF SCIENCE
May, 2008

CHARACTERIZATION OF THE EPIKARST OVER THE HUNTON ANTICLINE, ARBUCKLE-SIMPSON AQUIFER, OKLAHOMA

Thesis Approved:

Todd Halihan

Thesis Adviser

Estella Atekwana

Alex Simms

A. Gordon Emslie

Dean of the Graduate College

ACKNOWLEDGEMENTS

I would like to extent my sincere gratitude to those individuals and organizations that contributed in all aspects of this project. Special thanks are extended to the Oklahoma Water Resources Board for providing the funding for this project. Thanks to the ranchers and landowners for providing access to their land. I especially thank John Bruno for the generous use of his cabin as lodging.

I am sincerely grateful to my committee members for their time and efforts. To Dr. Todd Halihan, my advisor, thank you for the benefit of all the knowledge and wisdom you have shared with me over the years. I especially thank you for your considerable patience and the use of your field equipment for the data collection. I am also deeply grateful to Martha Halihan, Todd's wonderful wife who, with her husband, made me feel welcome, at ease, and well fed in their home. To Dr. Estella Atekwana, thank you for your encouragement and the knowledge you have given me through the classes I have taken with you. To Dr. Alex Simms, thank you for making the time to patiently answer all of my questions and most especially thank you for allowing me to use your lab equipment for the data analysis.

I would like to extend my gratitude to all the faculty, staff, and other professionals at Oklahoma State University that have provided me with advice and technical or material support in my research. Thank you to Dr. Jim Puckette

for answering random questions at odd hours. Thank you to Dr. Anna Cruse for the extended use of her lab equipment. Thank you to Dr. Jeffory A. Hattey and Dr. Brian J. Carter for your advice on sediment analysis. Thank you to Jimmy G. Ford and Gregory F. Scott of the United States Department of Agriculture for your assistance with the NRCS Soil Survey dataset. Thank you to Tim Sickbert, Devon Lab Coordinator, for your technical and field assistance. To Jason Faith of the United States Geological Survey thank you for your encouragement and the extended use of your camera. Special thanks to staff members Nancy Dryden and Sandy Earls for helping me negotiate all the administrative hurdles.

My sincere gratitude goes to all of the students who gave generously of their time to assist me without which there would be no thesis. Special thanks goes to Mat Riley for being a good friend, encouraging me along the way, and helping me learn how to operate a Geoprobe. To Niranjan Aryal and Marissa Raglin thank you for your technical assistance. To Matin Alavi, Meghan Dailey, Greg Federko, Shawn Hammond, Chris Mace, Robert Meyer, Khayyun Rahi, and Kathleen Thompson a special thank you for helping me with my field work.

I dedicate this thesis to my late parents William A. and Elizabeth A. Sample. Their wisdom and love have guided me through all of life's journeys. Last, but never least, I would like to recognize my sister Marianne Sample for being there with love and encouragement or a strong word whenever I needed it.

TABLE OF CONTENTS

LIST OF TABLES

LIST OF FIGURES

CHAPTER I

INTRODUCTION

The hydrologic properties of fractured karst aquifers are very complex and difficult to characterize. The epikarst zone is in the uppermost portion of a fractured karst aquifer in the weathered rocks above the phreatic zone. Studies have indicated that the potential for storage in epikarst zones is significant (Williams, 1983; Perrin et al., 2003; Klimchouk, 2004) and can potentially be more important than the storage in the underlying phreatic zone (Perrin et al., 2003). The characterization of the hydrologic properties of the epikarst zone is important for understanding the flow characteristics of a fractured karst aquifer and for quantifying the hydrologic budget of fractured karst aquifers which is required for the proper assessment and management of regional groundwater resources.

The fractured karst Arbuckle-Simpson aquifer, underlying portions of Carter, Coal, Johnston, Murray, and Pontotoc Counties in south central Oklahoma, has been the principle source of water for the about 39,000 people in the region (Figure 1.1). The aquifer has been the primary source of water for the city of Ada, Oklahoma and the 3.4 million visitors that annually visit the Chickasaw National Recreation Area. The U.S. Environmental Protection

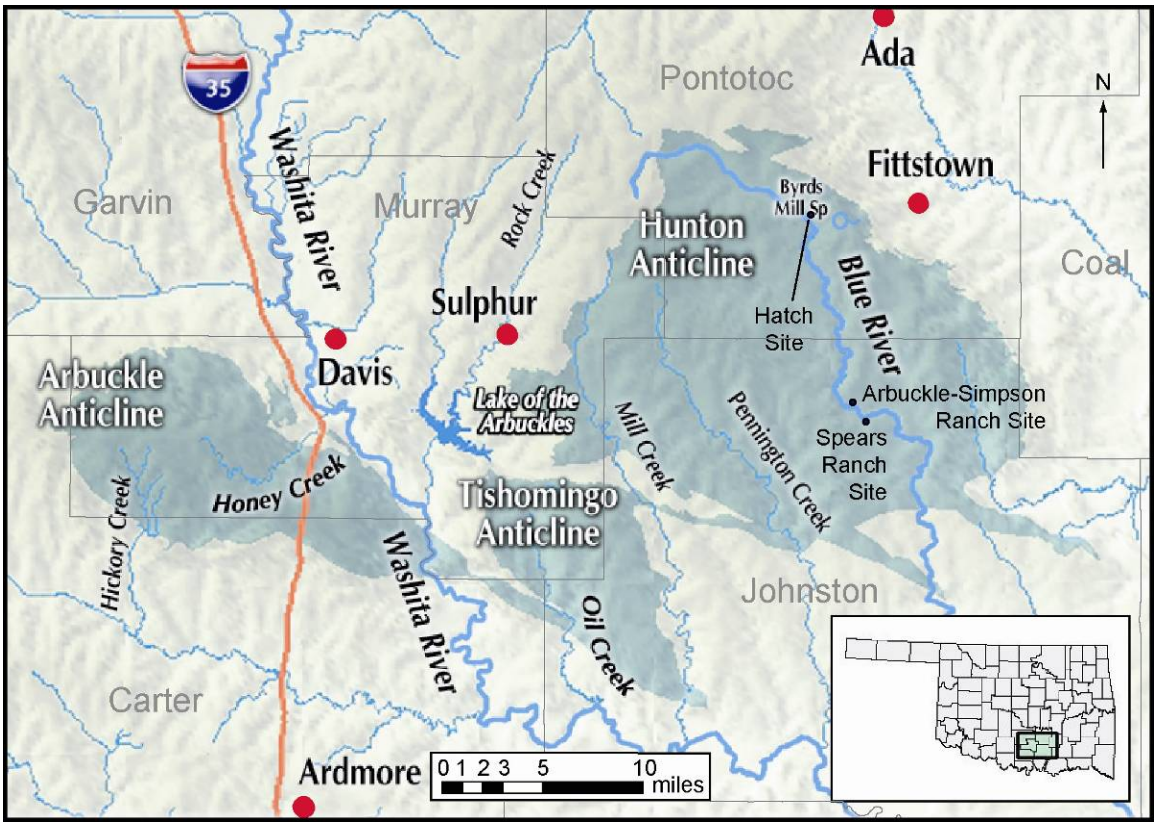

Figure 1.1. Arbuckle-Simpson aquifer outcrop location map with field site locations [after Oklahoma Water Resources Board, 2008; U.S. Geological Survey, 2008].

Agency designated the eastern portion of the Arbuckle-Simpson aquifer as a sole source aquifer in 1989 (Environmental Protection Agency, 1989).

Concerns over the potential impacts on the aquifer of a proposed plan to pump as much as 26 billion gallons (80,000 acre-feet) of water per year from the aquifer led to the passage of Oklahoma Senate Bill 288 in May of 2003 (Oklahoma State Senate, 2003). Senate Bill 288 established a temporary moratorium on the issuance of permits that would lead to municipal or public water supply use of groundwater from the aquifer until the Oklahoma Water Resources Board (OWRB) could conduct and complete a comprehensive

hydrologic study of the aquifer and approve a maximum yield that would not reduce the natural flow in streams and springs emanating from the aquifer (Oklahoma State Senate, 2003).

The work presented in this thesis was funded by the OWRB to characterize the epikarst zone of the Arbuckle-Simpson aquifer in terms of its thickness and the hydraulic properties of hydraulic conductivity and storativity. The focus of the study was concentrated in the eastern portion of the aquifer over a prominent uplift structure called the Hunton Anticline. Three field sites, the Hatch, Spears Ranch, and Arbuckle-Simpson Ranch sites, were selected for the project which provided a sampling of the diverse range of environments found across the Hunton Anticline. The field methods used to collect the data for the study were static water level measurements, direct push sediment cores and electrical conductivity logs, surface electrical resistivity imaging surveys, and concentric cylinder infiltration tests. The field data were collected between September 2006 and February 2008. Laboratory analyses of the field data included porosity and particle size distribution analyses of the direct push sediment cores.

Electrical geophysical methods have been widely used in groundwater exploration and aquifer evaluation. Empirical and semi-empirical relations have been found between the electrical properties of aquifer materials and hydrologic properties like hydraulic conductivity, porosity, and transmissivity (Mazac et al., 1985; Sri Niwas and de Lima, 2003; Singh, 2005). Relationships have largely been found in a variety of fully saturated granular aquifer environments. Less

work has been done in more complicated fractured carbonate aquifers or the unsaturated zone. Aquifer hydraulic conductivity determined at discrete points through sediment core particle size analysis, and from concentric cylinder infiltrometer analysis can be correlated to surface electrical resistivity imaging (ERI) and direct-push electrical conductivity (EC) logs data taken in the same location in the variably mantled epikarst setting of the Arbuckle-Simpson aquifer in southern Oklahoma. The available relevant literature on the subject of applying electrical methods to hydrologic problems will be presented in the following chapter.

The details of each of the field and laboratory methods used in the study will be described in detail in subsequent chapters. The remainder of this chapter will focus on brief discussions of epikarst, the geologic background of the study area, and descriptions of the field sites chosen for the study. The chapter will conclude with statements on the purpose and objectives of the study.

1.1 Epikarst

The epikarst zone is defined as the uppermost weathered layer of carbonate (limestone or dolomite) rock of fractured karst aquifers that lies beneath the lands surface and any mantling of soil but above the phreatic zone (Williams, 1983; Klimchouk, 2004) (Figure 1.2). The thickness of the epikarst zone can be highly variable (Klimchouk, 2004) and has been reported as ranging between a few meters to more than 160 meters thick (Bosak and Benes, 2003). Epikarst zones are most commonly reported as less than fifteen meters thick

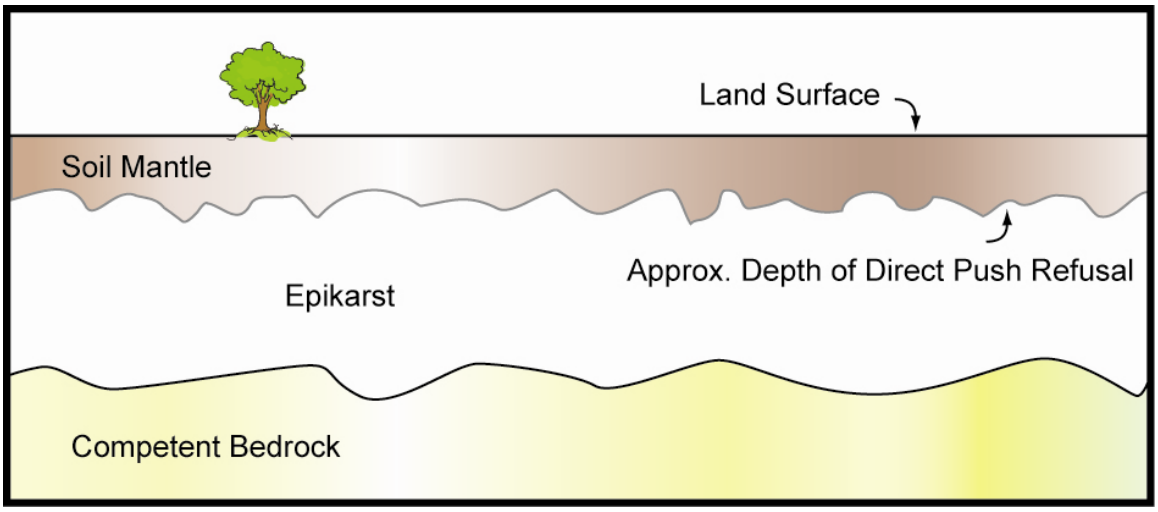

Figure 1.2. Schematic diagram and terms associated with epikarst.

(Klimchouk, 2004). The formation of epikarst is dependent on several environmental factors like climate, micro-climate, local topography, the composition, structure, and texture of the parent rock, and time (Klimchouk, 2004).

The formation of the soils mantling the epikarst is controlled by the same factors (Soil Survey Division Staff, 1993). The epikarst and mantling soil should then be expected to share similar characteristics. Soils forming in far removed areas with similar environmental factors will develop with similar physical and chemical characteristics which are used as the basis used for classifying soil types (Soil Survey Division Staff, 1993). Characteristics determined to be shared between the epikarst and mantling soil in one location should then be expected to exist in far removed areas with similar environments.

1.2 Geologic Background

The Arbuckle-Simpson aquifer is located in the Arbuckle Mountain physiographic province in south central Oklahoma (Fairchild et al., 1990) (Figure 1.1). The limestone, dolomite, and sandstone formations of the Arbuckle and Simpson Groups that make up the Arbuckle-Simpson aquifer were deposited from the Late Cambrian to Middle Ordovician times and achieved a combined thickness ranging from 5,000 to 9,000 feet across the region (Ham, 1969; Fairchild et al., 1990). Extensive faulting and folding due to major uplift experienced by the region during the Pennsylvanian Period led to the development of three major anticlinal structures, the Arbuckle, Tishomingo, and Hunton Anticlines, which are separated by large high angle faults (Ham, 1969; Fairchild et al., 1990).

The Arbuckle Anticline in the west experienced the most intense folding and faulting of the three structures during the Late Virgilian Arbuckle Orogeny (Ham, 1969). The Hunton Anticline in the East and the Tishomingo Anticline in the central portion experienced major epierogenic uplift during the Pennsylvanian Period but were largely unaffected by the intense folding of the Arbuckle Orogeny (Ham, 1969). Erosion of the uplifted areas have exposed the rocks containing the Arbuckle-Simpson aquifer at the land surface over the anticlines in an area greater than 500 mi^2 (Fairchild et al., 1990). The average saturated thickness of the Arbuckle-Simpson aquifer has been estimated as ~3500 feet. (Fairchild et al., 1990).

The area of investigation for this study was the Hunton Anticline. The topography of the Hunton Anticline is characterized by gently rolling plains over highly faulted and relatively flat-lying rocks (Fairchild et al., 1990). The Lower Ordivician West Spring Creek and Kindblade formations are the dominant lithologic units exposed at the surface over the Hunton Anticline. The West Spring Creek and Kindblade formations are described in the literature as limestone in the west and dolomite in the east and contains thin sandstones in the west which become thicker and more numerous to the east (Fairchild et al., 1990).

1.3 Site Description and Selection

Three field sites, the Hatch, Spears Ranch, and Arbuckle-Simpson Ranch sites, were selected for the project. The selected field sites provided a sampling of the diverse range of environments found across the Hunton Anticline. The field sites were selected based on several criteria. The sites selected needed to provide a sampling of the diverse range of environments found across the Hunton Anticline. The field sites had to be easily accessible and have sufficient space clear of obstacles at the surface and buried utilities to run the surface electrical resistivity imaging and direct push methods (> 150 meters in any one direction). Consideration was also given to locations of special interest to other researchers within the Arbuckle-Simpson Hydrology Study.

The Hatch site is located approximately four miles WSW of Fittstown in Pontotoc County, Oklahoma (Figure 1.1). The Hatch site is underlain by the

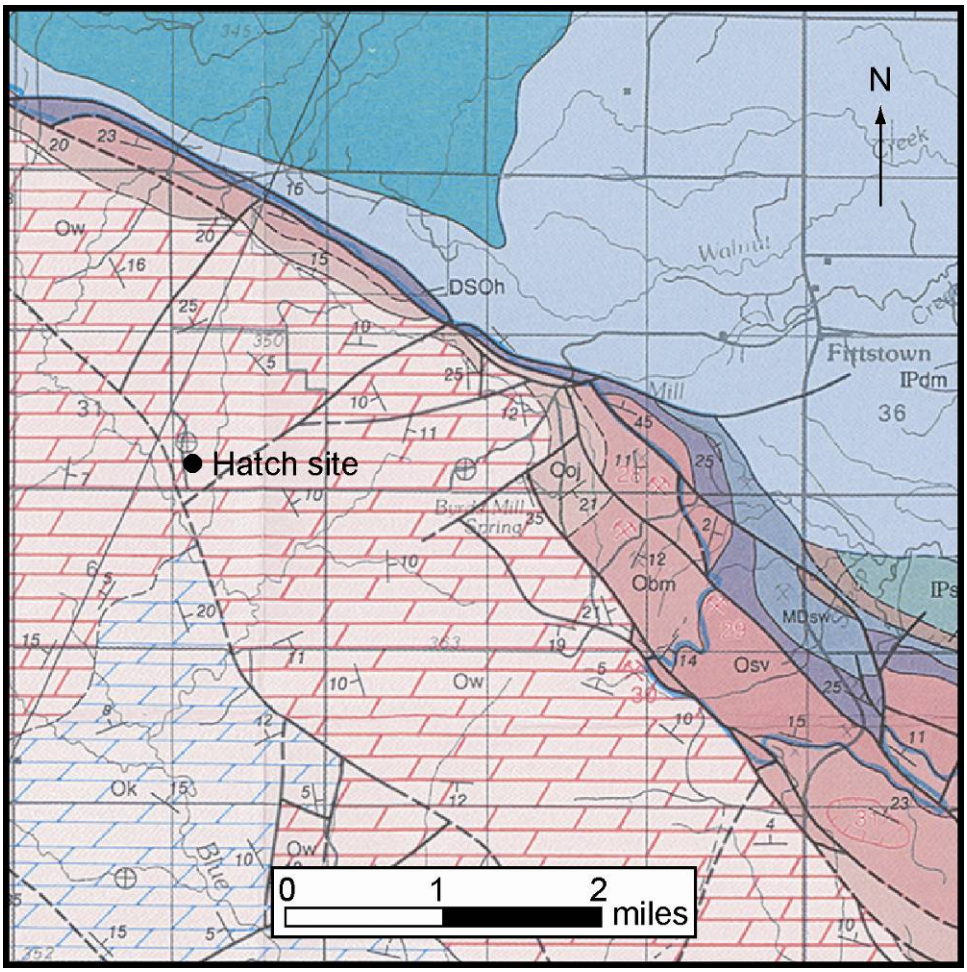

Figure 1.3. Bedrock geology underlying the Hatch site [from Plate 1; Geologic map of Arbuckle Mountains in Fairchild et al., 1990].

rocks of the West Spring Creek formation (Figure 1.3). The geologic map symbols in Figure 1.3 are defined in Figure 1.4. The topography at the site is gently rolling to essentially flat lying. The soil cover is essentially continuous across the site with bedrock exposed at the surface only in small and isolated spots. The site has a history as a dairy farm as evidenced by the unused dairy facility on the site and is currently in use as rangeland for cattle (Figure 1.5).

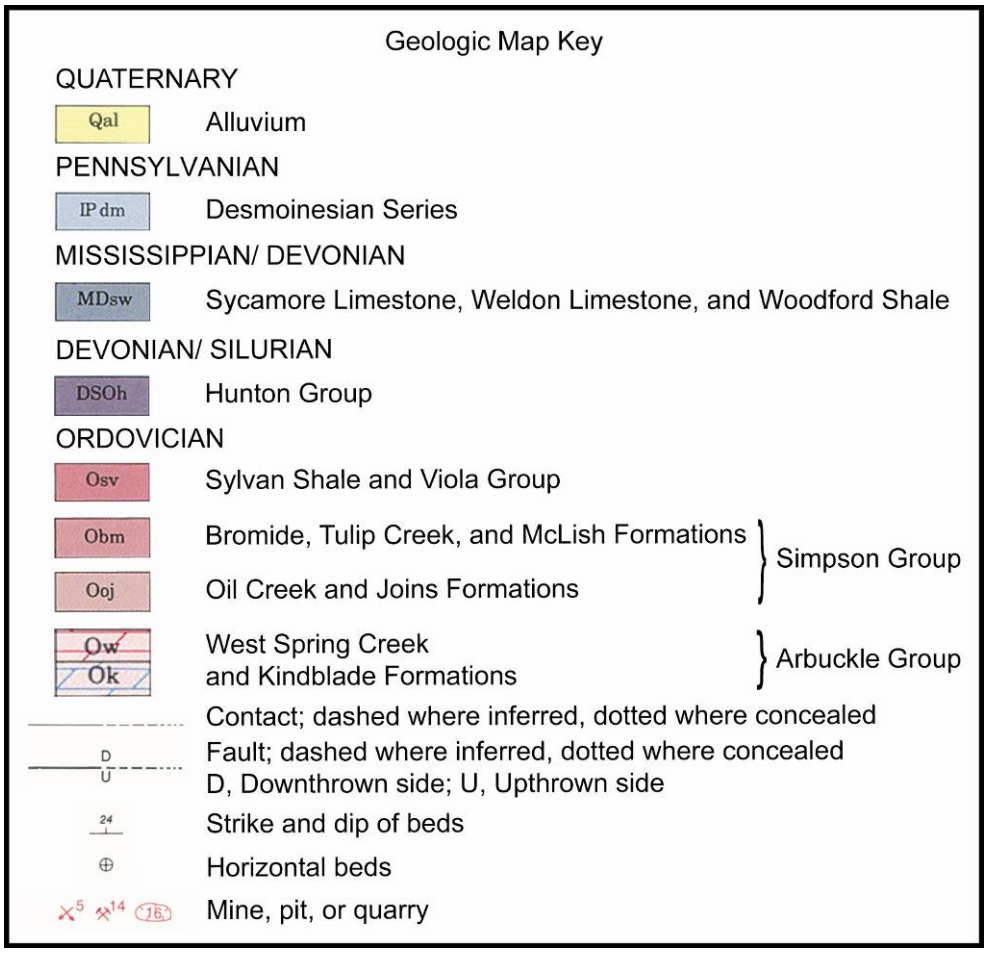

Figure 1.4. Geologic map key [after Fairchild et al., 1990]

A well is located on the site which is being used as a water level recording well by the OWRB. The decision to select the site was in part based upon knowledge of the site from a previous study (Sample and Halihan, 2004).

The Spears Ranch site is located approximately one mile west of Connerville in Johnston County, Oklahoma (Figure 1.1). The Spears Ranch site is underlain by the rocks of the West Spring Creek formation (Figure 1.6).

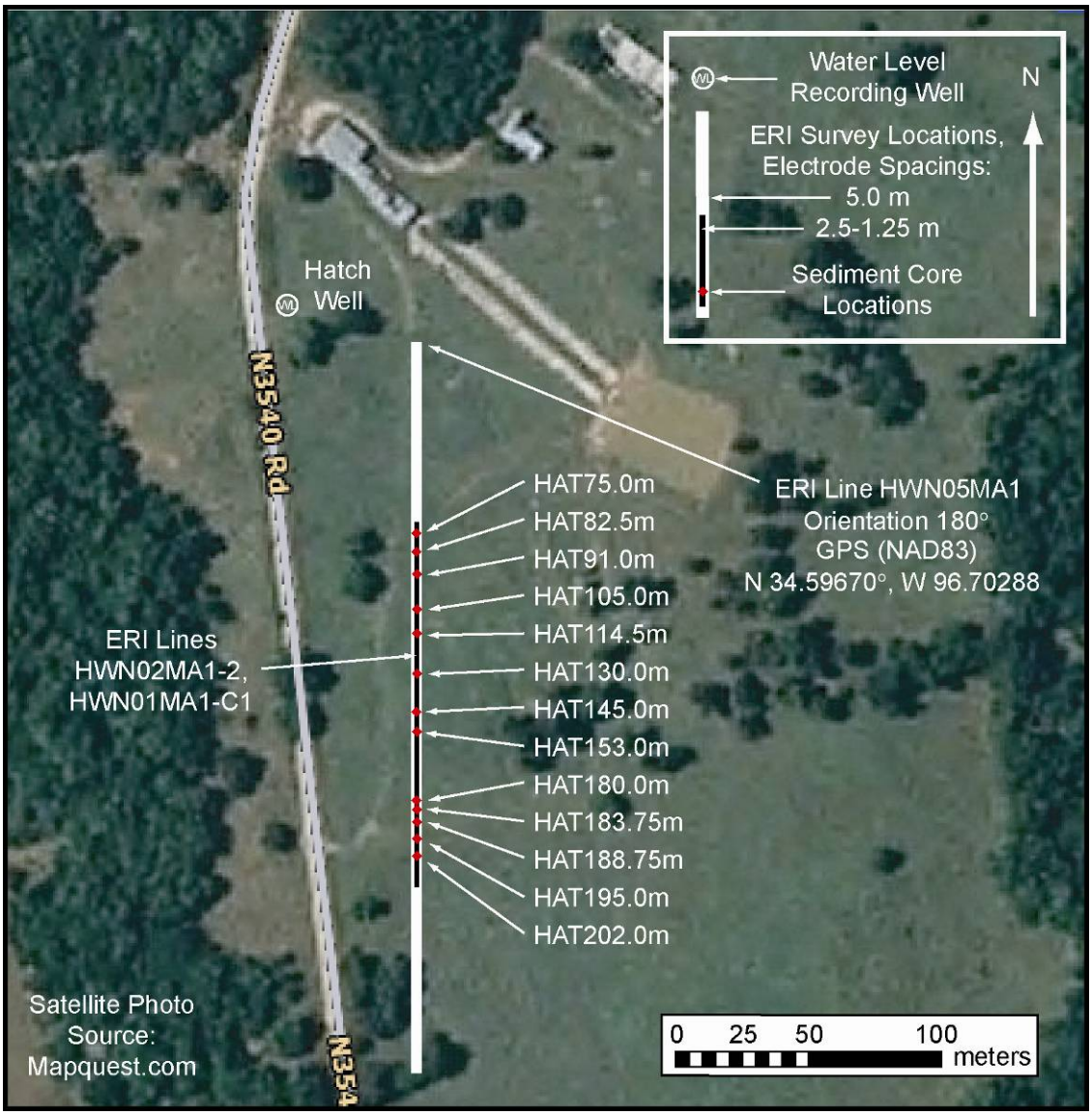

Figure 1.5. Hatch site map with surface electrical resistivity, direct push, and well locations.

The geologic map symbols in Figure 1.6 are defined in Figure 1.4. The area of investigation was just south of the Blue River. The topography at the site is gently rolling and slopes towards the Blue River. The slope of the terrain is greatest close to the Blue River. Soil cover appears essentially continuous in relatively flat lying areas and spotty to completely absent in areas with any slope.

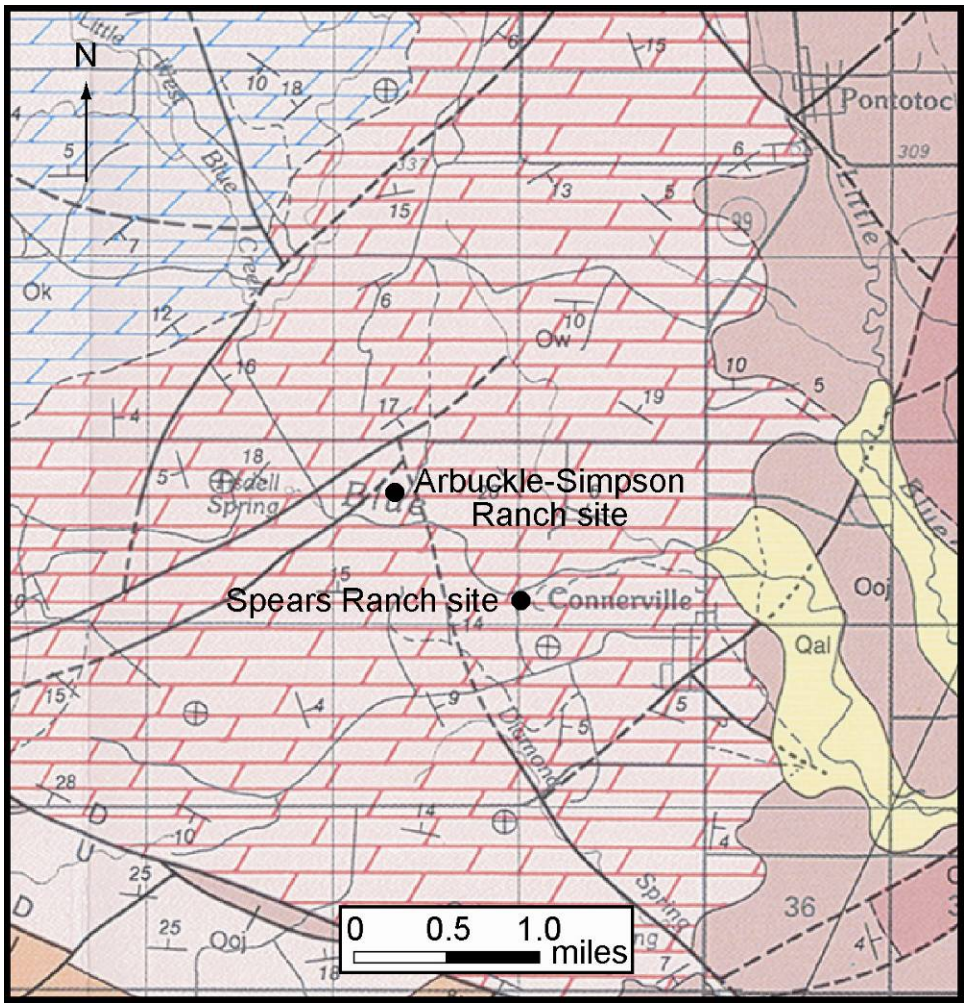

Figure 1.6. Bedrock geology underlying the Arbuckle-Simpson and Spears Ranch sites [from Plate 1; Geologic map of Arbuckle Mountains in Fairchild et al., 1990].

The site is currently in use as rangeland for cattle (Figure 1.7). Two wells are located on the site were installed by the United States Geological Survey for hydrologic research in connection with the Arbuckle-Simpson Hydrology Study.

The Arbuckle-Simpson Ranch site is located approximately 1.8 miles WNW of Connerville in Johnston County, Oklahoma (Figure 1.1). The Arbuckle-Simpson Ranch site is underlain by the rocks of the West Spring Creek

Figure 1.7. Spears Ranch site map with surface electrical resistivity and direct push locations and well locations.

formation (Figure 1.6). The geologic map symbols in Figure 1.6 are defined in Figure 1.4. The topography at the site is gently rolling to essentially flat lying. Soil cover is continuous in the flat lying area of investigation. Rocks were observed exposed at the surface to the west of the area of investigation and to

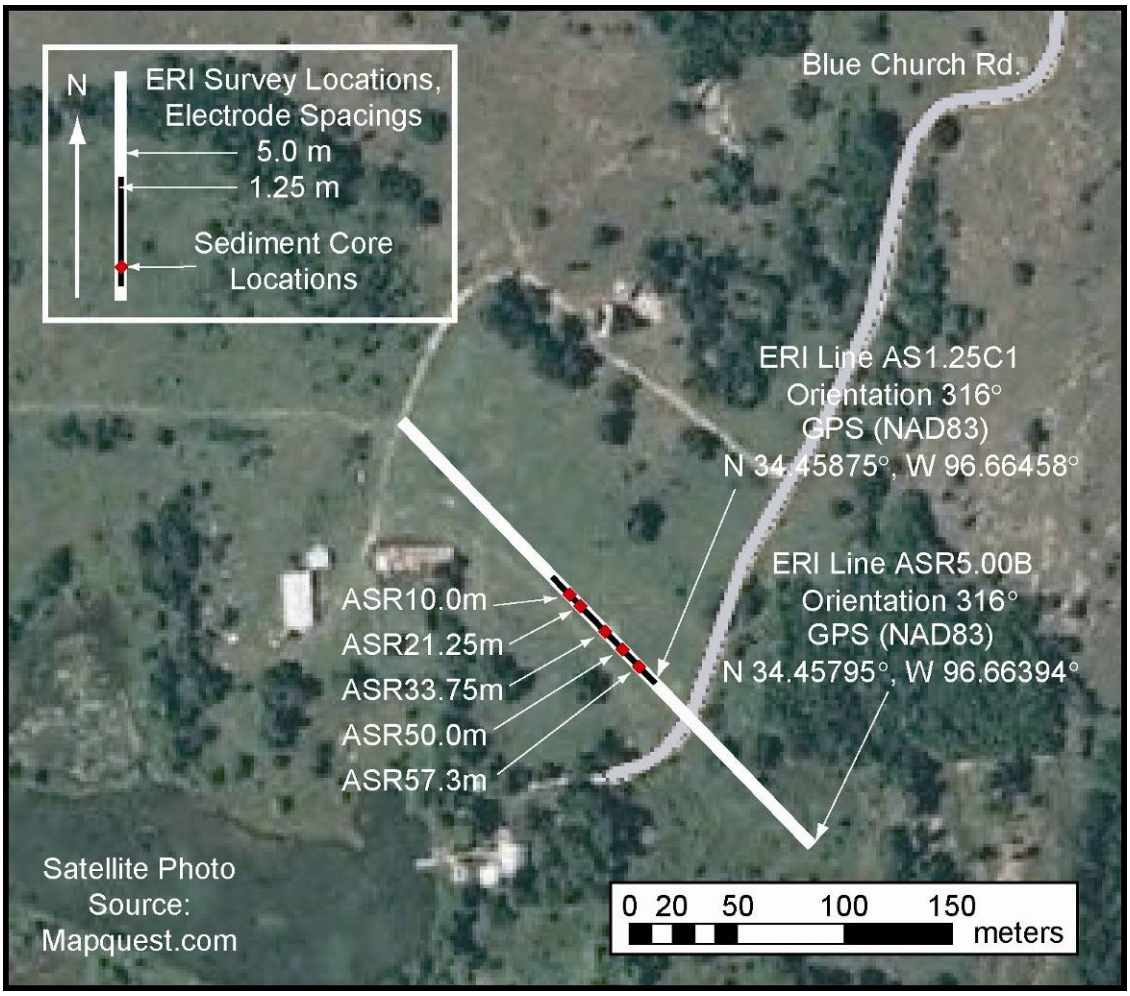

Figure 1.8. Arbuckle-Simpson Ranch site map with surface electrical resistivity and direct push locations.

the east on hill slopes. The site has a history of use as rangeland for cattle (Figure 1.8). A spring fed pond is located on the site and numerous springs have been identified on the property that contributes of the flow to the Blue River. An inferred fault is identified in the literature as crossing the site from the south west to the north east (Fairchild et al., 1990) (Figure 1.6).

1.4 Purpose and Objectives

The main purpose of this thesis was to determine a correlation between the aquifer hydraulic conductivity and electrical resistivity properties of the variably mantled epikarst setting of the Arbuckle-Simpson aquifer over the Hunton Anticline in southern Oklahoma. The major objective of this thesis was to characterize the variably mantled epikarst of the Arbuckle-Simpson aquifer in terms of its electrical and hydraulic properties. The specific tasks formulated to address the purpose and objective of this thesis were:

1) Determine the electrical properties of the variably mantled epikarst using surface electrical resistivity imaging data.
2) Determine the electrical properties of the variably mantled epikarst at discrete points using direct push electrical conductivity logging.
3) Determine a correlation between the surface electrical resistivity imaging and direct push electrical conductivity logging data.
4) Measure depth to water from wells present at the sites or estimate if possible from ancillary sources if wells were not available.
5) Determine the thickness of the soils mantling the epikarst using direct push electrical conductivity logging and sediment coring depth of refusal results.
6) Determine the thickness of the variably mantled epikarst using direct push depth of refusal results and surface electrical resistivity imaging data.
7) Determine the water content and porosity of the soils mantling the epikarst.

8) Determine the particle size distribution of the soils mantling the epikarst using dry sieving and laser diffraction particle size analysis.
9) Calculate the hydraulic conductivity of the soils mantling the epikarst from double-ring infiltrometer analysis and from the sediment core porosity and particle size analysis results using empirical methods.
10) Estimate the storativity and evaluate the storage potential of the mantled epikarst and the saturated thickness of the aquifer.
11) Determine a correlation between the hydraulic conductivity and electrical resistivity properties of the variably mantled epikarst using all of the data collected.

A review of the relevant electrical resistivity literature is discussed in chapter two. The field and laboratory methods employed are described in detail in chapters three and four respectively. The results of the field and laboratory analyses are presented in chapter five. The results are discussed in chapter six and the conclusions are presented in chapter seven.

CHAPTER II

LITERATURE REVIEW

Previous literature relevant to this study includes research on the application of electrical geophysical methods to determine hydrologic properties. These studies describe various methods used to develop empirical and semi-empirical relationships between the electrical and hydraulic properties of aquifer materials in a variety of geologic settings. These reports are described in this chapter following a brief historical background.

2.1 Brine Saturated Sands

The electrical properties of earth materials have been used in geophysical investigations since the 1830's where it began seeing practical use in the ore mining industry (Rust, 1938). In 1929, apparent resistivity measurements using four electrode arrays began being adapted for use in well logging for petroleum exploration (Rust, 1938). In 1942, Gus Archie established an empirical relationship between porosity (Φ) and what he termed the formation resistivity factor (F) for clean brine saturated sands, where F was the ratio of the resistivity of the rock saturated with water to the resistivity of the water filling the pore

spaces ($F = R_O/R_W$). The formation resistivity factor, or formation factor, was related to the porosity through the equation:

$$F = \Phi^{-m} \quad \text{(Eq. 1)}$$

where *m* was a constant called the cementation exponent which was the slope of the line of best fit for the log/log relationship between *F* and Φ (Archie, 1942). The constant *m* varied between 1.3 and 2.5 (Telford et al., 1990; Reynolds, 1997; Asquith and Kyrgowski, 2004) but was most commonly assumed to be 2.0 (Asquith and Kyrgowski, 2004).

Archie showed that as the porosity of brine saturated sandstones increased, the formation factor, *F*, decreased. Archie related the resistivity of the sand, *R*, to the fraction of the voids filled with water, *S*, through the equation:

$$R = R_O S^{-n} \quad \text{(Eq. 2)}$$

Where *n* was a constant approximately equal to 2.0 (Telford et al., 1990; Reynolds, 1997; Asquith and Kyrgowski, 2004). These relationships could be re-written to form the equation:

$$R = \Phi^{-m} S^{-n} R_W \text{ or } \rho = \Phi^{-m} S^{-n} \rho_W \quad \text{(Eq. 3)}$$

Archie also observed a similar relationship between permeability, *k*, and *F* in clean brine saturated sands but noted that because permeability and porosity do not relate in the same way in all sands that “the two relationships could not be held to apply with equal vigor” and thus no empirical relationship for *F* and *k* was offered (Archie, 1942).

A geometric factor, *a*, which accounted for the effects of tortuosity began being attached to Archie's equation by the early 1950's (Winsauer et al., 1952) yielding the form of the equation:

$$\rho = a^{*}\Phi^{-m}S^{-n}\rho_W \qquad \text{(Eq. 4)}$$

Tortuosity was defined as the ratio of the actual sinuous path traveled between two points by a fluid or electric current through the saturated pore channels of a rock to the straight line distance between the two points (Winsauer et al., 1952; Fetter, 2001; Weight and Sonderegger, 2001). The value of the geometric factor, *a,* could range between 0.5 and 2.5 (Telford et al., 1990; Reynolds, 1997; Asquith and Kyrgowski, 2004) but was most commonly set to 1.0 (Asquith and Kyrgowski, 2004).

2.2 Fresh Water Saturated Sands

Jones and Buford (1951) measured the variation of the formation factor and permeability in graded sands in developing a method to determine the quality of groundwater in granular aquifers from electric logs as an aid in groundwater exploration. The data from this study showed that for fresh water saturated sands a decrease in grain size resulted in a decrease in the value of the formation factor and permeability. This was the reverse of the relationship previously found in brine saturated sands from petroleum related studies.

Since Jones and Buford's (1951) observation of a direct relationship between formation factor and permeability in fresh water saturated sands, numerous studies have been undertaken in a wide variety of aquifer settings in

attempts to quantify a general relationship between the electrical and hydraulic properties of aquifer materials. The studies have largely been restricted to the fully saturated intervals of relatively simple granular aquifers. The observed relationships were found to be highly variable, dependent on the depositional environment, and can vary within the same depositional environment (Mazac et al., 1985; Huntley, 1986; Sri Niwas and de Lima, 2003; Singh, 2005). Both direct and inverse relationships have been observed.

Kosinski and Kelly (1981) found a direct relation between apparent formation factor and hydraulic conductivity in glacial outwash sediments using the results of VES with pumping test and boring log control. Kosinski and Kelly (1981) also found a direct relationship between a normalized aquifer electrical resistance and transmissivity. The normalized aquifer electrical resistance was defined as the product of the aquifer apparent formation factor, the aquifer thickness, and an average electrical resistivity of pore water. Kosinski and Kelly (1981) noted that, because of the problems of equivalence and suppression, resistivities derived from surface measurements could not be correlated to subsurface geology without independent geologic control such as that derived from well logs.

Kelly and Reiter (1984) used analytic and numerical models to study how anisotropy due to layering influenced the relations between hydraulic and electrical properties. Kelly and Reiter (1984) limited the data for their study to cases where a direct relationship between resistivity and hydraulic conductivity had been observed. Kelly and Reiter (1984) determined that the relation

between electrical resistivity and hydraulic conductivity was dependent on the degree of anisotropy.

Mazac et al. (1985) stated that direct relationships between the formation factor and hydraulic conductivity could be expected in environments where inverse relationships were observed between clay content and hydraulic conductivity or between porosity and grain size. Sri Niwas and de Lima (2003) indicated that a direct relationship between hydraulic conductivity and electrical resistivity could be expected in fully saturated aquifers where the substratum is very conductive. The hydraulic flow in this environment would be horizontal while the characteristic current flow was dominantly vertical. Direct relationships have also been found in carbonate aquifer settings.

Kwader (1985) analyzed the relationship between hydraulic conductivity and formation resistivity factor using core analysis, porosity and resistivity data from borehole logs, and hydraulic conductivity values derived from flow meter logs and pumping tests from wells in unconsolidated sand and Tertiary carbonate aquifers. Kwader (1985) found a good correlation between formation factor and hydraulic conductivity in a wide variety of granular and carbonate aquifers when several basic assumptions were held to be true. The basic assumptions were that no hydrocarbons (non-aqueous phase liquids) were present, the zone of interest was saturated with fresh or brackish water and acted like granular material, and the zone was relatively clay free and transmitted electrical current by surface conductance. The relationship between formation factor and hydraulic conductivity broke down in highly cemented carbonate settings or

where a high degree of fracture porosity was present and in settings with significant clay content because the portion of the electric current passing through the clay matrix could not be quantified (Kwader, 1985).

Inverse relationships have also been identified. Heigold et al. (1979) described an inverse relationship between aquifer resistivity and hydraulic conductivity determined from pumping test data and VES from a glacial outwash aquifer. Heigold et al. (1979) attributed the inverse relationship to differences in the degree of sorting of glacial sediments.

Biella et al. (1983) conducted lab experiments in clean sands to determine the effect of grain size and grain size distribution on the porosity/ formation factor relationship. Biella et al. (1983) observed an inverse relation between the intrinsic formation factor and porosity. The lab experiments conducted using samples with different grain size and size distributions led Biella et al. (1983) to conclude that the relationship was independent of grain size and size distribution which appears to disagree with Heigold et al. (1979). Biella et al. (1983) also found an inverse relation between hydraulic conductivity and intrinsic formation factor. Biella et al. (1983) determined that the hydraulic conductivity/ formation factor relationship could only be established if the mean grain size is constant.

Mazac et al. (1985) stated that in environments where porosity was the dominant factor controlling hydraulic conductivity and other factors were relatively constant an inverse relationship could be expected. Sri Niwas and de Lima (2003) indicated that an inverse relationship between hydraulic conductivity and electrical resistivity could be expected in fully saturated aquifers where the

substratum is highly resistive. The hydraulic flow and characteristic current flow in this environment would both be dominantly horizontal.

2.3 Unsaturated Sands

Much less work has been done in the vadose zone. Work done by Keller and Frischknecht (1966) indicated that the relationship between the degree of saturation and electrical resistivity is not constant for all saturations. Keller and Frischknecht (1966) stated that water is maintained as a continuous film on the surface of the rock matrix until a critical saturation level which is grain size dependent is achieved. The quantitative relationship between the degree of saturation and electrical resistivity changes when the saturation level drops below the critical saturation level. Small changes in saturation below the critical level begin to result in larger changes in the resistivity.

Curtis and Kelly (1990) demonstrated relationships between the electrical and recharge properties of the vadose zone using resistivity and hydraulic conductivity data from lab, literature, and field experiments. The hydraulic conductivity of soils and sediments were estimated from lab measurements, literature, and available field recharge test results. The electrical resistivities of various unsaturated sediments were determined from the correlation of surface resistivity measurements with borehole data. Unsaturated sediment types were found to have characteristic resistivities. The resistivity data were correlated with estimates of hydraulic conductivity to demonstrate a relationship between resistivity and recharge potential.

Gorman and Kelly (1990) conducted laboratory experiments on ideal sand mixtures to observe relationships between unsaturated zone sediments and their saturated hydraulic conductivity. The moisture content of the mixtures was varied from near specific retention to near saturation. A direct relationship was found between the formation factor of the mixtures at specific retention and the mixtures saturated hydraulic conductivity using the unsaturated form of Archie's equation.

$$F_{unsat} = a*\Phi^{-m}S^{-n} \quad \text{(Eq. 5)}$$

Gorman and Kelly (1990) observed that the formation factor varied with the degree of saturation in a constant and well defined manner over the range of moisture contents used.

2.4 Fractured Carbonate Settings

Work done to correlate the electrical and hydraulic properties in highly cemented and fractured carbonate aquifer settings is sparse. Kwader (1985) indicated that the relationships observed between formation factor and permeability breaks down in highly cemented and fractured carbonate aquifer settings or in settings with significant clay content. Singh (2005) indicated that the hydrological properties of fractured aquifers change too rapidly for relationships between the electrical and hydraulic properties to exist.

The epikarst of the Arbuckle-Simpson aquifer is by definition unsaturated (Williams, 1983; Klimchouk, 2004). The focus of the investigation for this project will essentially be confined to the soils mantling the epikarst due to the nature of

the methods employed. The electrical properties of the mantled epikarst materials will be indirectly measured using a surface electrical resistivity imaging method and directly measured for the mantling soils using an electrical conductivity probe inserted into the ground using a direct push method. Sediment cores will be collected from essentially the same locations as the electrical conductivity probe data using a direct push method. Direct measurements of the hydrologic properties (moisture content, porosity, and grain size distribution) of the sediment core materials will be derived from laboratory analysis. Relevant literature for the field and laboratory methods will be presented in the field and laboratory methods chapters.

CHAPTER III

FIELD METHODS

Several methods were employed at the field sites to collect the data necessary to characterize the epikarst over the Hunton Anticline, Oklahoma. The field methods applied during this study were, in the sequence of their application, surface electrical resistivity imaging (ERI) surveys, direct push electrical conductivity (EC) logging, direct push sediment core collection, and concentric (double ring) infiltrometry. All of the field methods were applied at each field site in as short a time period as possible (~ 3 days) in order to insure that subsurface conditions would remain essentially constant for the duration of the investigations. In addition static water level measurements were measured from water wells if present at the field sites.

ERI surveys were conducted at the start to insure that the electrical resistivity data collected reflected undisturbed field conditions and to identify the most appropriate locations to apply the remainder of the field methods. Preliminary field analysis of the ERI survey data was used to determine the range of electrical variability in the subsurface. Areas of interest were identified from the preliminary ERI data analysis which represented the full range of electrical variability in the subsurface. Discrete points on the surface centered

above the areas of interest were selected as the most appropriate locations for application of the remaining field methods.

Direct push EC logging was the next field method applied. The EC logging collected small scale, high resolution (0.05 ft), vertical electrical conductivity profiles at the locations above the selected areas of interest identified from the ERI surveys. The application of direct push EC logging before the remaining methods insured that the EC data reflected undisturbed subsurface conditions. The collection of EC log data reflecting undisturbed field conditions were critical for correlations with the surface ERI data.

Sediment cores were collected by direct push methods following the EC logging. The sediment cores were collected within one foot of each EC logging location. The collection of sediment cores in approximately the same locations as the EC logs was required for correlating both the ERI and EC data with the corresponding sediments at depth. The direct push sediment cores were collected prior to the infiltration experiments to insure that the moisture content in the sediment cores reflected essentially undisturbed field conditions.

The final field method applied at each area of interest was an infiltration experiment using a concentric (double ring) infiltrometer. The infiltration experiments were used to estimate saturated vertical hydraulic conductivity of the earth materials at the surface. This method was applied last because the process of estimating the saturated vertical hydraulic conductivity altered the near surface moisture conditions. The following sections describe in detail the methods used at each field site.

The field work for the project was accomplished during five trips to the study area over the period of September 2006 to February 2008. The Arbuckle-Simpson Ranch site was visited on July 25-28, 2007 and again on February 29, 2008. The Hatch Site was visited on September 2-4, 2006 and again on March 19-23, 2007. The Spears Ranch site was visited on June 11-15, 2007.

3.1 Static Water Level Measurements

Static water level measurements were collected from wells at the field sites. The depth to the static water level was measured from the top of the well casing (TOC). The distance from the land surface to the TOC, also known as the stick up, was measured. The depth to the static water level from the land surface was calculated by subtracting the stick up from the depth to the water level from TOC. The elevation of the static water level was determined by subtracting the depth to the static water level from the land surface from the elevation of the land surface at the well. The land surface elevation at the well locations were taken from previous studies at the sites if possible or estimated from USGS quadrangle maps if no data from previous studies were found.

3.2 Surface Electrical Resistivity Imaging

The resistance, R [ohms], of a volume of material to the flow of electric current, I [amp], is a fundamental property of the material. The resistance of a cubic volume of material, with length, L [m], and cross-sectional area, A [m^2], to

the flow of electric current results in a potential difference, *V* [volt], across opposing sides of the volume of material. The relationship between resistance, current and the potential difference is expressed in the equation known as Ohm's law (Telford et al., 1990; Giancoli, 1995; Reynolds, 1997).

$$R = V/I \qquad \text{(Eq. 6)}$$

The resistance of a material is directly related to the length of the material, *L* [m], and inversely related to its cross-sectional area, *A* [m^2], by the expression

$$R = \rho(L/A) \qquad \text{(Eq. 7)}$$

where ρ [ohm m], is a constant of proportionality called the resistivity (Telford et al., 1990; Giancoli, 1995; Reynolds, 1997). Resistivity is expressed as the resistance through a distance by the equation

$$\rho = (V/I)*(A/L) \qquad \text{(Eq. 8)}$$

Resistivity is a material dependent property that is independent of material geometry (Giancoli, 1995; Reynolds, 1997).

The electrical resistivity measurements were conducted using four electrodes in a variety of geometric configurations. A known electrical current was applied across two of the electrodes and the potential difference was measured at the other two electrodes in the configuration. The calculated resistance, *R* [ohms], was multiplied by a geometric factor, *K* [m], which is dependent on the electrode configuration used, to produce a measured apparent resistivity, ρ_a [ohm m] (Telford et al., 1990; Reynolds, 1997).

The measured apparent resistivities are not the same as the true resistivities and do not reflect the physical properties of the subsurface. Earth

Figure 3.1. The electrical resistivity imaging system with components. SuperSting R8 IP resistivity instrument and switch box and electrode cable with electrode stake in inset images. Graduate student Khayyun Rahi is shown monitoring the ERI data collection at the Arbuckle-Simpson Ranch site.

materials are not perfectly homogeneous and isotropic. As a result, the measured apparent resistivities for a given location differ depending on the electrode configuration used for the measurement. The true electrical resistivity values of the subsurface materials are obtained from interpretation techniques during the data processing (Telford et al., 1990; Reynolds, 1997).

One to six ERI surveys were conducted at each field site using a system manufactured by Advanced Geosciences, Inc. (AGI). The ERI system was comprised of a string of 56 electrodes connected to stainless steel stakes inserted into the ground at regular intervals along a line. The electrodes were

connected by a cable to an AGI SuperSting R8 IP 8-channel resistivity instrument and switch box (Figure 3.1).

The ERI surveys at each field site were conducted in the same location and orientation but at a variety of scales unless noted otherwise. Decisions on the locations for the ERI surveys at each site were largely a function of the availability of access to an open space large enough to conduct the ERI surveys. The ERI survey locations also had to be free of sources of anthropogenic noise like metal post fencing and buried pipes which would have had a significant effect on the ERI data.

The ERI surveys at the Hatch and Spears sites were set up at compass orientations which would show the greatest degree of variability in the electrical properties of the subsurface. The decision on the orientation of the ERI surveys at the Hatch site was based upon knowledge of the site from a previous study (Sample and Halihan, 2004). The decision on the orientation of the ERI surveys at the Spears Ranch site was based upon knowledge of the site from a previous study that has remained unpublished as of January, 2008.

An inferred fault was mapped in the literature as crossing the Arbuckle-Simpson Ranch site (Fairchild et al., 1990) (Figure 1.5). The ERI surveys at the field site were set up in a location that was estimated to cross the inferred fault based upon observations of a subtle change in vegetation along a trend that was similar to the mapped trend of the inferred fault. The ERI surveys were set up perpendicular to and centered on the observed trend in vegetation.

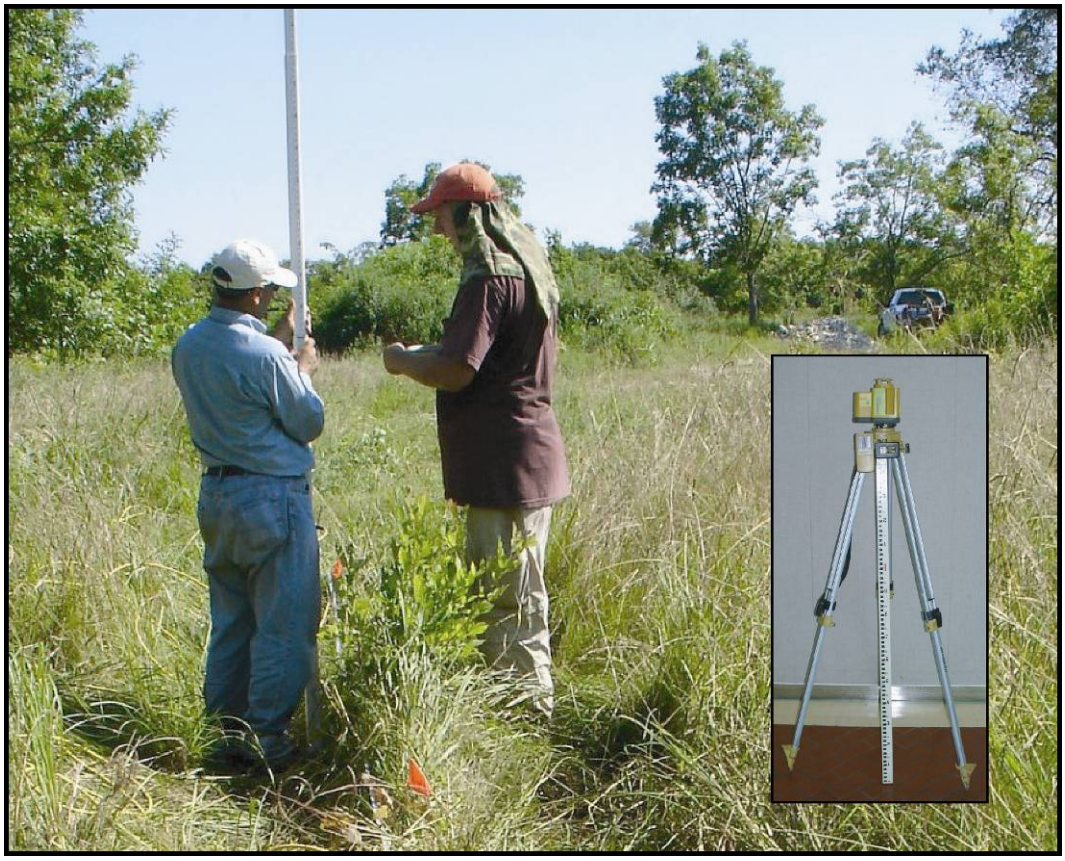

Figure 3.2. Topographic survey with Topcon rotating laser level survey equipment. OSU graduate students Khayyun Rahi (left) and the author (right) are shown conducting a topographic survey at the Arbuckle-Simpson Ranch site.

The ERI surveys were conducted at different scales to examine the electrical properties of the subsurface at different depths and resolutions. The scale of ERI surveys is a function of the spacing between the electrodes. The ERI system available at OSU permits a maximum electrode spacing of 32.8 feet (10 meters). The ERI surveys accomplished for the study were conducted using 16.4, 8.2, or 4.1 foot (5.0, 2.5, or 1.25 meter) electrode spacing. An ERI survey with 32.8 feet (5.0 meter) electrode spacing would collect electrical resistivity data along a line with a total length of 902 feet (275 meters). An ERI survey with an electrode spacing of 8.2 feet (2.5 meters) would collect data along a 451 foot

(138 meter) line and an electrode spacing of 4.1 feet (1.25 meters) would collect data along a 226 foot (69 meter) line.

The total length of the ERI survey lines determined the maximum effective depths to which quality electrical resistivity data could be collected. The maximum effective depth is approximately 20% of the total ERI line length. An ERI line with a total length of 902 feet (275 meters) could collect quality electrical resistivity data on the subsurface materials to a depth of about 180 feet (55 meters). A 451 foot (138 meter) ERI line would data to a depth of about 90 feet (28 meters) and a 226 foot (69 meter) ERI line would collect data to a depth of 45 feet (14 meters).

The electrode spacing determined the resolution of the ERI images. ERI surveys are capable of resolving features in the subsurface that are larger than about 50% the electrode spacing assuming there is a sufficient contrast in the electrical properties of the features with the background. An ERI survey line with an electrode spacing of 32.8 feet (5.0 meter) can resolve features in the subsurface that are at least 8.2 feet (2.5 meters) across. Features smaller than ½ the electrode spacing would not be seen unless grouped together in sufficient quantities or of sufficiently high contrast to create an anomaly.

At each field site all of the ERI surveys were tied together to a discrete point on the surface by establishing a common electrode location which was used for every ERI survey. A survey of the terrain was conducted along each ERI survey line using a Topcon RL-60B rotating laser level (Figure 3.2). The Topcon rotating laser level provided terrain data with an accuracy of ± 2.4 mm at

30.0 m. The terrain surveys were used to tie the ERI surveys to a common elevation datum. The terrain surveys were also used to resolve the effects of terrain in the ERI data processing. An Oklahoma State University proprietary method (the Halihan-Fenstemaker method) was used to acquire and process the ERI data into high resolution images.

3.3 Direct Push Methods

Direct push methods accomplished this through the insertion of tools into the subsurface on the end of small diameter pipes. The pipes were pushed into the ground through the use of a hydraulic hammer. Electrical conductivity logs and sediment cores were collected using the same system. The Direct push system used in this study was a Geoprobe® model 6200TMP (trailer mounted probe) (Figure 3.3).

The direct push methods can only push pipes into unconsolidated earth materials. The depth at which the pipes encountered consolidated material and could be pushed no deeper was referred to as the depth of refusal. The approximate thickness of the soils mantling the epikarst was defined as the average of the final depth of refusal for the soils encountered at the field sites.

Electrical conductivity, σ, is the inverse of resistivity and is a measure of a materials ability to carry electric current (Telford et al., 1990; Reynolds, 1997).

$$\sigma = 1/\rho \qquad \text{(Eq. 9)}$$

The standard unit of measurement for electrical conductivity is siemens per meter [S/m] which is equivalent to mhos per meter [$ohm^{-1}\ m^{-1}$] (Telford et al.,

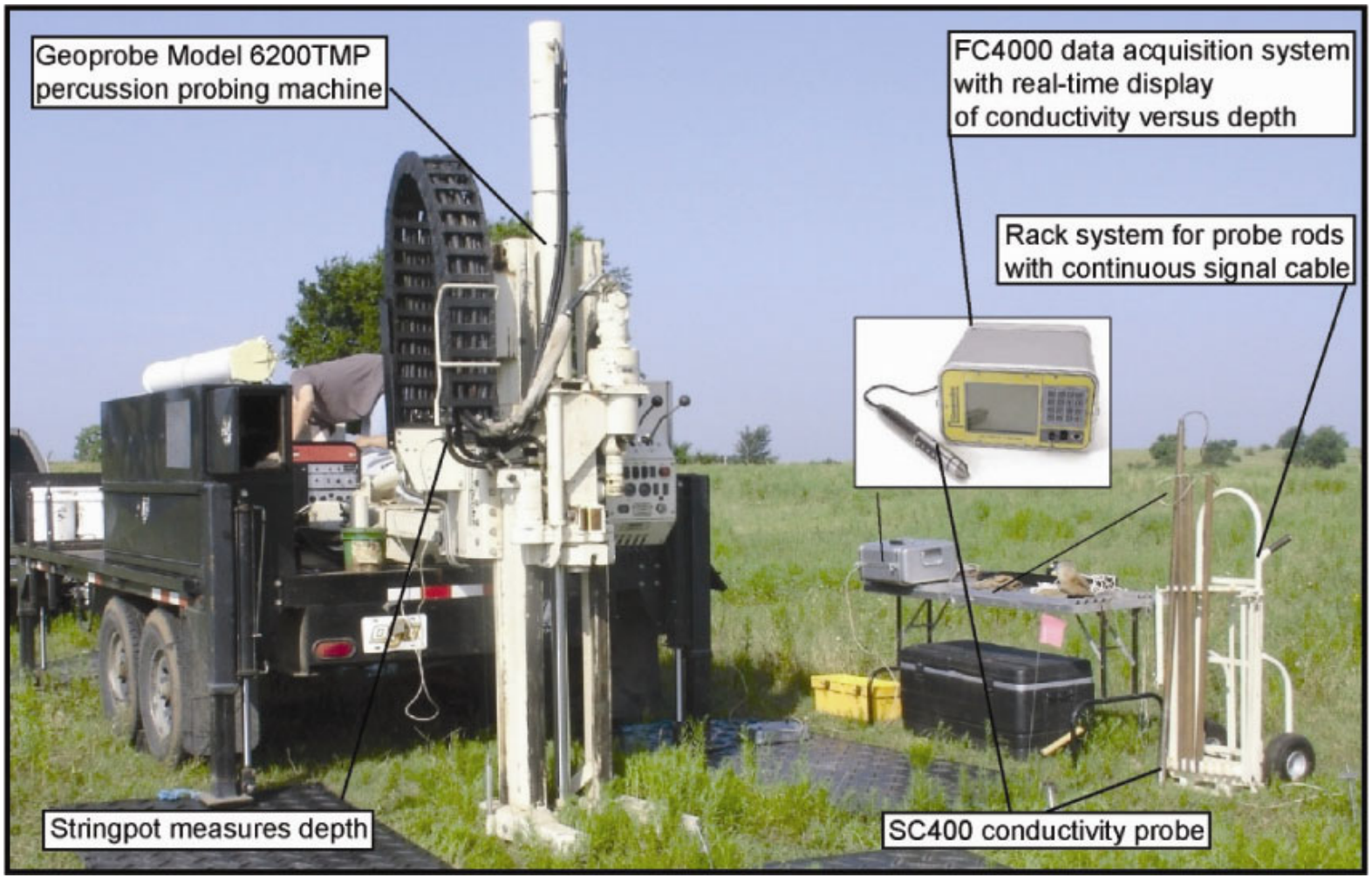

Figure 3.3. Geoprobe model 6200TMP direct push system configured for electrical conductivity probing. OSU undergraduate Chris Mace is shown on the Geoprobe at the Spears Ranch site.

1990; Reynolds, 1997). The electrical conductivity measurements collected by the direct push EC probe were collected in units of millisiemens per meter [mS/m].

Direct electrical conductivity measurements of the subsurface materials versus depth were collected at each area of interest using a Geoprobe® model SC400 conductivity probe and FC4000 field computer (Figure 3.3). The EC probe with a 1.5 inch outer diameter was attached to the end of a string of small diameter (1.0 inch) probe rods and inserted into the ground. Continuous electrical conductivity measurements with depth were collected as the EC probe was advanced into the ground by the direct push rig.

The EC probe collected the electrical conductivity data using a Wenner array of four electrodes spaced evenly apart over 2.5 inches. The EC probe collected measurements at 0.05 foot intervals while being inserted into the ground. The EC probe collected the electrical conductivity data in units of millisiemens per meter [mS/m]. The recorded depth of the EC measurements was controlled by a device called a stringpot which measured the vertical probe movements.

Continuous sediment cores were extracted at each area of interest using the direct push Geoprobe® DT22 dual tube soil sampling system (Geoprobe, 2006). The basic dual tube coring system consisted of a hollow cutting shoe at the base with an outer diameter (OD) of 2.375 inches and an inner diameter (ID) of 1.125 inches. The cutting shoe was threaded onto the bottom of a four foot outer probe rod section with an OD of 2.25 inches. A threaded drive head was

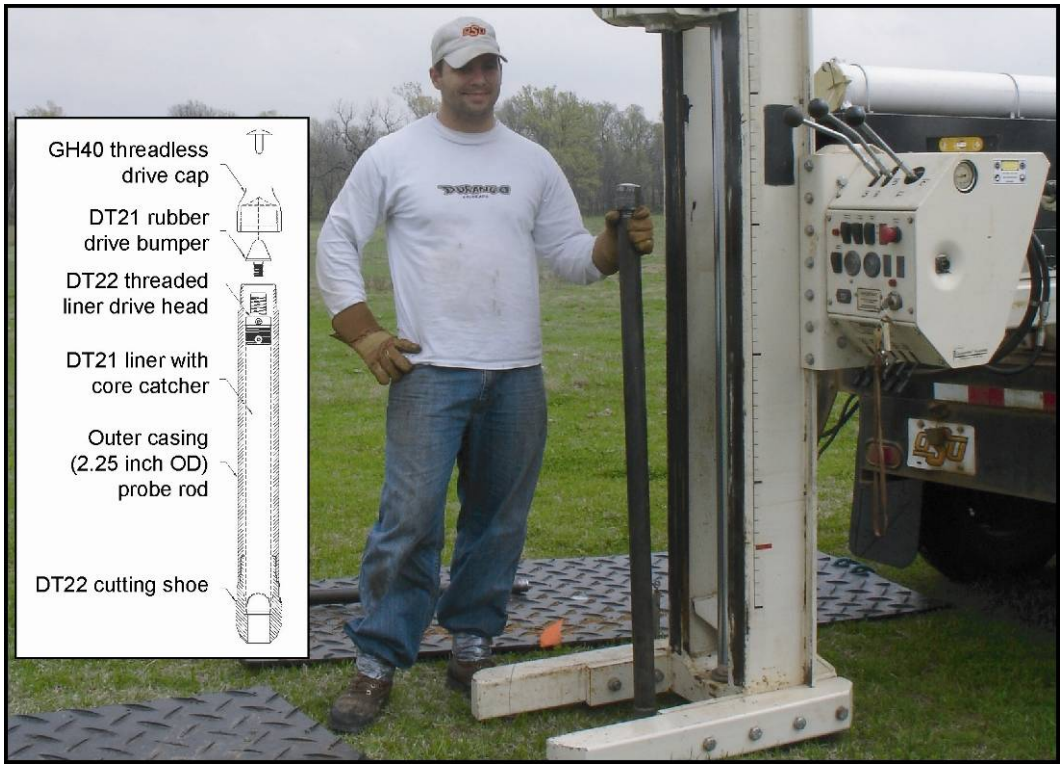

Figure 3.4. Direct push dual tube sediment coring system basic unit (after Geoprobe Systems, 2006). OSU undergraduate student Shawn Hammond is shown prepared to collect sediment core at the Hatch Site.

attached to the top of a four foot long clear plastic (PETG), 1.375 inch OD, core liner with a plastic core catcher integrated into its base. The core liner was inserted into the hollow space within outer probe rod casing until it seated firmly into the recess made for it in the cutting shoe. A rubber drive bumper was inserted into the top of the threaded drive head and a threadless drive cap was placed over the top of the outer probe rod to complete the basic unit of the dual tube coring system (Figure 3.4).

The initial dual tube coring system unit was inserted into the ground approximately three feet by the direct push rig (Figure 3.5-a). The cutting shoe sheared off a 1.1255 inch OD of sediment core which was collected into the core

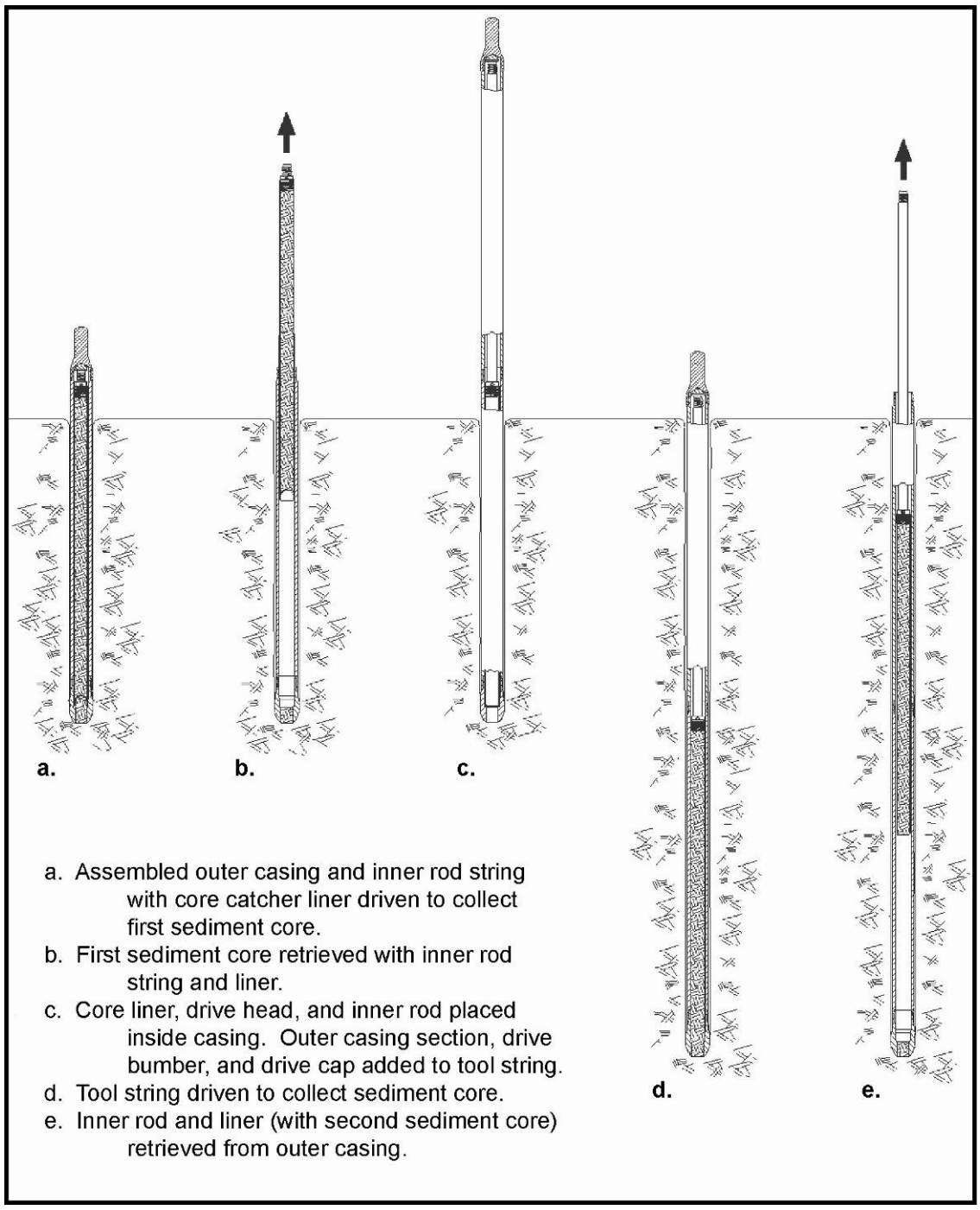

Figure 3.5. Direct push dual tube coring system operation (after Geoprobe, 2006).

liner as the coring system was inserted into the ground. A four foot section of 1.25 inch OD inner probe rod was screwed onto the threaded drive head at the top of the core liner and used to extract the sediment core from within the outer probe rods which remained in place (Figure 3.5-b).

The decision to stop the initial sediment core at three feet had a couple of benefits. The extra foot in the core liner provided extra accommodation space for any expanding soils encountered. The foot of probe rod left remaining above the ground facilitated the attachment of new probe rod sections to collection more sediment cores.

A new core liner and drive head was assembled and screwed onto a four foot section of 1.25 inch OD probe rod. This assembly was inserted into the 2.25 inch OD probe rod in the ground until the core lining seated firmly into the recess for it in the cutting shoe (Figure 3.5-c). The proper seating of the core liner and use of the rubber bumper was important to hold the liner in place to accept the sediment core and to prevent damage to the liner from the shock of impacts from use of the hydraulic hammer. A new four foot section of 2.25 inch OD probe rod was screwed onto the probe rod already in place and the rubber bumper and drive cap placed on the top of the assembly as before. The new dual tube coring assembly was inserted into the ground an additional four feet unless the presence of expanding soils necessitated that accommodation space be left at the top of the core tube (Figure 3.5-d). The new sediment core was retrieved and the process repeated until the depth of refusal was met (Figure 3.5-e).

As each section of sediment core was retrieved the actual total depth of penetration of the core section was measured in decimal feet and documented on the down-hole end of the core liner with a permanent marker. The coring depths were measured using a Keson model OTR10M100 fiberglass tape measure accurate to ± 0.01 ft and ± 0.002 m. The total coring depth was determined by measuring the stick up of the outer probe rod above the ground surface and subtracting the measured value from the total length of four foot probe rod sections involved at the time of the measurement. The actual depth of penetration of the top of each core was taken as the measured total depth of penetration recorded from the previous core up hole and documented on the up-hole end of the core liner with a permanent marker. The sediment core from each area of interest was given a unique name which was also documented on the core liner with a permanent marker. The unique sediment core name and total measured depth was recorded in the field notes.

Immediately following their retrieval the core sections were trimmed with a hack saw to remove any vacant space at the ends of the core sections. The ends of the core sections were capped with plastic core liner caps (red at the top and black at the bottom) and sealed with duct tape to preserve soil moisture conditions within the core. The cores sections were then visually analyzed to locate contacts where distinct changes in sediment texture occurred. The core sections were split into segments along the observed contacts and the ends of each core segment sealed as before (Figure 3.6).

Figure 3.6. Field processing of sediment core. OSU undergraduate student Megan Dailey processing sediment core at the Hatch site.

The top and bottom depths of each core segment were determined and recorded along with the unique core name on the core liner with a permanent marker. The actual length of sediment core could differ from the length determined from the depth of penetration measurements. The discrepancy between the measured and actual length was due to either the compaction of core materials during the collection process or from the swelling of expansive soils following the release of formation pressures. The majority of the discrepancies occurred in the top four foot section of the cores. When a discrepancy was present the actual depths represented by the core segments were estimated by averaging the difference over the whole length of the core section.

Any rock present at the bottom of a sediment core or lodged in the cutting shoe was assumed to be representative of the bedrock present at that location. Rock present at the bottom of a core was sealed in the core sleeve until it could be examined in the lab. Any rock lodged in the cutting shoe was collected into a sealable plastic bag, labeled, and stored with the sediment cores for examination in the lab.

3.4 Concentric (Double-Ring) Infiltrometry

Double-ring infiltrometers are widely used to estimate field saturated hydraulic conductivity, K_{fs} [μm/s], of soils based on *insitu* infiltration measurements (Bodhinayake et al., 2004; Reynolds et al., 2002c). This method used two thin-walled open-ended cylinders (12 and 24 inch diameters) that were inserted (hammered) concentrically into the soil 3 to 10 cm (Figure 3.7). Water was ponded and a constant head was maintained in both cylinders. The head in each cylinder was measured and monitored through the use of two mariotte tubes (3,000 cc and 10,000 cc capacities respectively) that were independently connected to the cylinders. Infiltration from the outer or buffer cylinder theoretically acted to absorb divergent flow which left only the vertical flow component of infiltration that was measured from the inner cylinder. The infiltration rate was measured over time until steady state flow was achieved (Bodhinayake et al., 2004; Reynolds et al., 2002a, b). Steady state flow conditions can be achieved in 10 to 60 minutes but could take several hours or days to achieve (Reynolds et al., 2002b). This method has been found suitable

Figure 3.7. Concentric cylinder infiltrometer set up.

for the estimation of soil hydraulic properties in terrains with slopes up to 20% grade (11.3 degrees) (Bodhinayake et al., 2004).

The hydraulic conductivity of soils is highly variable and can vary by more than a factor of ten within an area smaller than a square meter (Soil Survey Division Staff, 1993). The replication of hydraulic conductivity measurements (10 to 20 or more) would be required to achieve an adequate statistical distribution to arrive at a mean hydraulic conductivity for an area the size of an average plot (Reynolds et al., 2002c). Time constraints limited the collection of infiltration data to one experiment at each area of interest. Hydraulic conductivity measurements are also scale dependent and increase with the scale of the measurement regardless of the method used (Rovey and Cherkauer, 1995). The scale of measurement for a double-ring infiltrometer experiment is very small and was not

expected to have sampled the full range of hydraulic properties at any of the field sites.

Errors can be introduced in many ways with this method. Soil compaction during setup, plugging of soil pores by deflocculated silt and clay particles during measurements, or air trapped in the soil matrix by the infiltering water could cause the calculated K_{fs} to be too low (Reynolds et al., 2002b, c). Flow or leakage along the walls of the cylinders or the presence of a lateral divergent flow component could cause the calculated K_{fs} to be too high (Reynolds et al., 2002b, c). Numerous tests have shown that the buffer cylinder was often ineffective in isolating the measuring cylinder from the influence of divergent flow (Reynolds et al., 2002c). The natural variability of soils could sometimes cause erratic changes in the infiltration rate over time which would make identifying the true steady state conditions difficult (Reynolds et al., 2002a). Careful attention to proper procedure would reduce the effects of errors on the measurements. It was expected that this method would provide reliable order of magnitude measurements of saturated hydraulic conductivity in the near subsurface which was adequate for this study.

CHAPTER IV

LABORATORY METHODS

Upon returning to the lab from the field the sediment core segments were laid out, grouped by core, and arranged in order from the surface to the depth of refusal. Each core segment was inspected to insure that the duct tape seal on either end of the core segment remained intact. The duct tape seal was replaced if the seal appeared to be compromised in any way.

Laboratory analyses on the sediment cores were conducted in three steps. The sediment cores were described, divided into intervals based upon observed textural similarities, a representative core sample extracted from each core interval, and the water content (gravimetric and volumetric) and porosity were calculated for each core sample in the first step of the analyses. These analyses were conducted one core segment at a time in order to preserve the integrity of field soil moisture conditions assumed present within each sealed core segment. The second step consisted of particle size analyses of each core sample. The coarser particle size fractions (> 1 mm) were analyzed using mechanical sieve analysis and the finer particle size fractions ($\leq$ 1 mm) were analyzed using a Cilas 1180 laser diffraction particle size analyzer. The sieve and laser diffraction particle size analysis results were then combined into a

single coherent dataset for each core sample and analyzed to texturally classify each core sample. The third step in the laboratory analyses consisted of hydraulic conductivity calculations for each core interval using the Carmen-Kozeny and Fair-Hatch equations.

4.1 Water Content and Porosity Analysis

Each core segment was removed intact from its core tube and placed upon a sheet of freezer paper in order to facilitate its analysis. It was discovered that the sediment cores would slide from their encasing core tubes with relative ease and negligible disturbance by placing a long wooden dowel (broom handle) at one end of the core tube and sliding the core tube onto the dowel while holding the dowel in place. The core segments were labeled and photographed at each step of the analysis. The majority of extracted sediment core segments were observed to be continuous smooth cylinders of sediment. Irregularities along the lengths of the sediment cores were largely limited to the near surface where moisture content was low or in zones where coarse sand, gravel, or weathered bedrock was encountered (Figure 4.1-a).

Diameter measurements were collected along each core segment using a dial caliper accurate to $\pm$ 0.01 inch (Figure 4.1-b). The measurements in inches were converted into centimeters by multiplying the measured results by a factor of 2.54 cm/in. The diameter measurements were collected wherever changes in color or texture were observed and within each foot of the core segments when no changes were observed. The diameter measurements were recorded for use

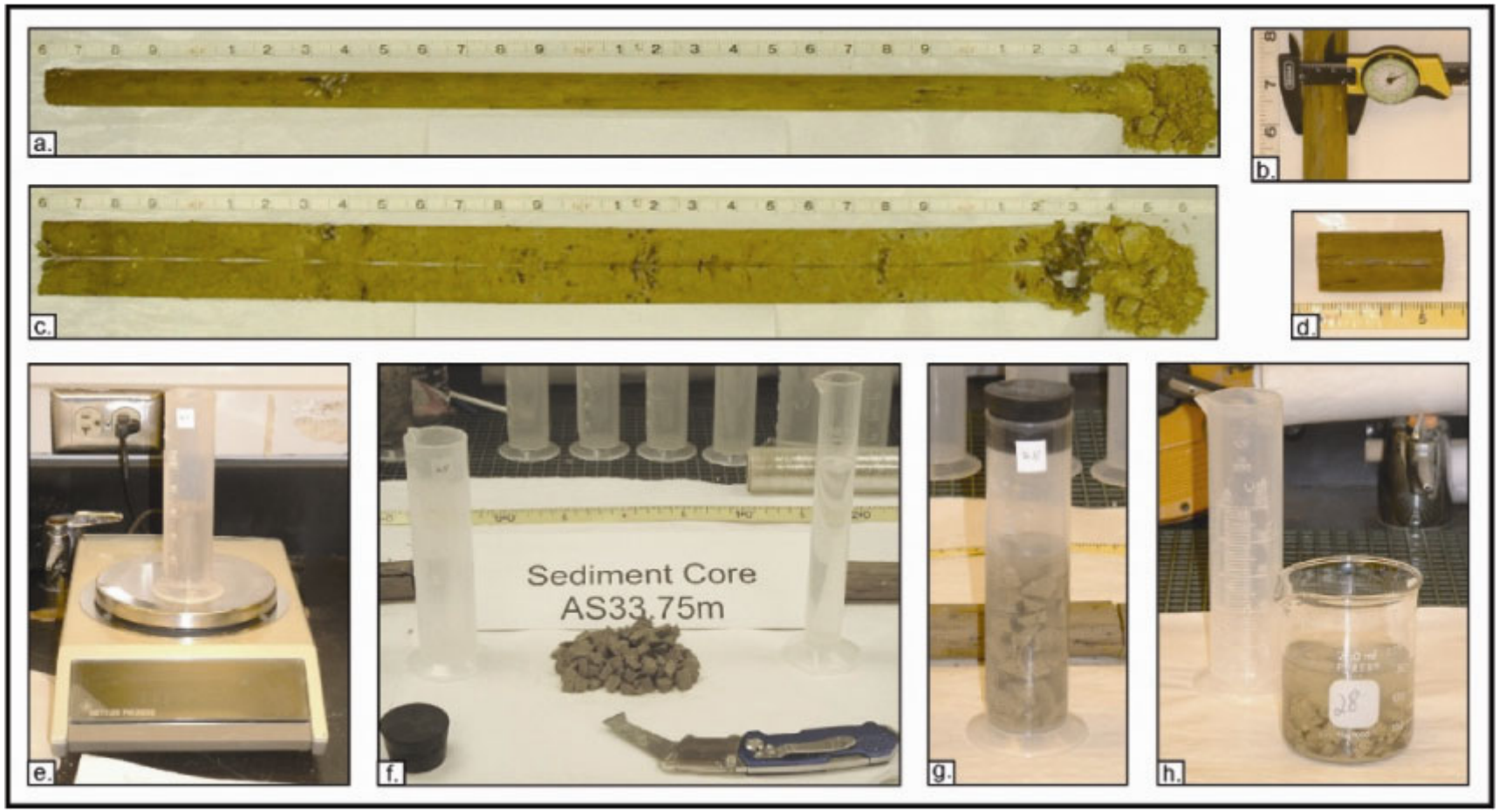

Figure 4.1. Sediment core property analysis steps (a) removing the core for analysis (b) measuring the core diameter (c) splitting the core to expose the cross section (d) extracting a representative sample (e) measuring the mass (f) preparing the sample for saturation (g) saturation the sample (h) preparing to oven dry the saturated samples.

in volume calculations for the representative core samples extracted from the cores.

After the diameter measurements were collected, each core segment was carefully split lengthwise with a utility knife to expose the cross section of the core (Figure 4.1-c). This was done to reveal sedimentary features obscured by smearing along the external surface of the core. Each core cross section was examined in detail to identify and describe sedimentary features, colors, and horizons where soil textures were observed to change with depth. Each core was subdivided into intervals observed to have essentially the same features. Each core interval was defined as a separate unit and given a unique designation.

Once the core intervals were identified and described the core section halves were carefully fitted back together to facilitate the extraction of representative samples from within each of the intervals. A representative sample was cut from near the center of each core interval with a utility knife and trimmed to a maximum length of 6.0 cm (Figure 4.1-d). The maximum length of 6.0 cm was chosen out of concern that a longer length could potentially produce a sample volume too large to be accurately analyzed in a 100 ml short-form graduated cylinder. Whenever possible the sample length of 6.0 cm was used in order to standardize procedures, promote repeatability, and to reduce the potential effects of errors inherent in analyzing smaller volumes. All interval and sample lengths were measured using a Keson model OTR10M100 fiberglass tape measure accurate to $\pm$ 0.01 ft and $\pm$ 0.002 m. Core intervals were

measured in decimal feet to facilitate comparison of core interval depth with the depths recorded on the electrical conductivity logs. The core sample lengths were measured in centimeters to facilitate volume calculations.

No core samples were extracted from core intervals that were observed to consist entirely of weathered rock. The methods used for the sediment core analyses were not appropriate for the analysis of rock fragments. Rock fragments extracted from the weathered rock core intervals were examined using reflected light microscopy, tested for hardness against metal (knife blade or tweezers), and exposed to dilute, 10%, hydrochloric acid to identify the rocks lithology. The results of the lithologic analyses of the weathered rock intervals were added to the sediment core description notes. The intervals of weathered rock were placed into sealable plastic bags which were labeled appropriately and stored for reference.

Standard glass graduated cylinders were used for the analyses at the start. Problems arising from the use of standard graduated cylinders led to a decision to change over to polypropylene (PP) short-form graduated cylinders. The narrow openings of the standard graduated cylinders were found to hinder the analyses of the core samples. Air bubbles frequently became trapped in the sediment matrix in the standard cylinders and were difficult to impossible to remove. Extraction of the core sample material from the standard cylinders for further analysis was found to be difficult to impossible. Two standard cylinders were broken in attempts to extract the core samples and those samples lost before further use of the standard cylinders was terminated. The short-form

graduated cylinders have a larger diameter opening which eliminated the problems associated with using the standard cylinders. Larger 250 ml graduated cylinders were available for use in the analysis but were rejected because of the significant decrease in measurement accuracy with the larger cylinders ($\pm$ 5.0 ml versus $\pm$ 2.0 ml).

The length, *l* [cm], of each representative core sample was recorded along with the diameter, *d* [cm], for the associated core interval. The volume of each representative core sample, V_t [cm^3], was calculated using the equation for the volume of a cylinder.

$$V_t = V_{cylinder} = \pi(d/2)^2 l \qquad \text{(Eq. 10)}$$

This method of sampling a volume of the core preserved conditions present within the core which came close to approximating undisturbed field conditions.

When a core interval was too irregular in shape to extract a representative core sample volume as a cylinder with any degree of accuracy such as when gravel was significant or when the sample was too dry to cut into a regular cylinder the sample volume was determined by immersing the core sample into a 100 ml short-form graduated cylinder containing a 50 ml volume of water. The volume of the core sample was calculated by subtracting the volume of the water from the observed combined volume at the instant of immersion. It was recognized that measuring core sample volume by this immersion method would introduce error into the sample volume calculations in that water would invade, at least in part, what would have otherwise been air filled pore spaces within the sample volume. This type of error would lead to a calculated sediment core

sample volume that was too small. If air bubbles become trapped in the graduated cylinder along with the sediment core sample as it is being immersed then the resulting sediment core sample volume would be too large.

Errors in the sediment core sample volume measurements would affect the results of the bulk and particle density, volumetric water content, porosity, and water saturation calculations. Sediment core sample volume measurements that are too low would lead to bulk and particle densities, volumetric water contents, and water saturations that are too high and total porosities that are too low. Sediment core sample volume measurements that are too high would lead to bulk and particle densities, volumetric water contents, and water saturations that are too low and total porosities that are too high. Great care was taken to measure sediment core sample volumes as accurately as possible to minimize the effects of potential measurement errors.

A 100 ml short-form graduated cylinder was labeled and its mass was measured and recorded for each core sample. Each core sample was placed in its cylinder and the combined mass measured. The initial mass of the core samples, M_t [g], were obtained by subtracting the mass of the cylinder from the combined sample + cylinder mass. All mass measurements were taken using a Mettler PM2000 electronic scale accurate to $\pm$0.01 g (Figure 4.1-e).

The volume of the air filled pore spaces in vadose zone sediments can be significant in porosity determinations. The volumes of the air filled pore spaces in the core samples were calculated by immersing the core sample into a 100 ml short-form graduated cylinder containing a 50 ml volume of water, allowing the

core samples to become fully saturated, and recording the resultant observed combined volumes. The volumes of the air filled pore spaces in the core samples, V_a [cm^3], were determined as the difference between the observed saturated water + core sample volumes and the calculated water + core sample volumes. All water volumes were calculated using a standard 50 ml graduated cylinder with an accuracy of $\pm$ I ml.

The core samples were broken apart or cut up with a utility knife into small pieces prior to their immersion into the water (Figure 4.1-f). The smaller pieces increased the surface area of the core samples in direct contact with the water. This was done to reduce the time required to bring the core samples to saturation and reduce the possibility of air bubbles being trapped in the matrix of the core samples. The short-form graduated cylinders were immediately sealed with a rubber cork to prevent moisture loss through evaporation that could have affected the resultant observed volume (Figure 4.1-g). The sealed cylinders were manually agitated to remove any trapped air bubbles. The sediments were allowed to settle and if necessary the cylinders were manually agitated again to remove any remaining air bubbles. The core samples were allowed to come to saturation over a period of no less than 12 hours.

Once the core samples had come to saturation the excess water was poured off and measured in a 50 ml graduated cylinder. The volume of the excess water was subtracted from the observed combined volume of the core samples + water to determine the saturated core sample volume, V_{sat} [cm^3]. Any differences between the original field, V_t [cm^3], and saturated, V_{sat} [cm^3], core

sample volumes could have been caused by measurement (uncertainty) errors, trapped air bubbles, or the presence of expanding clay in the samples. A minute amount of core sample material was often transferred to the 50 ml graduated cylinder along with the excess water. The volume of core sample material transferred along with the excess water was deemed too small to significantly effect the volume calculations but significant enough to potentially effect the results of the dry core sample mass measurements and particle size analyses which followed. The excess water with the minute amount of core material was retained and recombined with the core samples to preserve the total sample masses.

The saturated core samples were transferred to 250 or 300 ml glass beakers to allow the core samples to be oven dried (Figure 4.1-h). A 250 or 300 ml glass beaker was acquired, labeled, and it's mass determined for each core sample. The saturated core samples were transferred to the glass beakers along with the excess water. A long handled laboratory spatula and small amounts of additional water were used to facilitate the complete transfer of core material from one container to the other. Great care was taken to insure that all of the core sample material was transferred to the glass beakers.

The core samples were oven dried in a VWR model 1310 gravity convection oven with a temperature uniformity of $\pm$ 4°C (Figure 4.2). The VWR oven was preheated to ~ 105 °C. The core samples were placed in the oven and allowed to dry for period of no less than 18 hours.

Figure 4.2. The VWR oven.

Short-form glass cylinders would have been preferred for the analyses so that no transfer of material would have been required in order to oven dry the samples but the short-form cylinders were not available in a glassware version. Two of the PP short form graduated cylinders were damaged while testing the feasibility of using the PP short form graduated cylinders for drying the core samples in. The two core samples used in the test were successfully retrieved and transferred to glass beakers.

A partial re-hydration of the oven dry core samples prior to the dry mass measurements and the dry mechanical sieve analyses which followed could have been a potentially significant source for error given the relatively small sample sizes. No desiccation cabinet was available to cool and store the dry core samples prior to the analyses. The potential for re-hydration of the core samples was minimized by limiting the extraction of dry core samples from the oven to

three at a time and completing the dry analyses on those samples before retrieving any additional dry core samples from the oven. The time estimated to measure the mass and conduct the dry mechanical sieve analyses on three core samples was considered too short for any significant re-hydration of the core samples to occur.

The hot dry core samples were removed from the oven and covered with clean dry paper towels to minimize mixing of the dry air in the core sample beaker with the more humid lab air. The covered core samples were allowed to cool until no longer hot to the touch. The dry masses of the core sample particles, M_p [g], were determined by subtracting the beaker masses from the measured combined beaker + dry core sample masses.

The observed and measured quantities up to this point were used in a number of calculations leading to values for the gravimetric and volumetric water contents and porosities present in the core samples. The mass of water, M_w [g], initially present in the undisturbed core samples were calculated by subtracting M_p from M_t. The volumes of the water, V_w [cm^3], in the initial core samples were calculated by assuming a water density of 1.0 g/cm^3. The total volumes of the pore spaces in the core samples, V_v [cm^3], were defined as the sums of V_a plus V_w for each of the core samples. The dry particle volumes of the core samples, V_p [cm^3], were calculated by two different methods. The dry particle volumes of the core samples were calculated as the difference between V_t and V_v. The dry particle volumes of the core samples were also calculated by dividing M_p by an assumed particle density, ρ_p [g/cm^3], of 2.65 g/cm^3. The particle density value of

2.65 g/cm^3 is a commonly used average density value for earth materials (Eshel et al., 2004; U.S. Department of Agriculture; Natural Resources Conservation Service, 2007). Particle densities for the core samples were also calculated by dividing M_p by V_p. The particle densities calculated by this method were used to test the validity of using the assumed particle density in the porosity calculations. The bulk densities, ρ_b [g/cm^3], of the core samples were calculated as the quotient of M_p divided by V_t.

The gravimetric water contents, θ_g [%], of the core samples were calculated and expressed as a percentage as follows:

$$\theta_g = M_w / M_p * 100 \qquad \text{(Eq. 11)}$$

The volumetric water contents, θ_v [%], of the core samples were calculated and expressed as a percentage as follows:

$$\theta_v = V_w / V_t * 100 \qquad \text{(Eq. 12)}$$

The saturation ratio's, R_s [%], for the core samples were calculated and expressed as a percentage using the expression:

$$R_s = V_w / V_v * 100 \qquad \text{(Eq. 13)}$$

The total porosities, Φ [dim], of the core samples were calculated as follows:

$$\Phi = 1 - (\rho_b / \rho_p) \qquad \text{(Eq. 14)}$$

The total porosity values in this form were used in hydraulic conductivity calculations. The total porosity values were also expressed as a percentage by multiplying the values by 100. This was done to facilitate side by side comparative analyses of total porosities with gravimetric and volumetric water contents, and saturation ratio's.

The methods for determining water content and porosity described in this section were arrived at through an iterative process. The Hatch site sediment cores were the first to be analyzed. The Hatch site sediment core sample volumes (001 – 048) were not calculated until after the gravimetric water content analysis was complete. The volumes of the Hatch site sediment core samples (001 – 048) were determined by packing the oven dry sediment core material into containers and measuring the volumes. The volumes of Hatch site sediment core samples (001 – 031) were evaluated in glass beakers using subsets of the samples due to a temporary shortage of appropriate sized containers. The volumes of Hatch site sediment core samples (032 – 037) were evaluated using standard graduated cylinders in an attempt to improve the accuracy of the volume measurements. The short form graduated cylinders arrived in time to accomplish the volume measurements for Hatch site sediment core samples (038 – 048). The volumes of the void spaces in Hatch site sediment core samples (001 – 048) were determined by saturating the sediment core samples with a known volume of water and measuring the volume of the excess water that was poured off. The bulk and particle density and porosity calculations of Hatch site sediment core samples (001 – 048) were determined using these bulk and void volume measurements. All subsequent sediment core sample water content and porosity analyses were accomplished using the methods previously described.

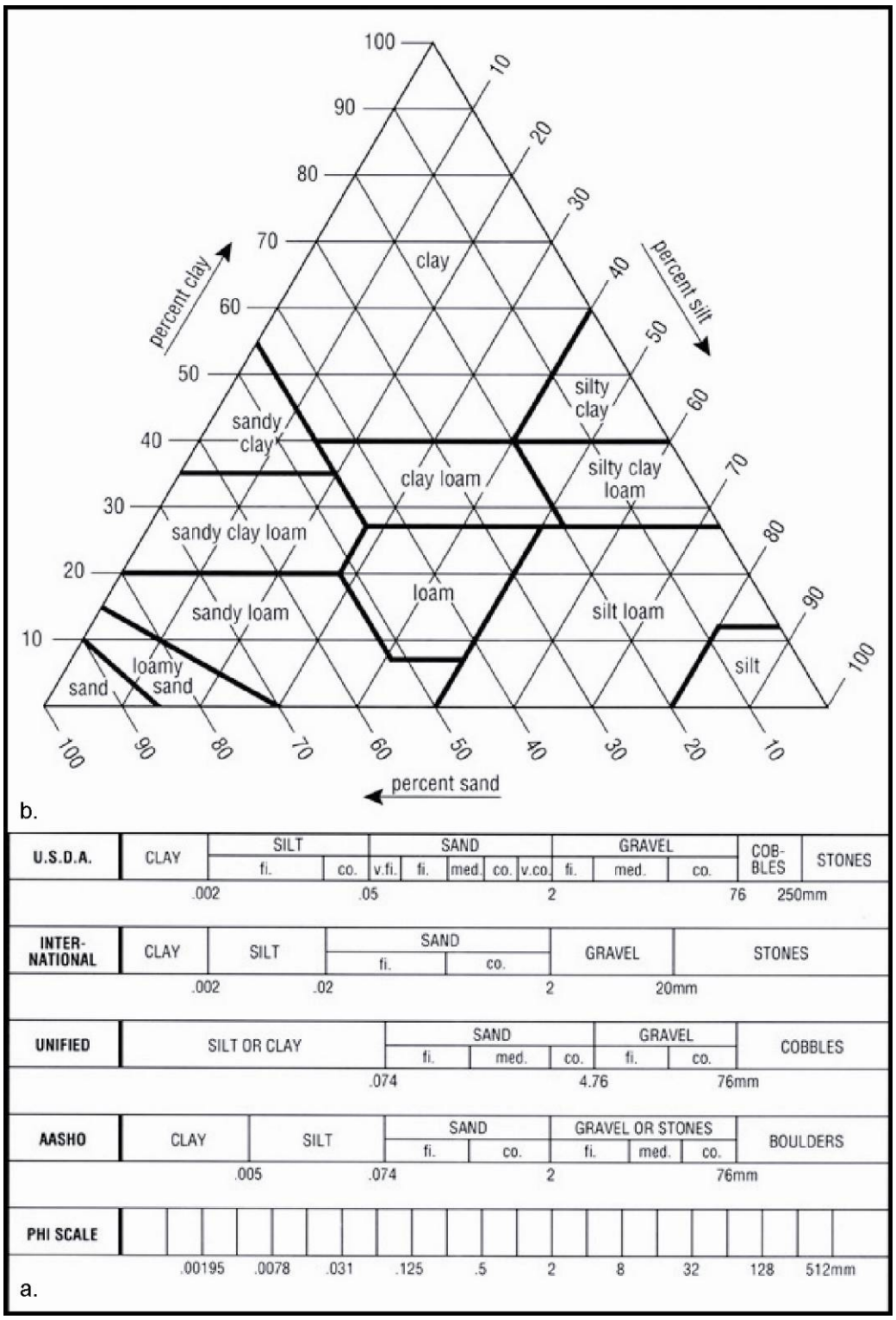

Figure 4.3. USDA (a) particle size and (b) soil texture classification schemes (after Soil Survey Division Staff, 1993).

4.2 Particle Size Analysis

Particle size analysis (PSA) has been accomplished to determine the size distribution of individual particles in soils. Soil aggregates were dispersed into individual particles by a combination of mechanical, chemical, and ultrasonic means and separated into discrete size units by sieving and sedimentation, or by instrumentation methods. Particles smaller than 2000 μm were divided into three general size groups (sand, silt, and clay) using a system of classification adopted by the U. S. Department of Agriculture (Gee and Bauder, 1986; U.S. Department of Agriculture; Natural Resources Conservation Service, 2007) (Figure 4.3-a). The percent distribution of sand, silt, and clay particles in a soil defined its texture. Soil textures were classified using a system of classification adopted by the U. S. Department of Agriculture (Gee and Bauder, 1986; U.S. Department of Agriculture; Natural Resources Conservation Service, 2007) (Figure 4.3-b). Particle size analysis results can be used to determine the properties of sediments (Gee and Bauder, 1986; Beuselinck et al., 1998; Lindsay et al., 1998; Blott et al., 2004; Eshel et al., 2004; Sperazza et al., 2004).

In this section various PSA methods are compared followed by an introduction to the laser diffraction method used in this study. Next, the dry sieve analysis procedures used in this study are described followed by a discussion on sample preparation procedures which occurred prior to the laser diffraction analyses. Finally, the Cilas 1180 laser diffraction particle size analyzer is introduced and the standard operating procedures used for the analyses are described.

4.21 Particle Size Analysis Methods Comparison

The sieving and sedimentation methods (pipette and hydrometer) are considered the classical methods for PSA (Gee and Bauder, 1986; Beuselinck et al., 1998; Lindsay et al., 1998; Eshel et al., 2004; Sperazza et al., 2004). The pipette and hydrometer are based on Stokes' law which describes the relationship between particle diameter and settling velocity. The pipette method requires the extra step of separating the sand size fraction (2000-50 μm) from the silt and clay (< 50 μm) by wet sieving (Gee and Bauder, 1986; Eshel et al., 2004). The sand size fractions are passed through a series of sieves stacked in order of descending size. The sand fractions are determined by measuring the dry mass of the material remaining on the sieves. The pipette and hydrometer methods provide results that are comparable if similar sample preparation techniques are used (Eshel et al., 2004).

Several disadvantages are experienced by the classical methods. The sieving method is limited in usefulness to particle sizes > 50 μm (Eshel et al., 2004). The sedimentation methods are time consuming, especially for determination of the size fraction < 2 μm, requires relatively large samples (40 g for the hydrometer and 10-20 g for the pipette), and has a limited capacity to resolve size fractions into subgroups (Allen, 1981; Eshel et al., 2004; Sperazza et al., 2004). Sedimentation results for particles < 1 μm are increasingly unreliable due to the effects of Brownian motion on the settling rate of the particles (Allen, 1981; Blott et al., 2004; Eshel et al., 2004).

When a particle is small enough, collisions with fluid molecules can measurably displace the particle which result in random 'Brownian' motion of the particle in addition to gravitational motion (Allen, 1981). Brownian motion exceeds gravitational motion for 1 μm particles that have a specific gravity of two (Allen, 1981). Non-spherical particles like the platy form of some silts and clays also have slower settling velocities than spherical particles of equivalent size (Blott et al., 2004; Eshel et al., 2004). The slower settling velocities of these particles result in an overestimation of the fine size fractions at the expense of coarser size fractions (Blott et al., 2004; Eshel et al., 2004).

Sedimentation methods are also sensitive to variations in particle density. Particle densities can range from around 1.2 g/cm^3 to > 6.0 g/cm^3 (Telford et al., 1990). Uncertainty regarding the actual density of the particles can bias size distribution analysis in sedimentation methods (Eshel et al., 2004).

The main source for error in the hydrometer method is inaccuracy in the readings (Gee and Bauder, 1986; Eshel et al., 2004). An error of ± 1 g/L on a hydrometer reading will result in an error of ± 2 wt% for the clay size fraction (Gee and Bauder, 1986). The main source for error in the pipette method is associated with sampling and weighing (Gee and Bauder, 1986). Error in the sieve-pipette method has been reported as high as 40% (Sperazza et al., 2004).

Instrumentation methods including microscopy (optical, transmission and scanning electron), electrical sensory zone, and laser light scattering (diffraction) techniques have been developed by industry for applications including the analysis of powders and gels (Gee and Bauder, 1986; Eshel et al., 2004).

Instrumental methods have several advantages over the classical methods. Instrumental methods are generally quicker, require small samples, and provide information over a wide range of particle sizes with a single analysis. The results obtained from instrumental methods are generally considered as reproducible as the classical methods (Beuselinck et al., 1998; Lindsay et al., 1998). The main disadvantage to instrumental methods has been the high cost of the instruments (Eshel et al., 2004).

4.22 Laser Diffraction Particle Size Analysis Theory

Laser diffractometry is an instrumental method that determines the size distribution of a volume of particles by relating the optical properties of the particles to an optical model (Blott et al., 2004). PSA using laser diffraction is based on two optical models: the Fraunhofer theory and Mie scattering (McCave et al., 1986; Lindsay et al., 1998; Eshel et al., 2004; Sperazza et al., 2004). The Fraunhofer theory states that monochromatic laser light scattered by a spherical particle of a given size will be diffracted through a given angle, that the angle of diffraction is inversely proportional to the size of the particle, and that the intensity of the diffracted light is directly proportional to the particles size (McCave et al., 1986; Lindsay et al., 1998; Eshel et al., 2004). A monochromatic laser beam is passed through a moving suspension containing the particles and the resultant diffracted light is focused onto a detector. The Fraunhofer model assumes that the laser beam is normal to the detector and that the distance is very large relative to the size of the particles (Eshel et al., 2004). The detector

senses the angular distribution of the resultant diffraction (Airy's) pattern which gives the intensity of the diffracted light (McCave et al., 1986).

The Fraunhofer model works well for approximating particle size when particle diameters are much larger than the wavelength of the laser light. When particle diameters approach the wavelength, λ [μm], of the laser light the particles no longer diffract light in the manner predicted by Fraunhofer's theory and the model begins to break down. The approximation of particle diameter, d [μm], using the Fraunhofer model becomes progressively worse below $d \approx 10\lambda$ (McCave et al., 1986; Lindsay et al., 1998). Fraunhofer based PSA tends to underestimate the particle sizes close to the wavelength of the laser light (McCave et al., 1986; Blott et al., 2004; Sperazza et al., 2004).

The mode of light scattering for particles with diameters close to or smaller than the wavelength of the laser light is called Mie scattering. The Mie solution is a complete analytical solution of the Maxwell equations which govern the behavior of electromagnetic waves in space (Eshel et al., 2004). Mie scattering is dependent on differences in the refractive indices and sizes of the particles (Lindsay et al., 1998). The use of Mie scattering in PSA requires knowledge of the refractive indices of the particles and of the medium composing the suspension (Lindsay et al., 1998; Eshel et al., 2004; Sperazza et al., 2004).

Laser diffraction results are independent of particle density but can be affected by particle shape (Blott et al., 2004; Eshel et al., 2004). The Fraunhofer optical model assumes a spherical particle (Lindsay et al., 1998) and assigns a particle size based on the projected cross-sectional area of the particle in the

Figure 4.4. The Cilas 1180 laser diffraction particle size analyzer

diffraction pattern (Eshel et al., 2004). The projected cross-sectional area of non-spherical particles can be larger than their spherical equivalent. Flocculated clay particles also present a larger cross-sectional area to the laser light (Sperazza et al., 2004). The larger projected cross-sectional area results in particles being assigned to a larger bin size than they belong to which skews the particle size distribution towards the coarser fractions at the expense of the finer fractions (Blott et al., 2004; Eshel et al., 2004; Sperazza et al., 2004).

The laser diffraction particle size analyzer used for this study was the Cilas 1180 (Figure 4.4). The Cilas 1180 provides particle size distribution data over an operating range of 0.04 – 2,500 μm (Cilas, 2004). The Cilas 1180 provides results with a repeatability of 0.5% and a reproducibility of < 2% (Cilas, 2008). Standard operating procedure established at the lab for use of this machine dictated that particles > 1,000 μm be removed from the samples prior to

all analyses. The particles > 1,000 μm were removed and analyzed using the dry sieve method.

4.23 Dry Sieve Analysis

Dry sieve analyses immediately followed the dry mass measurements of the oven dry core samples. The oven dried core sample material adhered together and had to be mechanically disaggregated into individual particles through the use of a ceramic mortar and pestle prior to being sieved. The mechanically disaggregated core sample material was then passed through a stacked series of ASTM E-11 (ISO 3310-1) test sieves (Figure 4.5). The sieve sizes used in the analyses were the No. 5 (4.0 mm), No. 10 (2.0 mm), and No. 18 (1.0 mm) sieves.

The test sieves were stacked from top to bottom in order of descending size. A pan was attached to the bottom of the stacked sieves to retain the fraction of particles ≤1.0 mm. The dry particles were introduced into the uppermost (largest) test sieve and the stacked sieves were mechanically agitated to facilitate the separation of the particles by size in the sieves. The particles retained by each sieve, starting with the largest (4.0 mm) were further disaggregated using the mortar and pestle and passed through the sieves until it was determined that further disaggregating of the core samples into individual particles was no longer possible. Care was taken to prevent the shattering of larger individual particles during the disaggregating process. The dry sieve analysis distributed the core sample particles into four size fractions (x > 4.0 mm,

Figure 4.5. Dry analysis procedures.

4.0 mm ≥ x > 2.0 mm, 2.0 mm ≥ x > 1.0 mm, 1.0 mm ≥ x) and which were quantified on a mass basis and recorded.

Particles > 4.0 mm were observed using reflected light microscopy, tested for hardness against metal (knife blade or tweezers), and exposed to dilute, 10%, hydrochloric acid to determine if the particles were carbonate or silicate in nature. With few exceptions such as the fossiliferous chert found in core sample ASR21.25m_S016 the coarser fractions (> 1.0 mm) were disposed of following the mechanical sieve analysis. The fine particle size fractions (≤ 1.0 mm) were preserved for analyses in the Cilas 1180 by collecting the fraction into sealable jars, labeling them, and setting them aside (Figure 4.5).

4.24 Sample Preparation for Particle Size Analysis

Soils often contain organic matter and can contain carbonate or iron oxide coatings that can bind the individual particles together (Gee and Bauder, 1986). Clay sized particles are prone to flocculation (agglomeration) as a result of their higher surface area to volume ratio (McCave et al., 1986; Sperazza et al., 2004). The separation and dispersion of particle aggregates is a key step in PSA (Gee and Bauder, 1986). Chemical and physical means are employed to enhance the separation and dispersion of particle aggregates (Gee and Bauder, 1986). The most appropriate (successful) method to use in promoting the separation and dispersion of the particles is largely dependent on individual soil characteristics (Gee and Bauder, 1986). Different dispersion methods can result in clay contents that can differ by as much as a factor of four or greater (Gee and Bauder, 1986).

Chemical methods can be used to remove organic matter and carbonate or iron oxide coatings. Organic matter can be removed from the soil samples by oxidizing it with 15% H_2O_2 (Beuselinck et al., 1998). The effects of organic matter on grain size distribution have been studied and it was found that for most soils the organic matter present was not significant, had no effect on measurement accuracy or reproducibility, and did not affect grain size distributions (Beuselinck et al., 1998; Blott et al., 2004). It has been suggested that organic matter removal be restricted to sediments like lacustrine mud where the organic content was high (Blott et al., 2004).

Iron oxides can be removed with a bicarbonate buffered solution of sodium dithionite-citrate with an optimum pH of 7.3. Iron oxides should not be removed if they are part of the dominant mineralogy. Carbonate can be removed with a 1 M solution of NaOAC at a pH of 5. Hydrocloric acid is not used for carbonate removal because it can destroy the crystalline lattice of clay minerals (Gee and Bauder, 1986).

Chemical methods are used to disperse flocculated particles, usually clays. Chemical dispersion works by elevating the electro-kinetic (zeta) potential that exists across the interface of all liquids and solids. The most common method of accomplishing this is to saturate the ion exchange complex with sodium using Na-hexametaphosphate (HMP), Na_2PO_7, NaOH, Na_2CO_3, or NaOBr. HMP is the most common dispersing agent used. The amount of chemical dispersing agent needed to fully disperse the flocculated particles is dependent on the type of soil (Gee and Bauder, 1986).

Physical dispersion methods use the turbulent mixing or shearing action of electric mixers, and mechanical shakers to effect particle dispersion. Ultrasonic dispersion uses the transmission of vibrating sound waves to produce microscopic bubbles which collapse and produce cavitations. The energy released by cavitations blasts soil aggregates apart. Ultrasonic dispersion is very effective when used on calcareous and organic soils and soils where clays are significant. Physical and chemical dispersion methods are often used together for maximum effectiveness (Gee and Bauder, 1986).

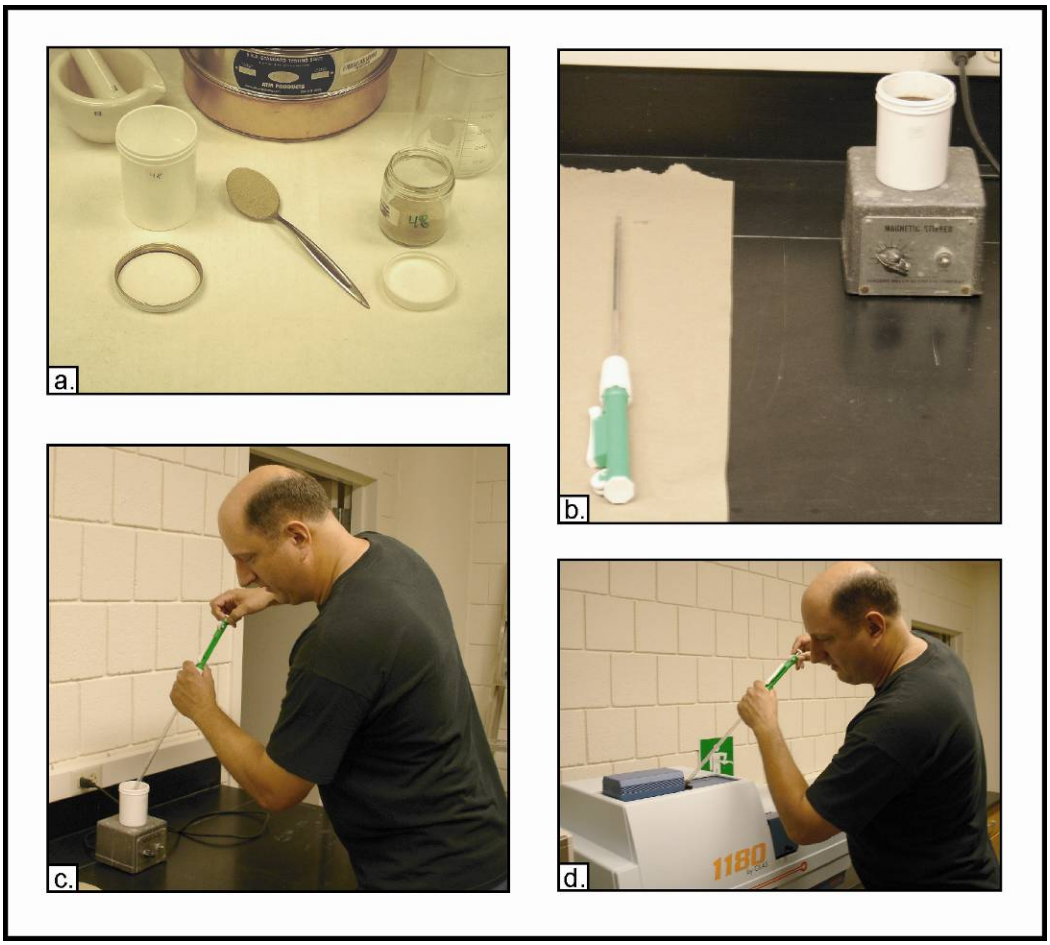

Figure 4.6. Cilas sampling procedure steps (a) Preparing the sample solution for laser diffraction analysis (b) homogenizing the sample solution on magnetic stirrer (c) the author extracting sample in preparation for analysis (d) the author inserting sample into Cilas for analysis.

The organic matter and any carbonates and iron oxides present in the core samples were not chemically removed prior to the PSA. The organic matter content was estimated to be too low to warrant the need for chemical removal. The carbonate component in the core samples was expected to be significant because the parent material for most of the core samples was expected to be dolomite. Although no mineralogical analyses were done on the fine fractions of the core samples, the reddish color present in many of the samples suggested

that iron oxides were present in potentially significant amounts. The carbonate and iron oxide material were not chemically removed from the core samples prior to the PSA in favor of relying on ultrasonic means to accomplish the necessary dispersion.

A solution of liquid Calgon® water softener (sodium hydroxide, 5-10% by weight) and water was prepared as a dispersing agent to assist in the deflocculating of silt and clay sized particles in the fine fractions. Approximately 20 ml of liquid Calgon® was mixed with ~ 150 ml water in a 200 ml sealable jar. This resulted in an initial Calgon® solution of about 0.588 – 1.176% weight by volume. Approximately 10 ml of the initial Calgon® solution was added to ~ 150 ml of water in labeled sealable 200 ml jars. This final Calgon® solution with a concentration of about 0.04 – 0.07% weight by volume was used to chemically disperse the fine particle size fractions. A spoonful (~ 12 ml) of the fine particle size fractions were added to the jars containing the final Calgon® solution (Figure 4.6-a). The jars were sealed, agitated by hand to mix the contents, and set aside to allow the fine particle size fractions to saturate for a minimum of 12 hours. Once the fine particle size fractions had become saturated, the sample jars were moved to the lab containing the Cilas 1180. The sample jars were unsealed one at a time for analysis and placed on a magnetic stirrer (Figure 4.6-b). The fine particle size fraction and Calgon® solutions were agitated for several minutes until their introduction into the Cilas 1180. The mixing action of the magnetic stirrer was used to promote further dispersion of any remaining flocculated particles in the samples and to homogenize the distribution of the

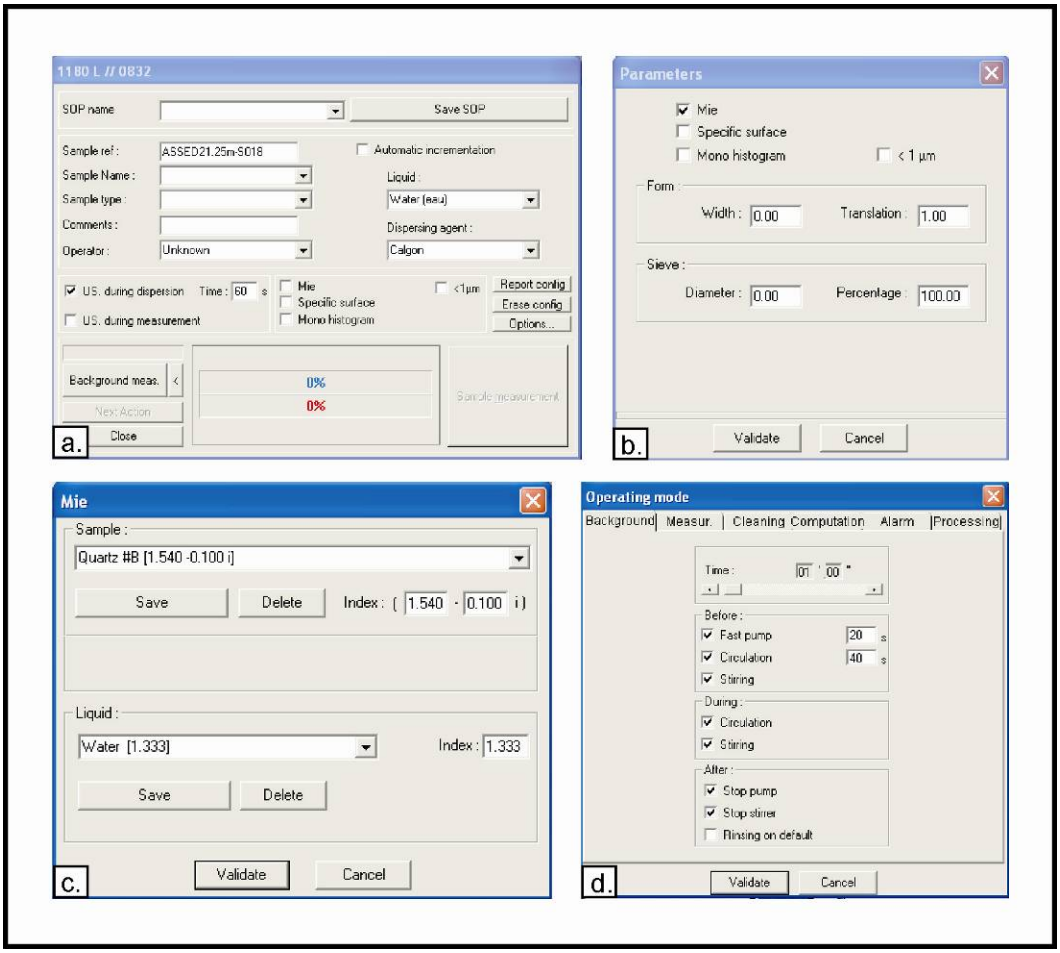

Figure 4.7. Cilas analysis settings (a) ultrasound settings (b) interpretation settings (c) Mie analysis option (d) background settings.

particles in the sample solutions within the sample containers. The magnetic stirrer was set to the same mixing velocity for every core sample to ensure that every sample was dispersed in the same way.

4.25 Cilas 1180 Analysis Procedure

Before samples were run through the Cilas 1180 several basic measurement parameter options had to be set on the machine. The parameter settings regulated ultrasound timing, the method of result interpretation, and the

background, measurement, cleaning, computation, alarm, and processing parameters. The sum of all the instrument settings could be saved as a list of standard operating parameters (SOP).

The ultrasound settings established the time and duration of ultrasound during dispersion and or measurement of the sample material (Figure 4.7-a). Ultrasound was selected to occur for 60 seconds during the dispersion phase of the sample analysis. The use of ultrasound during sample measurement was not chosen.

The result interpretation settings defined the method used to process and display the measurement results such as Mie or specific surface (Figure 4.7-b). The Mie option permitted the use of the Mie solution in place of the Fraunhofer theory for estimating particle size. All of the core samples were analyzed using the Fraunhofer Theory to determine the particle size distribution. Several core samples were also analyzed using the Fraunhofer theory and the Mie solution to compare the results. The refractive indices of quartz #B and water were chosen from the drop down menu for the sample and liquid types used in the Mie analysis (Figure 4.7-c).

Specific surface was the ratio of the total surface area to the weight of the particles. This option could have been used to calculate the measurement results on a specific surface basis in place of the default volume basis. This option required knowledge of the density of the particles. The specific surface option was not used in the analysis.

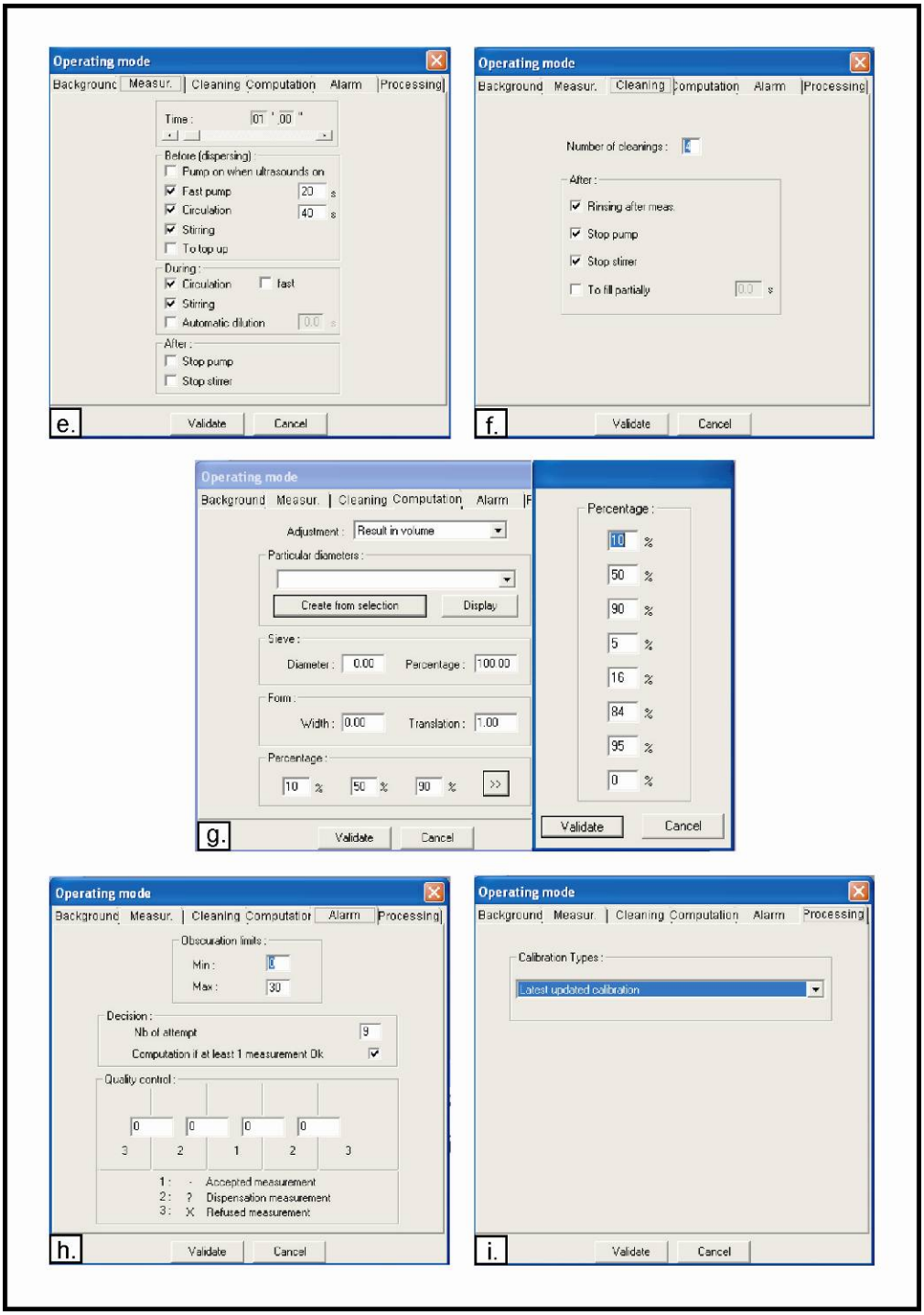

Figure 4.7. Cilas analysis settings (e) measurement settings (f) cleaning parameter settings (g) computation settings (h) alarm settings (i) processing settings.

The background settings established the various timing and activities like pumping, stirring, and circulation that occurred whenever background measurements occurred (Figure 4.7-d). Background measurements established a baseline to account for any noise in the measurement process. Background measurements were taken at the beginning of every analysis session and before new samples were introduced into the machine. Background measurements were set to occur over a period of 60 seconds.

The measurement settings established the various timing and activities like pumping, stirring, and circulation that occurred before, during, and after each measurement cycle (Figure 4.7-e). Parameters were set to pump and circulate water through the system for 60 seconds prior to sample measurements. The sample measurements were set to occur over an additional 60 second period.

The cleaning parameter settings established the number and duration of rinse cycles following the measurement cycles (Figure 4.7-f). The rinse cycles flushed the remaining sample material out of the machine to clear it for the next sample analysis. A series of four sixty second rinse cycles were set to initiate after each measurement cycle.

The computation settings configured the specific parameters used to format the measurement results (Figure 4.7-g). The results were set to display the particle size distribution in a volume basis for the entire range of particle sizes. Particle diameters of 5, 10, 16, 50, 84, 90, and 95% of volume were assigned to be calculated and presented with the measurement results for possible future statistical analyses.

The alarm settings defined the limits of measurement parameters for the acceptance of measurement results. Obscuration, a measurement of the percentage of incoming laser light obscured by the sample material in solution, was set to between 0 and 30% (Figure 4.7-h). The maximum number of attempts to collect valid measurements was set at nine and computations were set to be made if at least one valid measurement was collected. Measurements falling outside of the bounds set by the limits were rejected. A quality control option designed specially for routine analysis was available but not used.

The processing settings permitted the selection of a calibration type if more than one was available (Figure 4.7-i). The calibration type chosen was the latest updated calibration. The latest updated calibration was in February of 2006.

The Cilas 1180 can operate in either a liquid or dry particle mode. The analyses conducted in this study were accomplished using the liquid mode. The Cilas 1180 was put through a series of four 60 second rinse cycles at the start of every analysis session. The rinse cycles ran filtered water through the machine to flush out any material remaining from previous analyses and to exchange the stale water in the system for fresh filtered water.

The core samples were assigned unique sample reference numbers in the Cilas database. The nature of the liquid (water) and the dispersing agent (Calgon®) used during the analyses were entered for the samples. Background measurements were taken at the beginning of each core sample analysis.

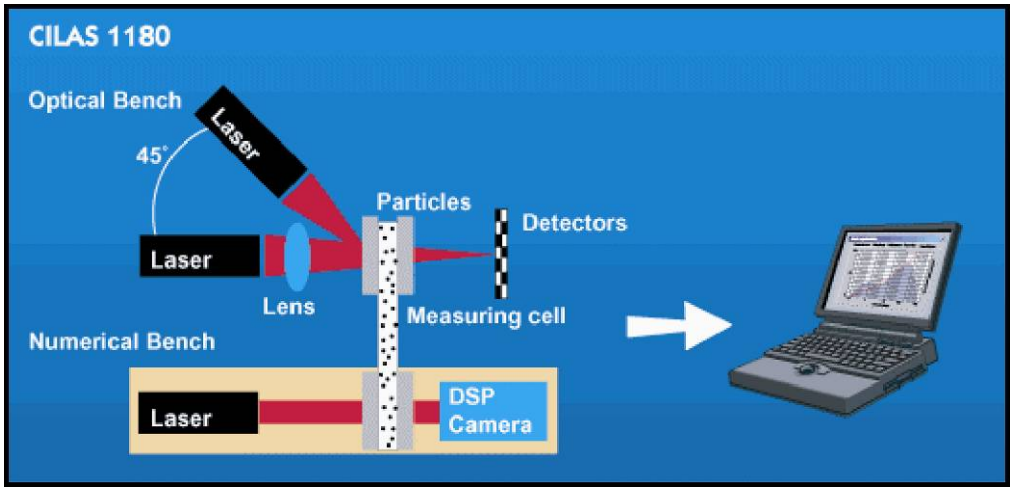

Figure 4.8. Cilas analysis techniques. Image courtesy of www.cilasus.com.

The amount of core sample material required for analysis in the liquid mode was < 5 g. A 10 ml pipette equipped with a fast release pump was used to extract a small amount (1-3 ml) of the homogenized solution from the core sample container on the magnetic stirrer (Figure 4.6-c). The pipette was inserted into the sample container to a measurement depth approximately two thirds of the way into the sample container and about one quarter of the sample container diameter away from the outer edge of the container. The pipette was inserted into the core sample containers in approximately the same location for every analysis. This was done to ensure consistent results for every core sample analysis.

The core samples were introduced into the sample receiving tank on the top of the Cilas 1180 (Figure 4.6-d). The receiving tank contained a mechanical stirrer and integrated ultrasonic dispersion system. The samples were stirred and sonicated in the tank for 60 seconds prior to the actual analysis. The

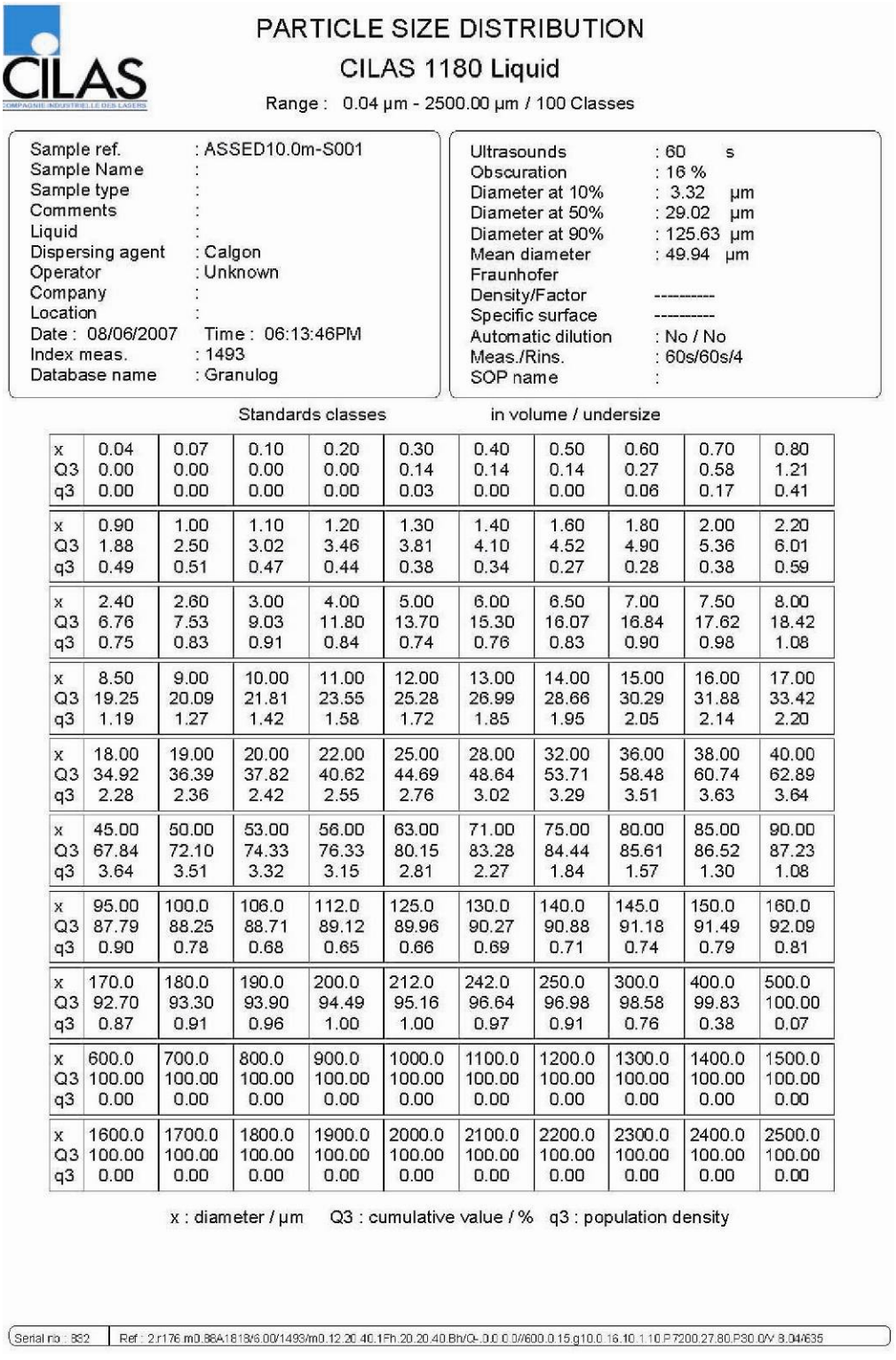

PARTICLE SIZE DISTRIBUTION

CILAS 1180 Liquid

Range : 0.04 µm - 2500.00 µm / 100 Classes

Sample ref.	: ASSED10.0m-S001	Ultrasounds	: 60 s
Sample Name	:	Obscuration	: 16 %
Sample type	:	Diameter at 10%	: 3.32 µm
Comments	:	Diameter at 50%	: 29.02 µm
Liquid	:	Diameter at 90%	: 125.63 µm
Dispersing agent	: Calgon	Mean diameter	: 49.94 µm
Operator	: Unknown	Fraunhofer	
Company	:	Density/Factor	----------
Location	:	Specific surface	----------
Date : 08/06/2007	Time : 06:13:46PM	Automatic dilution	: No / No
Index meas.	: 1493	Meas./Rins.	: 60s/60s/4
Database name	: Granulog	SOP name	:

Standards classes in volume / undersize

x	0.04	0.07	0.10	0.20	0.30	0.40	0.50	0.60	0.70	0.80
Q3	0.00	0.00	0.00	0.00	0.14	0.14	0.14	0.27	0.58	1.21
q3	0.00	0.00	0.00	0.00	0.03	0.00	0.00	0.06	0.17	0.41
x	0.90	1.00	1.10	1.20	1.30	1.40	1.60	1.80	2.00	2.20
Q3	1.88	2.50	3.02	3.46	3.81	4.10	4.52	4.90	5.36	6.01
q3	0.49	0.51	0.47	0.44	0.38	0.34	0.27	0.28	0.38	0.59
x	2.40	2.60	3.00	4.00	5.00	6.00	6.50	7.00	7.50	8.00
Q3	6.76	7.53	9.03	11.80	13.70	15.30	16.07	16.84	17.62	18.42
q3	0.75	0.83	0.91	0.84	0.74	0.76	0.83	0.90	0.98	1.08
x	8.50	9.00	10.00	11.00	12.00	13.00	14.00	15.00	16.00	17.00
Q3	19.25	20.09	21.81	23.55	25.28	26.99	28.66	30.29	31.88	33.42
q3	1.19	1.27	1.42	1.58	1.72	1.85	1.95	2.05	2.14	2.20
x	18.00	19.00	20.00	22.00	25.00	28.00	32.00	36.00	38.00	40.00
Q3	34.92	36.39	37.82	40.62	44.69	48.64	53.71	58.48	60.74	62.89
q3	2.28	2.36	2.42	2.55	2.76	3.02	3.29	3.51	3.63	3.64
x	45.00	50.00	53.00	56.00	63.00	71.00	75.00	80.00	85.00	90.00
Q3	67.84	72.10	74.33	76.33	80.15	83.28	84.44	85.61	86.52	87.23
q3	3.64	3.51	3.32	3.15	2.81	2.27	1.84	1.57	1.30	1.08
x	95.00	100.0	106.0	112.0	125.0	130.0	140.0	145.0	150.0	160.0
Q3	87.79	88.25	88.71	89.12	89.96	90.27	90.88	91.18	91.49	92.09
q3	0.90	0.78	0.68	0.65	0.66	0.69	0.71	0.74	0.79	0.81
x	170.0	180.0	190.0	200.0	212.0	242.0	250.0	300.0	400.0	500.0
Q3	92.70	93.30	93.90	94.49	95.16	96.64	96.98	98.58	99.83	100.00
q3	0.87	0.91	0.96	1.00	1.00	0.97	0.91	0.76	0.38	0.07
x	600.0	700.0	800.0	900.0	1000.0	1100.0	1200.0	1300.0	1400.0	1500.0
Q3	100.00	100.00	100.00	100.00	100.00	100.00	100.00	100.00	100.00	100.00
q3	0.00	0.00	0.00	0.00	0.00	0.00	0.00	0.00	0.00	0.00
x	1600.0	1700.0	1800.0	1900.0	2000.0	2100.0	2200.0	2300.0	2400.0	2500.0
Q3	100.00	100.00	100.00	100.00	100.00	100.00	100.00	100.00	100.00	100.00
q3	0.00	0.00	0.00	0.00	0.00	0.00	0.00	0.00	0.00	0.00

x : diameter / µm Q3 : cumulative value / % q3 : population density

Figure 4.9a. An example of Cilas analysis results in table format.

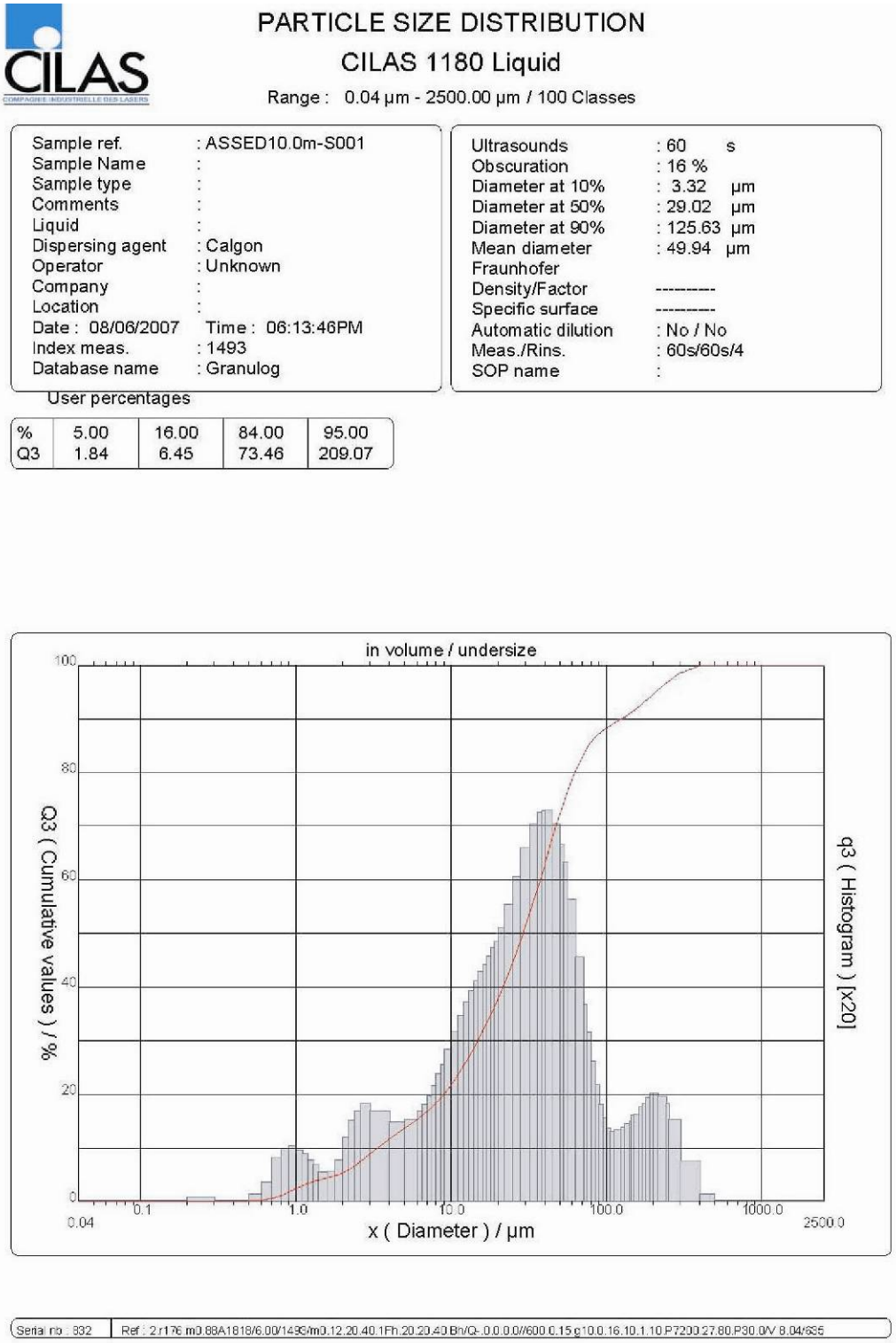

Figure 4.9b. An example of Cilas analysis results in histogram format.

samples were circulated through the analysis process using two peristaltic pumps.

The samples were analyzed using two different techniques (Figure 4.8). In the first technique the fine particles were measured by capturing the diffraction pattern (optical Fourier transform) from the particles using an inverse Fourier lens and custom multi-cell silicon detectors and applying either the Fraunhofer or Mie theory. In the second technique the coarse particles were measured using a real-time fast Fourier transform of an image captured with a CCD (charge-coupled device) camera equipped with a digital signal processing unit (DSP). Three fiber and collimated laser diodes with wavelengths of 635 nm and 830 nm (0.635 μm and 0.830 μm) were used during the analysis. A proprietary algorithmic transformation was used to combine the two datasets and provide a continuous particle size distribution curve. The distribution curve consisted of 100 size fractions on a volume basis over the 0.04 – 2,500 μm operating range of the Cilas 1180.

The measurement results were displayed in table and graphical formats. The table format listed the De Brouckere mean diameter, x [μm], for each particle size fraction, the cumulative curve value, $Q3$ [%], which represents the proportion of the sample with diameter $\leq x$, and the population density, $q3$, for each particle size fraction (Figure 4.9a). The measurement results were displayed in histogram and overlay curve formats. The histograms display the $Q3$ and $q3$ values versus x [μm] diameters for the entire range of particle size fractions using an x20 vertical exaggeration for the q3 values (Figure 4.9b).

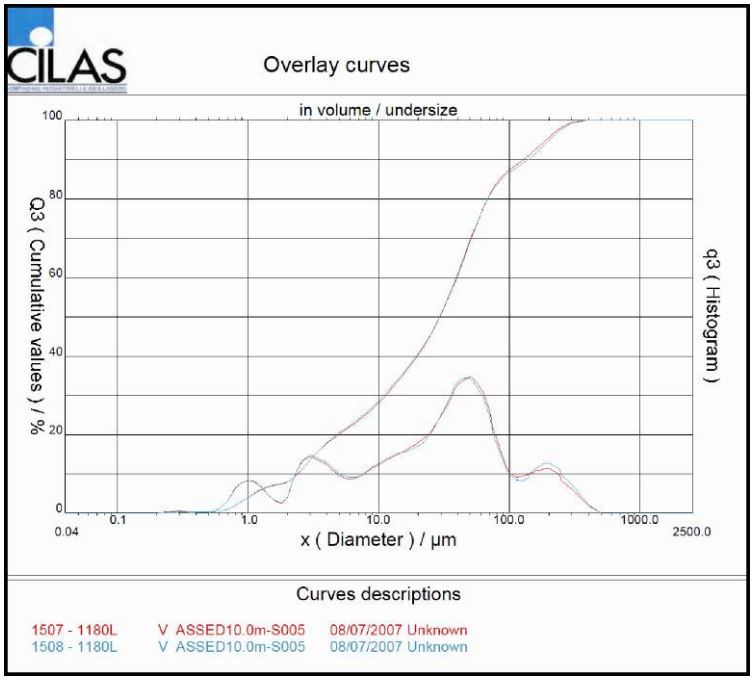

Figure 4.10a. Graphical example of Cilas analysis result repeatability (a) essentially identical results

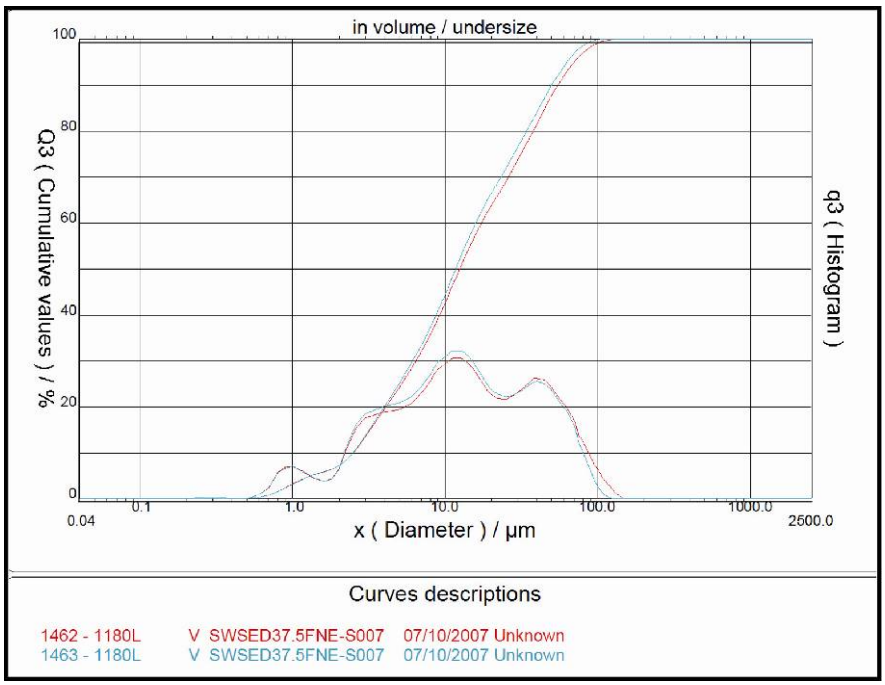

Figure 4.10b. Graphical example of Cilas analysis result repeatability (b) minor differences

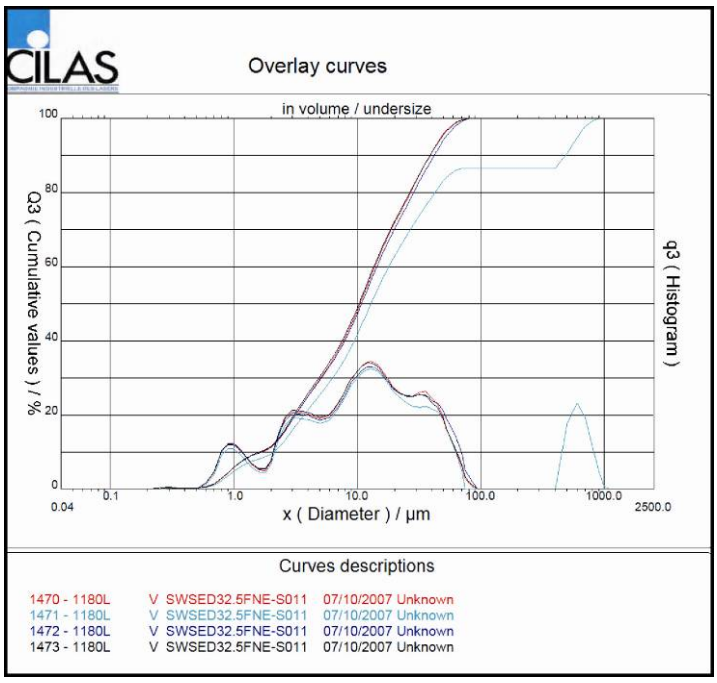

Figure 4.10c. Graphical example of Cilas analysis result repeatability (c) arriving at a consensus.

Each of the core samples were analyzed in the Cilas 1180 at least twice to ensure repeatability of the results. It was realized that differences between analysis results would occur due to minor variations in the distribution of particles in the separate measurements even though they came from the same core sample. Variations in the distribution of particles could be caused by imperfect homogenization of the particles during the mixing process. Extracting volumes of the core sample solution from different locations within the sample container could also effect the resultant particle size distribution.

The Cilas 1180 results for each core sample were compared to determine which of the results best represented the distribution of particles from that core sample. If both results were essentially the same the first of the two results were chosen (Figure 4.10-a). If both results were essentially the same but one

displayed a slightly larger particle diameter maximum then the results with the larger diameter maximum was chosen (Figure 4.10-b). If significant differences existed between the first two analysis results then the sample was analyzed additional times until a consensus could be reached in the results. In this instance the analyses with similar results were compared and the median result from that group was selected (Figure 4.10-c). The selected Cilas 1180 results were combined with the corresponding sieve analysis results to provide a single complete particle size distribution dataset for each core sample which was used for textural analysis and hydraulic conductivity calculations.

4.26 Textural Analysis

The mechanical sieve analysis results for each core sample were converted from a mass to a volume in order to enable the combination of the sieve and Cilas 1180 datasets. The volume of each sieved size fraction ($x > 4.0$ mm, $4.0 \text{ mm} \geq x > 2.0$ mm, $2.0 \text{ mm} \geq x > 1.0$ mm, $1.0 \text{ mm} \geq x$) was determined by dividing the measured mass of the size fraction by an assumed constant particle density of 2.65 g/cm^3. The sieve and Cilas 1180 datasets were combined by dividing the volume of the fine size fraction ($1.0 \text{ mm} \geq x$) determined from the sieve analysis by the sum of the population densities, *q3*, of all the Cilas 1180 size fractions and multiplying the resultant value by the population density of each of the Cilas 1180 size fractions. The volumes of the coarser size fractions ($x > 4.0$ mm, $4.0 \text{ mm} \geq x > 2.0$ mm, $2.0 \text{ mm} \geq x > 1.0$ mm) were then added to the Cilas 1180 results to complete the combined dataset. The

cumulative value, *Q3* [%], for each particle size fraction of the combined dataset was also calculated.

The percentage of clay, silt, sand, and gravel within each core sample was quantified using the combined dataset and applying the USDA soil particle size classification scheme (Figure 4.3). The core samples were then classified texturally by calculating the percentage of clay, silt, and sand without the gravel size component and applying the USDA textural classification scheme (Figure 4.3). The textural modifier "gravelly" was added as a prefix to the textural classification for a core sample when the gravel component was $\geq$ 15 but < 35% of the total core sample volume. The textural modifier "very gravelly" was added as a prefix to the textural classification for a core sample when the gravel component was $\geq$ 35 but < 60% of the total core sample volume. The resulting soil textural classification for each core sample was added to the appropriate core sample description. The textural classifications of the sediment core samples were used to identify the specific soil type sampled by the sediment core.

The 'sa_miads_soils' layer in the Arbuckle-Simpson Hydrology Study GIS dataset was used to identify the soil types present in the area of investigation at each field site. If the 'sa_miads_soils' layer indicated that more than one soil type was present in the area of investigation at a field site then the experimentally derived properties of the sediment core material were compared against the properties of the indicated soil types as defined in the NRCS soils database (Soil Survey Staff, 2005). The soil type in the NRCS soils database

with properties most closely matching the experimentally derived properties of the sediment core material was selected as the soil type sampled by the sediment core at the field site.

4.3 Hydraulic Conductivity Calculations

Hydraulic conductivity, *K* [μm/s], values were estimated for each sediment core location from the concentric cylinder infiltration test results and calculated for each core sample from the sediment core analysis results. Hydraulic conductivity, *K* [μm/s], is a measure of the ability of a permeable medium to allow a fluid, usually water, to flow through it (Fetter, 2001; Weight and Sonderegger, 2001). Hydraulic conductivity, *K* [μm/s], is defined by the equation:

$$K = k(\rho g/\mu) \qquad \text{(Eq. 15)}$$

where, *k* [μm^2], is the intrinsic permeability of the material which is a measure of the ability of the medium to transmit a fluid that is independent of the nature of the fluid, ρg [$g/s^2\mu m^2$], is the specific weight of the fluid and, μ [g/s-μm], is the dynamic viscosity of the fluid.

4.31 Infiltration Hydraulic Conductivity

Saturated hydraulic conductivity was defined as the infiltration rate present when steady state conditions were met. Saturated hydraulic conductivities were estimated from plots of the experimentally derived infiltration rates versus time. If possible, the saturated hydraulic conductivity was estimated directly from the

plotted infiltration experiment results. If steady state conditions were not reached during the infiltration experiments or if the infiltration experiment results displayed erratic changes in the infiltration rate then the saturated hydraulic conductivity was estimated by fitting a power function trend line to the infiltration experiment results. The power function trend line was extrapolated out to a time which was deemed to approximate steady state conditions to determine the rate.

Where erratic changes were observed in the infiltration experiment results which made estimation of the steady state infiltration rate problematic smoothing techniques like moving averages were used on the data to facilitate the estimation of steady state conditions. Extremely erratic data points were removed from the infiltration rate datasets in order to permit the estimation of the steady state infiltration rate. Twenty nine percent of the infiltration test results (six tests) required these smoothing techniques to arrive at an estimation of the steady state infiltration rate. The saturated hydraulic conductivity value for one location at the Arbuckle-Simpson Ranch site (ASR21.25m) could not be determined from the infiltration experiment results.

4.32 Sediment Core Hydraulic Conductivity

All hydraulic conductivity calculations were made assuming that the fluid involved was fresh water and that the temperature and pressure conditions were constant at 20°C and 1 ATM. The density, ρ [g/μm^3], of fresh water at 20°C and 1 ATM is 9.982*10^{-13} g/μm^3 (Fetter, 2001). The acceleration due to gravity, g [μm/s^2], is 9.80*10^6 μm/s^2 (Reynolds, 1997). The specific weight, ρg [g/s^2μm^2], of

fresh water at 20°C and 1 ATM is then equal to $9.782*10^{-6}$ g/s^{2}μm^2. The dynamic viscosity, μ [g/s-μm], of fresh water at 20°C and 1 ATM is $1.005*10^{-6}$ g/s-μm (Fetter, 2001). A micrometer per second [μm/s] was selected as the standard unit of measurement for the hydraulic conductivity calculations to facilitate comparison with the properties of the soils present at the field sites as reported in the NRCS soils dataset. Micrometers were also used as the units of length reported in the Cilas 1180 particle size analyses.

The hydraulic conductivity values calculated for the core samples were arrived at using the Carmen-Kozeny (Bear, 1988, c1972; Charbeneau, 2000) and Fair-Hatch (Todd, 1959; Charbeneau, 2000) methods. Both methods use expressions resulting from independent attempts at deriving Darcy's Law from elemental fluid mechanics equations (Charbeneau, 2000). Each method calculates values for intrinsic permeability, k [μm^2], by expressing the relationships between intrinsic permeability, k [μm^2], and the various material properties that exert a measure of control over fluid flow through a medium including porosity and grain size distribution, packing, and shape (Charbeneau, 2000).

The Carmen-Kozeny equation calculates the intrinsic permeability using the equation:

$$k = [\Phi^3/ (1 - \Phi)^2]*[d_e^2/ 180] \qquad \text{(Eq. 16)}$$

where Φ is the total porosity of the material, d_e is the effective grain size, and 180 is a shape coefficient. The effective grain size used for this study was defined as d_{10} [μm] which is the size fraction that is 10% finer by mass (Weight and

Sonderegger, 2001; Fetter, 2001). The effective grain size, *d10* [μm], was calculated for each core sample from the complete particle size analysis results through linear interpolation using the equation

$$d_{10} = X1 + (((X2 - X1)*(10.0 - Y1))/ (Y2 - Y1)) \qquad \text{(Eq. 17)}$$

The calculated effective grain size, *d10* [μm], for each core sample was also used to observe trends in grain size distribution within each sediment core and between sediment cores at each field site.

The Fair-Hatch equation calculates the intrinsic permeability using the equation

$$k = 1/ [m*((1 - \Phi)^2/ \Phi^3)*((\theta/ 100)*\Sigma(P/ dm))^2] \qquad \text{(Eq. 18)}$$

where Φ is the total porosity of the material, *m* is a dimensionless packing factor experimentally determined to be about 5.0 (Todd, 1959), θ is a dimensionless shape factor that varies between 6.0 for spherical grains and 7.7 for angular grains (Todd, 1959), *P* is the percentage of particles between adjacent size fractions, and *dm* is the geometric mean of rated sizes of adjacent size fractions. All grains were assumed spherical for the calculations thus the value of the shape factor was set at 6.0.

The value for Σ(P/ dm) for each core sample was calculated from the complete particle size analysis results. The percentage of particles between adjacent size fractions, *P*, was calculated by dividing the population density *q3* of each size fraction by the sum of all the population densities in the dataset and multiplying the quotient by 100. The geometric mean of rated sizes of adjacent

grain size fractions was calculated using the “GEOMEAN” function in Excel for each pair of adjacent grain size fractions.

Hydraulic conductivity values calculated for each core sample using the Carmen-Kozeny and Fair-Hatch methods were compared individually and collectively to determine trends. The Calculated hydraulic conductivity values from core samples taken from near the surface were compared to the estimated hydraulic conductivity values derived from the infiltration experiments. The hydraulic conductivity values empirically calculated from the sediment core analysis do not have any directional orientation and thus can not be used to say anything specific about vertical anisotropy in the sediments above the epikarst zone.

The results from all of the datasets described in this chapter were compiled for a detailed side by side analysis. The compiled datasets were used to determine if any relationships could be observed between datasets at a field site or between field sites. Special attention was taken to discern any possible relationship between the physical (water content, porosity, effective grain size, and hydraulic conductivity) of the core samples and the corresponding electrical (Resistivity) properties.

CHAPTER V

RESULTS

This chapter presents the results of the field work and subsequent laboratory analyses of the data collected. The results of the field work (static water level measurements, electrical resistivity imaging, direct push electrical conductivity logging and sediment coring, and infiltration experiments) accomplished are presented first. The results of the laboratory analyses of the sediment cores (core description, particle size distribution, porosity, and water content) are presented next. Hydraulic conductivity calculation results are presented at the end. A compilation of the results from all of the methods at each location was constructed to facilitate side by side comparisons of the data (APPENDIX). All the data is available in electronic format.

5.1 Static Water Level Measurements

The depth to static water level measurements were collected from wells at the Hatch and Spears Ranch field sites (Table 1). A static water level measurement was collected from the well at the Hatch site on September 6, 2006. The elevation of the static water level was measured as 1,055 feet (depth of 79.8 ft). No static water level measurement was collected from the Hatch well

Table 1. Static waterlevel measurements.

Location	Hatch Site Well
Date of Measurement	September 6, 2006
Elevation of Land Surface	~1135.00 ft
Top of Casing (TOC) Stick Up	0.79 ft
Depth to Water from TOC	80.54 ft
Elevation of Static Water Level at Well	1055.25 ft
Land surface elevation estimated from USGS “Fittstown, OK” quadrangle map	
Location	Spears Ranch Site Well (SW1)
Date of Measurement	June 11, 2007
Elevation of Land Surface	1010.61 ft
Top of Casing (TOC) Stick Up	0.31 ft
Depth to Water from TOC	25.75 ft
Elevation of Static Water Level at Well	985.17 ft
Land surface elevation from differential GPS data	
Location	Arbuckle-Simpson Ranch Site
Date of Observation	July 28, 2007
Elevation of water surface in the pond on the site	~999 ft
Water surface elevation estimated from USGS “Connerville, OK” quadrangle map	

in March, 2007. The total depth of the well measured by the OWRB was 201 feet. No information was found that indicated the depth to which the surface casing extended. The land surface elevation at the Hatch site well was estimated from the USGS “Fittstown, OK” quadrangle map.

A static water level measurement was collected from the Spears well #1 on June 11, 2007. The elevation of the static water level in the well was measured as 985 feet (depth of 25.4 ft). The surface water elevation of the Blue River was measured in the same time period using a pressure transducer in the river at the site as at an elevation of 974 feet. The total depth of the Spears well # 1 was logged as 628 ft and the surface casing extends to a depth of 80 ft. The

Table 2. Electrical resistivity imaging results summary.

Field Site	Filename	Electrode Spacing [ft (m)]	Survey Length (ft)	Common Electrodes			Data in Inversion (%)	RMS Error (%)
Hatch	HWN05MA1	16.4 (5.00)	902.3		28		92.9	4.04
	HWN02MA1	8.2 (2.50)	451.2	1	28		95.5	4.40
	HWN02MA2	8.2 (2.50)	451.2	1	28		94.4	2.74
	HWN01MA1	4.1 (1.25)	225.6	1	55	56	95.3	4.16
	HWN01MB1	4.1 (1.25)	225.6		28	29	94.8	4.46
	HWN01MC1	4.1 (1.25)	225.6			1	94.8	4.65
Spears Ranch	SW2.50A1	8.2 (2.50)	451.1	1	15		94.2	2.49
	SW1.25A1	4.1 (1.25)	110.7	1			97.7	3.60
	SW1.25A2	4.1 (1.25)	110.7		1	28	98.8	3.42
	SW1.25B1	4.1 (1.25)	225.6		1	28	93.9	3.64
	SW1.25C1	4.1 (1.25)	225.6			1	99.6	2.61
Arbuckle-Simpson Ranch	AS1.25C1	4.1 (1.25)	225.6	1	29	53	87.8	2.73
	ASR5.00B	16.4 (5.00)	902.2	22	29	35	91.3	2.57
						Minimum	**87.8**	**2.49**
						Maximum	**99.6**	**4.65**
						Average	**94.7**	**3.50**

land surface elevation at the Spears Ranch site well #1 was taken from differential GPS data

No well was available for a static water level measurement at the Arbuckle-Simpson Ranch site. The static water level for the Arbuckle-Simpson Ranch site was estimated from the water surface elevation of the pond located on the site (Table 1). The water surface elevation of the pond was estimated from the USGS “Connerville, OK” quadrangle map.

The approximate elevation of the static water level was plotted as a line on the electrical resistivity imaging results for each field site to determine if the

Table 3. ERI data quality criteria

ERI data not meeting these criteria were removed from the datasets prior to inversion	
Minimum Voltage	≥ 0.1 mV
Minimum Absolute (V/I)	≥ 1E-6 (ohm)
Maximum Repeat Error	≤ 2%
Minimum Apparent Resistivity	≥ 0.01 (ohm-m)
Maximum Apparent Resistivity	≤ 100,000 (ohm-m)

transition from unsaturated to saturated conditions could be determined from plotted static water levels were also used to determine if any relationships could be discerned between the phreatic zone and the approximate average depth to the bottom of the epikarst zone as determined from the ERI images. The observed effects of the static water level on the electrical resistivity results are presented in the following electrical resistivity imaging section.

5.2 Surface Electrical Resistivity Imaging

Electrical resistivity data were collected from the field sites during thirteen surface ERI surveys. The ERI surveys were conducted at different scales using a 16.4, 8.2, or 4.1 foot (5.0, 2.5, or 1.25 meter) electrode spacing. Smaller scale ERI surveys were nested within the same space as the larger scale ERI surveys unless noted otherwise. The nested ERI surveys were linked together in space through the use of common electrode locations (Table 2).

The ERI data collected at the field sites are of good quality. The inversions of the data had low root mean squared (RMS) errors of between 2.49

and 4.65%. Between 87.8 and 99.6% of the data were used in the inversions (Table 2). The remaining data did not meet the initial data quality criteria for inversion (Table 3) or were noisy data (> 50% data misfit) that were trimmed from the dataset during the inversion process. The data not meeting the initial quality criteria for inversion accounted for 0.4 – 11.0% of the total data. The noisy data that were trimmed from the inversions accounted for 0.0 – 2.0% of the total data.

The images generated from the ERI data show electrical resistivity values that range between 3.0 and 7,300 ohm-m. In general the electrical resistivity values in the ERI images are observed to increase with depth. The ERI data collected at different scales at each field site display similar features. The electrical resistivity value ranges and the features observed in the ERI images from each field site were very different. The degree of variability in the observed electrical properties of the subsurface materials between the field sites would make a comparison between the field sites on the basis of electrical properties difficult.

Six ERI surveys were conducted at the Hatch site at a variety of scales (Table 2). The Hatch site ERI surveys were conducted along a north-south line (Figure 1.5). Five of the Hatch site ERI surveys were conducted during the September, 2006 trip (Figure 5.1). The sixth Hatch site ERI survey (HWN02MA2) was conducted during the March, 2007 trip over the same space as ERI survey HWN02MA1 (Figure 5.2). The sixth ERI survey was required in order to have surface electrical resistivity data that reflected conditions within the subsurface at the time that the direct push and infiltration experiment methods

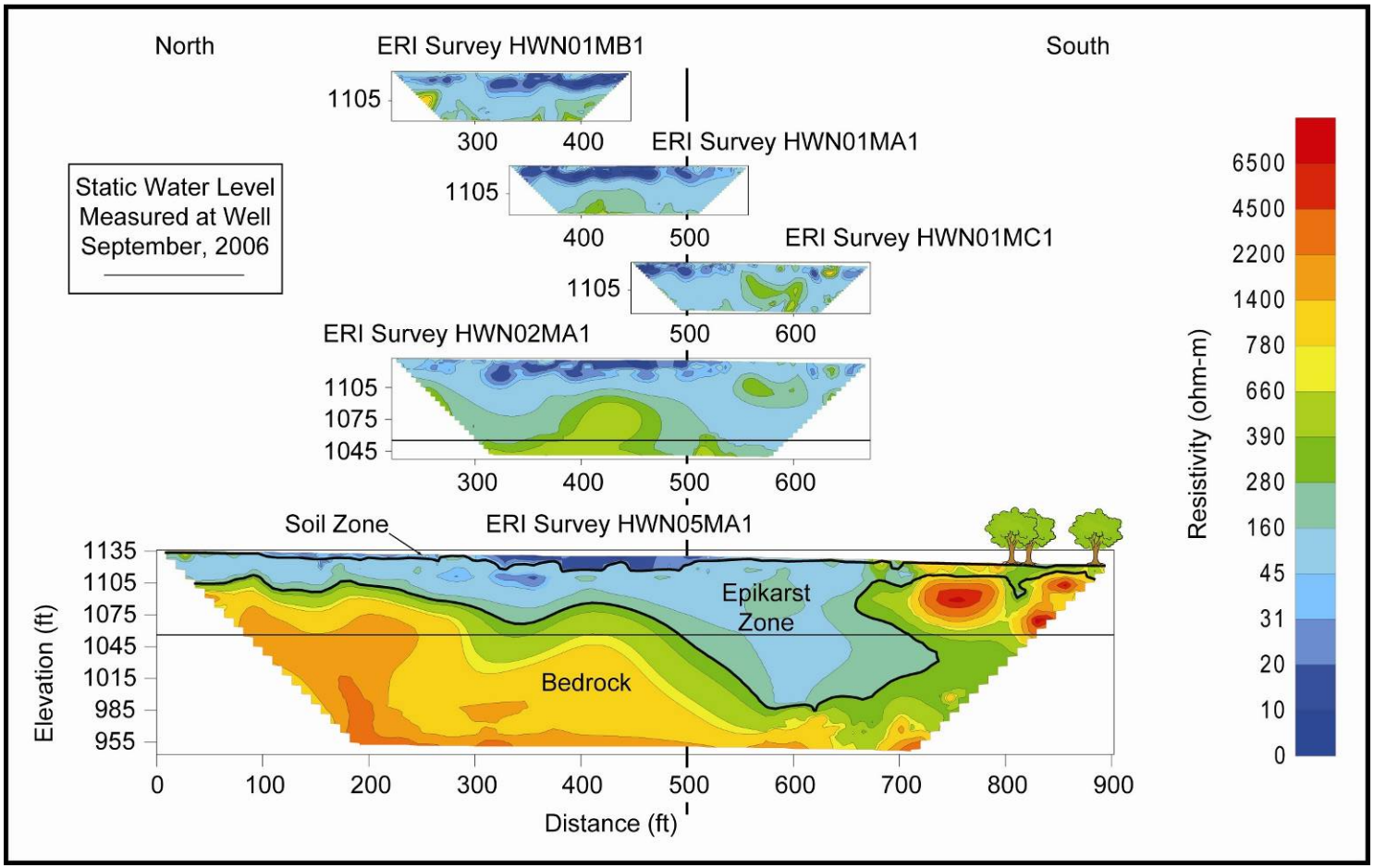

Figure 5.1. Hatch site ERI results; all ERI data images are aligned horizontally in space and to scale.

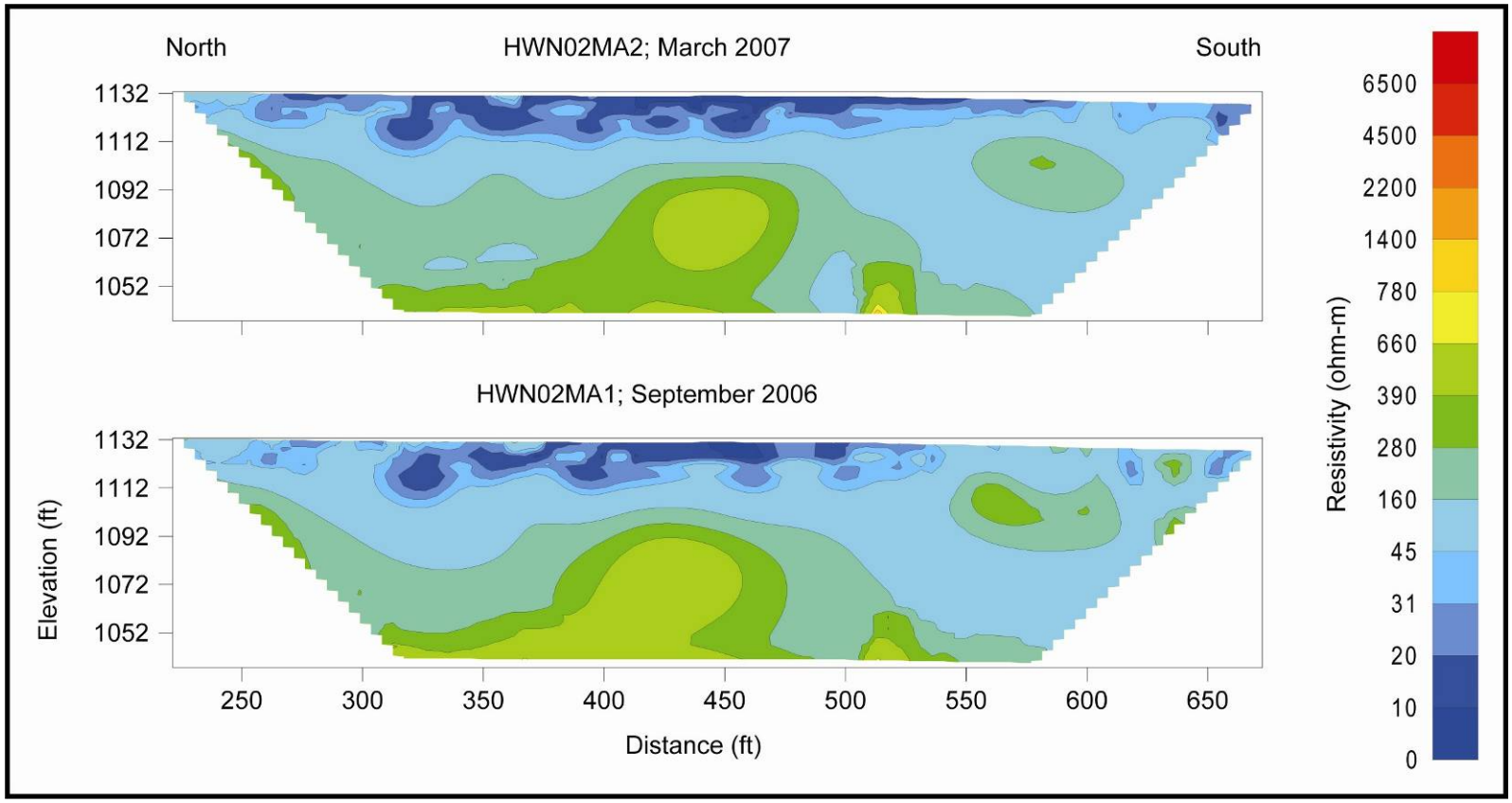

Figure 5.2. Hatch site ERI results; ERI data images from the same location at different times. All ERI data images are aligned horizontally in space and to scale

were employed. The sixth ERI survey was also used to observe changes in the electrical properties of the subsurface materials over the seven month time period between the trips to the site.

ERI survey HWN05MA1 conducted using 16.4 foot (5.0 meter) electrode spacing was the largest scale ERI survey completed at the Hatch site (Figure 5.1). ERI surveys HWN02MA1 and 2 were conducted using 8.2 foot (2.5 meter) electrode spacing and the ERI surveys HWN01MA1 – C1 were conducted using 4.1 foot (1.25 meter) electrode spacing (Table 2). The smaller scale ERI survey locations were nested within the space of the larger scale HWN05MA1 ERI survey. The total observed range of electrical resistivity values from all of the Hatch site ERI surveys was from 3.1 to 7,300 ohm-m).

A laterally extensive resistive feature (> 280 ohm-m) is observed in the HWN05MA1 ERI image below an elevation of ~ 1,100 feet (depth of ~ 40 feet) at the north end of the image. The resistive feature continues to the southern end of the image and appears to dip into the subsurface to the south at an apparent dip angle of approximately 15 degrees. Another resistive (> 280 ohm-m) feature can be seen close to the land surface in the southern end of the image. This resistive feature also appears to dip into the subsurface at the same orientation. The geologic map of the area from Circular 91 (Fairchild et al., 1990) indicates horizontal beds at a location just north of the field site (Figure 1.3). A more conductive feature (< 280 ohm-m) appears to separate the two resistive features at depth. Electrical resistivity values in the more conductive feature appear to

remain relatively conductive (< 160 ohm-m) to an elevation of ~ 990 feet (depth of ~ 139 feet) at a distance of between 575 and 675 feet along the line.

The observed electrical resistivity values near the surface are generally more conductive (< 280 ohm-m) down to an average elevation of about 1,080 (average depth of about 53 ft) except at a distance of about 700 ft along the line where electrical resistivity values rise to >1,000 ohm-m at or near the surface (Figure 5.1). The smaller scale HWN01MA-C1 ERI images show that the electrical properties are highly variable and relatively conductive with electrical resistivity values that are generally less than 280 ohm-m throughout. The thickness of the observed shallow conductive zone appears to vary considerably across the site. No clear relationship appears to exist between the measured static water level elevation obtained from the Hatch well (Table 1) and any observed features in the northern 700 feet of the electrical resistivity data from the Hatch field site (Figure 5.1). The measured static water level correlates well with the bottom of the shallow resistive feature observed at a distance of between 700 and 800 feet along the ERI line.

The images for ERI surveys HWN02MA1 and 2 display changes in the electrical properties of the subsurface that occurred at the site between September, 2006 and March, 2007(Figure 5.2). The HWN02MA1 (September, 2006) and HWN02MA2 (March, 2007) ERI images display similar electrical resistivity value ranges and show similar features throughout. Below an average elevation of about 1,080 (average depth of about 53 ft) the image from September, 2006 shows features that are, in general, slightly more resistive and

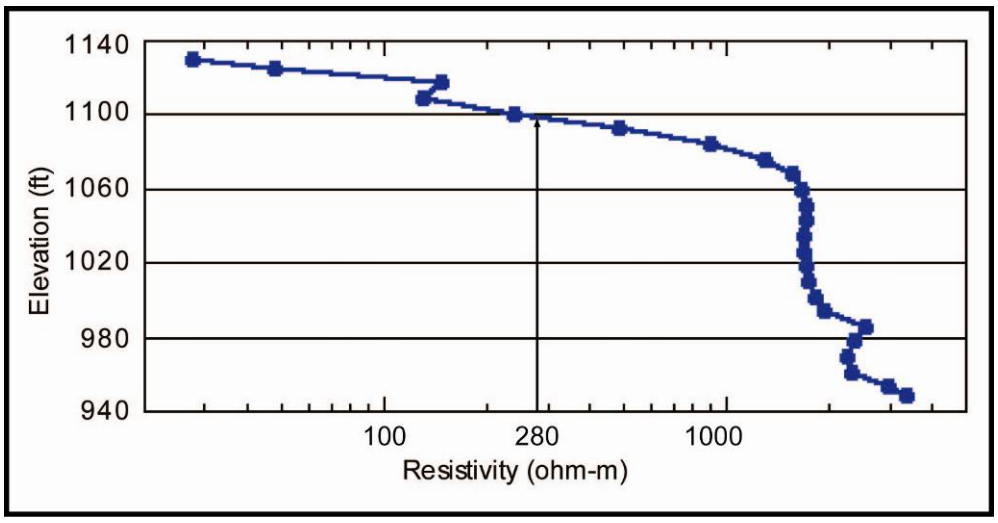

Figure 5.3. An example of a one dimensional electrical resistivity versus depth profile taken from the HWN05MA1 ERI data at the distance of 200 feet along the ERI line

less variable than in March, 2007. Features observed in the September 2006 ERI image above an average elevation of about 1,080 (average depth of about 53 ft) show slightly higher electrical resistivity values and a slightly higher degree of variability.

The weathered rocks of the epikarst zone were expected to be significantly more conductive than the underlying competent bedrock. The gradational shift from weathered to competent rock was expected to be reflected in the electrical properties of the rocks. Vertical one dimensional (1-D) profiles of electrical resistivity versus depth were constructed to determine the electrical resistivity value at each site that most closely marked the approximate transition from weathered to competent rock. The contour line corresponding to the electrical resistivity value at the transition also marked a reasonable depth for the boundary at the base of the epikarst. Figure 5.3 shows an example of a 1-D

electrical resistivity versus elevation (depth) profile that was taken from the HWN05MA1 ERI data at the distance of 200 feet along the ERI line. The apparent gradational zone between the weathered conductive material near the surface and the competent resistive material at depth is clear in the 1-D profile. The electrical resistivity value at the point approximately 1/3 the distance along the apparent gradational zone was selected as an estimate of the value that corresponded the transition from weathered to competent rock at the base of the epikarst zone. The contour line corresponding to the 280 ohm-m electrical resistivity value was selected as the possible location of the transitional boundary at the Hatch site (Figure 5.3). The drilling of the soil zone down to competent bedrock at one or more points along the ERI profile would be necessary to more clearly define the electrical properties that marked the transition at the base of the epikarst zone. The 280 ohm-m contour is generally above the elevation of the measured static water level except in the deep conductive zone between the distance of about 575 and 675 feet.

The soil zone was expected to be on average more conductive than the epikarst zone at each site. A method similar to the one used for determining the base of the epikarst zone was used in conjunction with the direct push results to determine the approximate electrical resistivity value contour bounding the soil zone at each site. The approximate electrical resistivity value contour bounding the soil zone at the Hatch site was determined to be about 45 ohm-m (Figure 5.3).

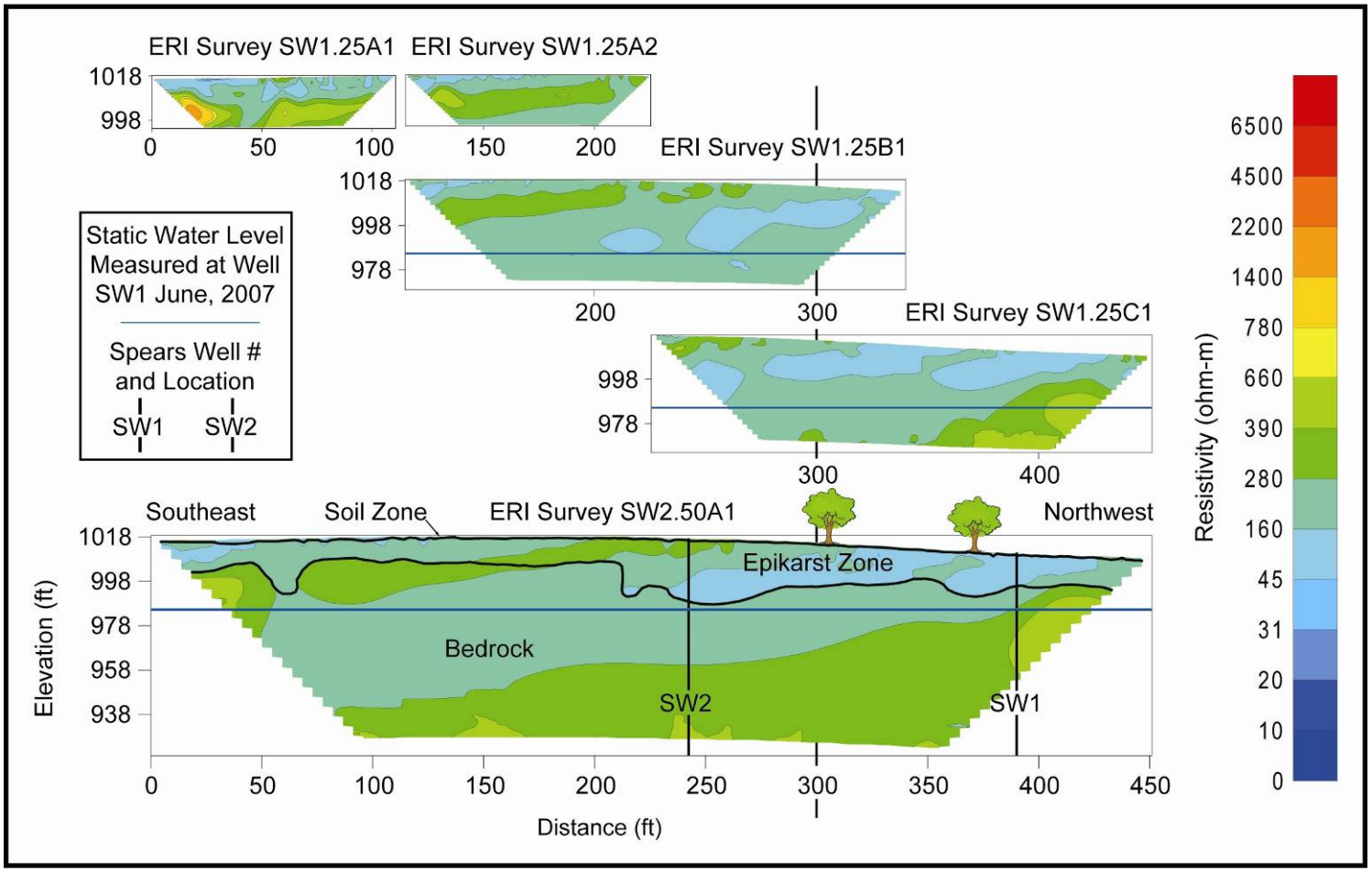

Figure 5.4. Spears Ranch site ERI results; all ERI data images are aligned horizontally in space and to scale.

Five ERI surveys were conducted at the Spears Ranch site at a variety of scales (Table 2). The Spears Ranch site ERI surveys were conducted along a line with a compass orientation of 315 degrees (Figure 1.7). The Spears Ranch site had the smallest total range of electrical resistivity values (19 to 1,900 ohm-m) of all of the field sites (Figure 5.4).

ERI survey SW2.50A1 conducted using 8.2 foot (2.5 meter) electrode spacing (Table 2) was the largest scale ERI survey completed at the Spears Ranch site (Figure 5.4). ERI surveys SW1.25A1, A2, B1, and C1 were conducted using 4.1 foot (1.25 meter) electrode spacing (Table 2). ERI surveys SW1.25A1 and A2 were conducted using an array of 28 electrodes instead of the full set of 56 electrodes resulting in the collection of electrical resistivity data over a much smaller area for those surveys. The smaller scale ERI survey locations were nested within the space of the larger scale SW2.50A1 ERI survey (Figure 5.4).

In general the observed electrical resistivity values in the ERI images from the Spears Ranch site appear to display an apparent pattern of layering with alternating conductive and resistive zones (Figure 5.4). The apparent layering dips to the southeast with an apparent dip angle of approximately 8.5 degrees. The geologic map of the area from Circular 91 (Fairchild et al., 1990) indicates that the dip angles of beds in the vicinity of the field site varies from horizontal to 14° and generally have an easterly component to the dip directions (Figure 1.6).

In general the observed electrical resistivity values appear more conductive (< 280 ohm-m) at or near the surface down to an average elevation of

about 1,001 feet (average depth of about 17 ft) (Figure 5.4). The observed electrical variability in the upper ~17 feet of the ERI images also appears to be more significant than the variability at depths below ~17 feet. The observed shallow conductive zone appears to be somewhat variable in thickness across the site.

The 280 ohm-m contour line was selected as the possible location of the transitional boundary between the epikarst and the bedrock at the Spears Ranch site (Figure 5.4). The cuttings recovered from the drilling of the Spears wells #1 and #2 could possibly be used to better define the approximate depth to the base of the epikarst zone. The 160 ohm-m contour line was selected as the approximate base of the soil zone at the Spears Ranch site (Figure 5.4). The soil zone was not well defined by the electrical properties and was largely interpreted from the direct push results.

The measured static water level obtained from the Spears well #1 (Table 1) appears to correlate reasonably well with features observed in the electrical resistivity data. A relatively conductive feature observed to dip into the subsurface at a distance of between 250 and 400 feet along the ERI survey line appears to terminate at a depth close to the measured static water level (Figure 5.4). The measured static water level is observed to be below the 280 ohm-m contour line.

Two ERI surveys (ASR5.00B and AS1.25C1) were conducted at the Arbuckle-Simpson Ranch site at different scales (Table 2). The two ERI surveys were conducted in the same location and orientation but at different times. The

ERI surveys were conducted along a line with a compass orientation of 316 degrees (Figure 1.8). ERI survey AS1.25C1 was conducted in July of 2007 and ERI survey ASR5.00B was conducted in February of 2008.

Changes in the electrical properties of the subsurface were expected to have occurred in the time between July 2007 and February 2008 due to seasonal variations in moisture content. The water surface level in the pond was lower in February 2008 than in July 2007 which would indicate the possibility of drier conditions in the shallow subsurface at the site. In general, drier conditions in the shallow subsurface would result in higher electrical resistivity values than when conditions were moister. Because the conditions in the ground in February 2008 were expected to be different than in July 2007 when the direct push EC and sediment core data were collected the ASR5.00B ERI data were not used in the comparative electrical and hydraulic property analyses.

ERI survey ASR5.00B conducted using 16.4 foot (5.0 meter) electrode spacing (Table 2). ERI survey AS1.25C1 was conducted using 4.1 foot (1.25 meter) electrode spacing. The smaller scale ERI survey location was nested within the space of the larger scale ERI survey (Figure 5.5). The two ERI surveys were linked together using common electrode locations which were determined from the existing borehole locations. The total observed range of electrical resistivity values at the Arbuckle-Simpson Ranch site was 3.0 to 3,500 ohm-m.

The observed electrical resistivity values near the surface in the ASR5.00B ERI survey (Figure 5.5) are relatively conductive (< 280 ohm-m) and

laterally continuous down to an average elevation of about 975 feet (average depth of about 29 feet) across the ERI image. The thickness of the observed shallow conductive zone appears to vary across the site. A laterally extensive resistive feature (> 280 ohm-m) is observed below the average elevation of about 980 feet (average depth of about 29 feet) in the southeastern 650 feet of the ERI data. A vertical conductive feature (< 160 ohm-m) is observed in the ERI data from the distance of about 650 feet along the line to the northwestern end of the ERI image. The vertical conductive feature appears to extend from the surface to the bottom of the ERI image. A resistive (> 700 ohm-m) feature is also observed at the northwestern edge of the ERI image near the surface.

The apparent resistive zone at depth appears to be sub-horizontal in orientation across the ERI image (Figure 5.5). The geologic map of the area from Circular 91 (Fairchild et al., 1990) indicates that the dip of beds in the vicinity of the field site is variable and ranges between approximately 20° SW and 6° NNE (Figure 1.6). The observed sub-horizontal and generally continuous nature of the top and bottom of the more resistive zone can not be used to infer an apparent dip angle for the beds because the relationship between the orientation of the ERI data and the strike of the beds is unknown.

The vertical conductive feature (<160 ohm-m) feature observed at the distance of about 650 feet along the ERI line appears to coincide fairly well with the approximate location of an inferred fault mapped in the literature as crossing the location (Fairchild et al. 1990) (Figure 1.6). The horizontal contrast observed

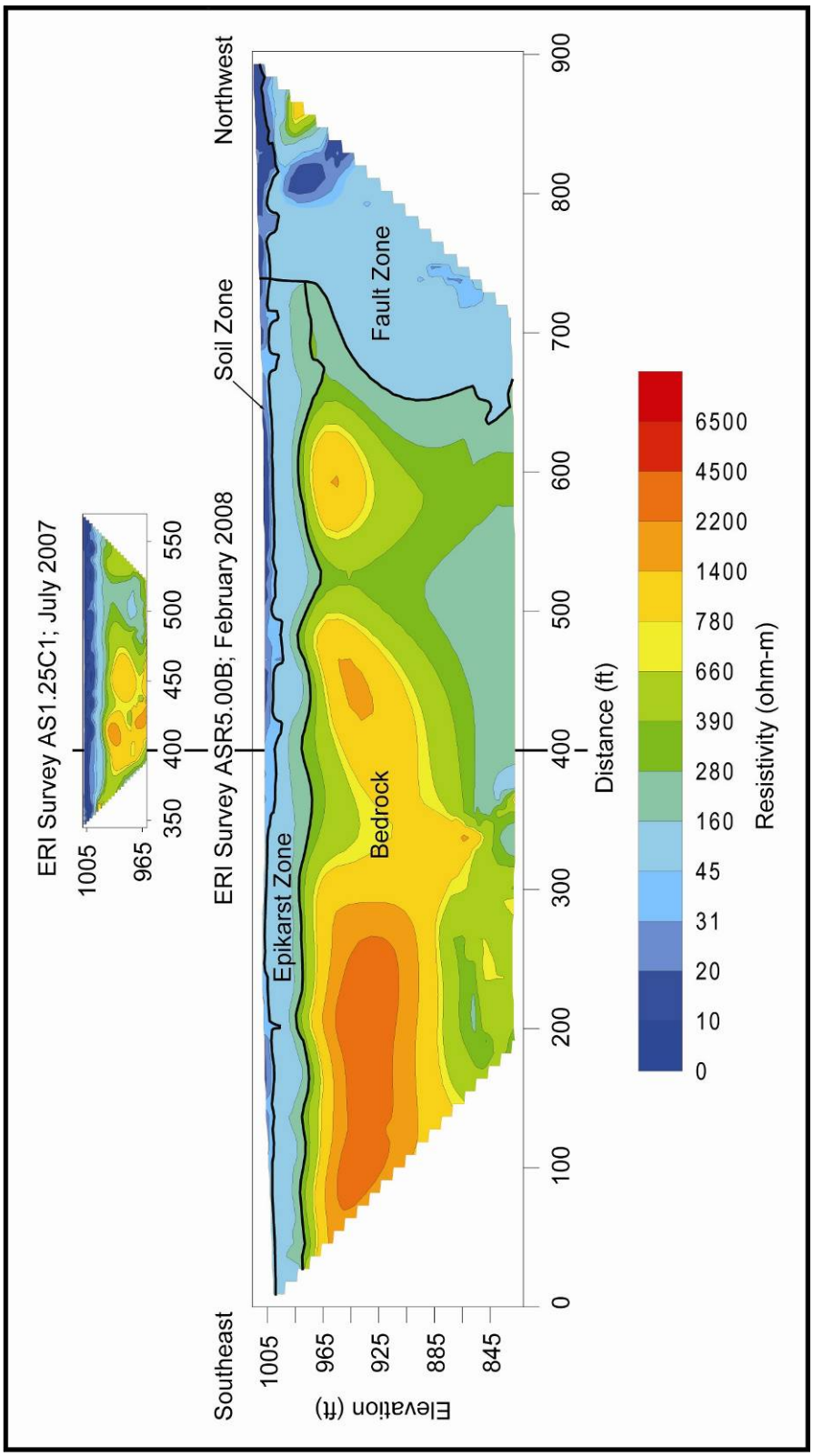

Figure 5.5. Arbuckle-Simpson Ranch site ERI results. All ERI data images are aligned horizontally in space and to scale.

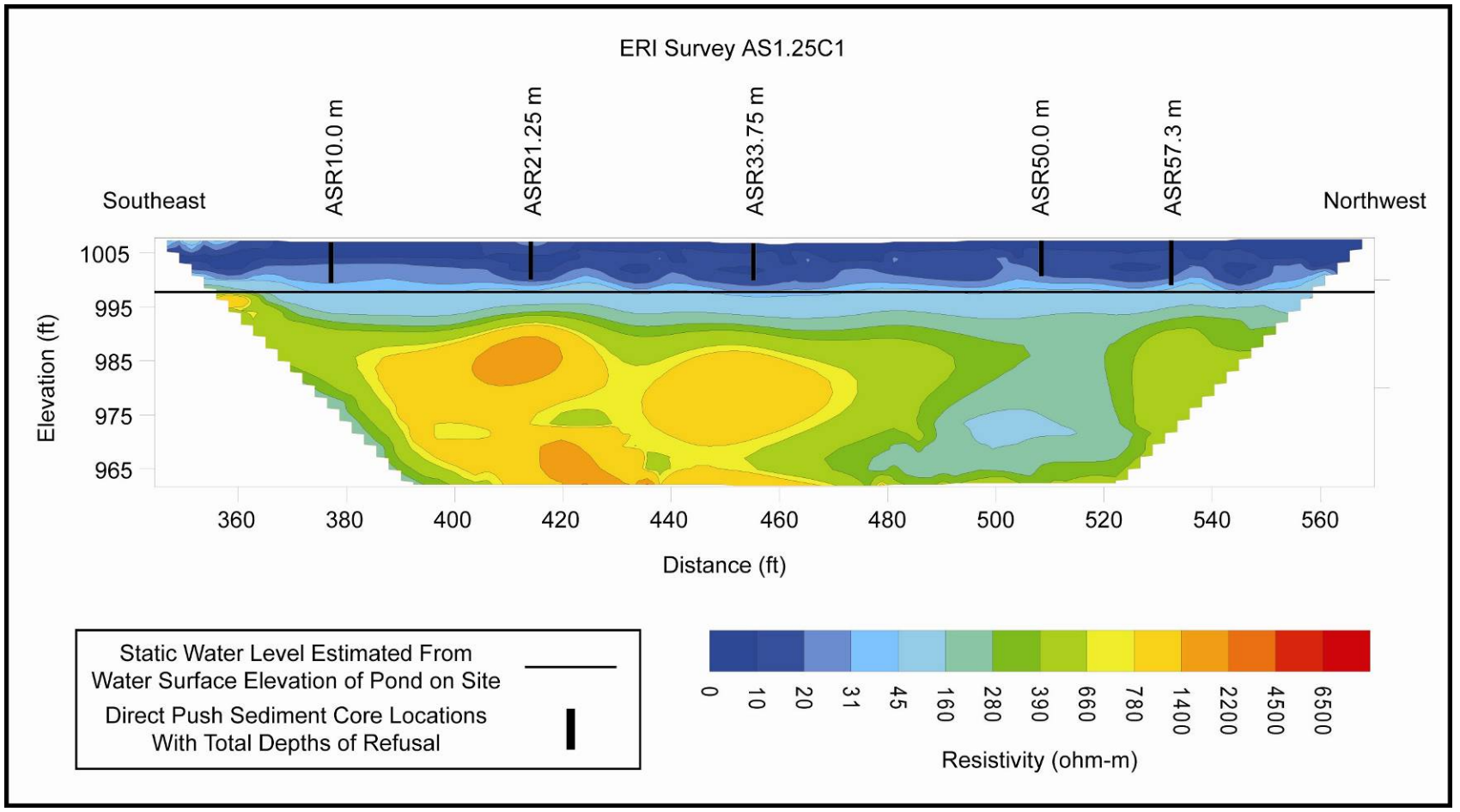

Figure 5.6. Arbuckle-Simpson Ranch site ERI results. Detail of AS1.25C1 ERI image with direct push locations and final depths of refusal.

in the electrical properties of the earth materials at the distance of about ~650 feet along the ERI image would be consistent with the changes in electrical properties expected to be observed in a fault zone. The electrical properties in the vertical conductive zone would also be consistent with the conditions expected in an area with an extensive network of water filled fractures.

The image for ERI survey AS1.25C1 ERI data image (Figure 5.6) displays a relatively conductive (< 45 ohm-m) and laterally continuous feature from the surface down to an average elevation of about 1,000 feet (average depth of about eight feet). The electrical resistivity values observed near the surface appear more conductive in the AS1.25C1 ERI image than in the ASR5.00B ERI image which would be consistent with the expected temporal variations in the moisture conditions in the shallow subsurface. The electrical resistivity values observed in the shallow conductive zone appear to rise quickly to values that are generally > 280 ohm-m below an average elevation of about 980 feet (average depth of about 29 feet).

The 280 ohm-m contour line was selected as the possible location of the transitional boundary between the epikarst and the bedrock at the Arbuckle-Simpson Ranch site (Figure 5.5). The drilling of the soil zone down to competent bedrock at one or more points along the ERI profile would be necessary to more clearly define the electrical properties that marked the transition at the base of the epikarst zone. The 45 ohm-m contour line was selected in conjunction with the direct push data as the approximate location of the base of the soil zone at the Arbuckle-Simpson Ranch site (Figure 5.5).

The static water level estimated from the water surface elevation of the pond present at the field site is located at an elevation of approximately 999 feet (average depth of about seven feet) (Table 1). The estimated static water level elevation corresponds well with the bottom of the shallow conductive zone in the AS1.25C1 ERI image (Figure 5.6). The interpreted epikarst zone appears to extend to well below the measured static water level at the site.

Vertical electrical resistivity profiles corresponding to the approximate locations of the direct push conductivity logs and sediment cores and infiltration experiments were extracted from the ERI data. Because the extraction of vertical electrical resistivity profiles from the exact locations of the direct push conductivity logs and sediment cores and infiltration experiments were generally not possible two vertical electrical resistivity profiles which bracketed the locations were extracted. The extracted vertical electrical resistivity profiles for each location were plotted along with the corresponding EC log results for comparison. The vertical electrical resistivity profiles for each location are presented in the APPENDIX. The EC log results are presented in the following direct push electrical conductivity logging section.

5.3 Direct Push Electrical Conductivity Logging

Sixteen direct push electrical conductivity logs were collected from the field sites. The EC data values were multiplied by 10^{-3} to convert the units from millisiemens per meter [mS/m] into units of siemens per meter [S/m]. The new electrical conductivity values were inverted to convert the values into equivalent

Table 4. Electrical resistivity and conductivity ranges of various common earth materials [Modified from Telford et al., 1990; Reynolds, 1997].

Earth Materials	Electrical Resistivity Range (ohm-m)	Electrical Conductivity Range (S/m)
Consolidates shales	$20 – 2x10^{3}$	$5x10^{-4} – 0.05$
Conglomerates	$2x10^{3} – 10^{4}$	$1x10^{-4} – 5x10^{-4}$
Sandstones	$1 – 7.4x10^{8}$	$1.4x10^{-9} – 1$
Limestones	$50 – 10^{7}$	$10^{-7} – 2x10^{-2}$
Dolomite	$3.5\ x10^{2} – 5\ x10^{3}$	$2x10^{-4} – 2.8x10^{-3}$
Marls	3 – 70	$1.4x10^{-2} – 0.33$
Clays	1 – 100	$10^{-2} – 1$
Alluvium and sand	$10 – 8x10^{2}$	$1.3x10^{-3} – 0.1$
Soil (40% clay)	8	0.13
Soil (20% clay)	33	$3x10^{-2}$
Top soil	250 – 1700	$5.9x10^{-4} – 4x10^{-3}$
Unconsolidated wet clay	20	$5x10^{-2}$
Clay (very dry)	50 – 150	$6.7x10^{-3} – 2x10^{-2}$
Gravel (dry)	1400	$7.1x10^{-4}$
Gravel (saturated)	100	10^{-2}
Quaternary/Recent sands	50 – 100	$1x10^{-2} – 2x10^{-2}$
Lateritic soils	120 – 750	$1.3x10^{-3} – 8.3x10^{-3}$
Dry sandy soil	80 – 1050	$9.5x10^{-4} – 1.3x10^{-2}$
Sand clay/clayey sand	30 – 215	$4.7x10^{-3} – 3.3x10^{-2}$
Sand and gravel	30 - 225	$4.4x10^{-3} – 3.3x10^{-2}$

electrical resistivity units [ohm-m] for comparison with the surface electrical resistivity measurements. The EC derived electrical resistivity data were plotted versus depth with the corresponding vertical profiles of the ERI data for each sediment core location (APPENDIX).

Several electrical conductivity values recorded within the first few readings at the surface were anomalously low for the earth materials being probed (Table 4) and included several recorded values of 0.00 mS/m. The EC values collected at the locations immediately beneath the anomalous readings provided electrical conductivity values that were reasonable for the earth materials being probed.

Table 5. Hatch site direct push depth of refusal summary.

Soil Type Encountered	Method	File Name	Distance Along ERI Line (ft)	Total Depth of Refusal (ft)
Verdigris silty clay loam	Electrical Conductivity Log	EC0111.DAT	246.0	10.40
		EC0113.DAT	270.7	5.50
	Sediment Core	HAT75.0m	246.1	8.64
		HAT82.5m	270.7	6.12
		HAT91.0m	298.6	12.75
		HAT145.0m	475.7	8.18
		HAT180.0m	590.6	6.40
		HAT183.75m	602.9	0.94
		HAT188.75m	619.3	2.65
		HAT195.0m	639.8	3.50
Verdigris Soil Type Minimum Depth of Refusal				0.94
Verdigris Soil Type Maximum Depth of Refusal				12.75
Verdigris Soil Type Average Depth of Refusal				6.51
Stephenville fine sandy loam	Sediment Core	HAT105.0m	344.5	10.49
		HAT114.5m	375.7	9.43
		HAT130.0m	426.5	10.49
		HAT153.0m	502.0	8.30
		HAT202.0m	662.8	11.75
Stephenville Soil Type Minimum Depth of Refusal				8.30
Stephenville Soil Type Maximum Depth of Refusal				11.75
Stephenville Soil Type Average Depth of Refusal				10.09
Surface distance measured relative to north end of ERI line HWN05MA1				

The anomalously low EC values at the surface were assumed an indication of poor coupling between the electrodes on the EC probe and the earth material at the locations the readings were collected. Recorded electrical conductivity values of < 0.1 mS/m were considered suspect and not used in any analysis. The electrical resistivity values derived from the conductivity data gave values ranging between 0.08 and 8,300 ohm-m which were considered reasonable for the earth materials probed.

Table 6. Spears Ranch site direct push depth of refusal summary.

Soil Type Encountered	Method	File Name	Distance Along ERI Line (ft)	Total Depth of Refusal (ft)
Kiti very flaggy silt loam	Electrical Conductivity Log	EC0117.DAT	12.3	0.70
		EC0119.DAT	32.8	0.20
		EC0120.DAT	49.2	0.35
		EC0126.DAT	287.1	0.65
		EC0125.DAT	328.1	1.20
		EC0124.DAT	344.5	2.90
		EC0123.DAT	369.1	0.90
		EC0122.DAT	401.9	2.75
		EC0121.DAT	438.8	4.35
	Sediment Core	SPR3.75m	12.3	1.40
		SPR10.0m	32.8	0.80
		SPR15.0m	49.2	0.70
		SPR87.5m	287.1	1.00
		SPR100.0m	328.1	1.20
		SPR105.0m	344.5	3.50
		SPR112.5m	369.1	0.90
		SPR122.5m	401.9	1.40
		SPR133.75m	438.8	0.55
Kiti Soil Type Minimum Depth of Refusal				0.20
Kiti Soil Type Maximum Depth of Refusal				4.35
Kiti Soil Type Average Depth of Refusal				1.41
Surface distance measured relative to southern end of ERI line SW2.50A				

Two EC logs were collected at the Hatch site in September, 2006 (Table 5). No EC logs were collected at the site in March, 2007. The direct push electrical resistivity data ranged between 0.08 and 7,100 ohm-m. Total depths of refusal for the two EC logs were 5.5 and 10.4 feet. The range in total depths of refusal appears to suggest that the thickness of the soil mantle is highly variable across the site.

Table 7. Arbuckle-Simpson Ranch site direct push depth of refusal summary.

Soil Type Encountered	Method	File Name	Distance Along ERI Line (ft)	Total Depth of Refusal (ft)
Gowton loam	Electrical Conductivity Log	EC0129.DAT	32.8	7.55
		EC0130.DAT	69.7	5.95
		EC0131.DAT	110.7	6.85
		EC0132.DAT	164.0	5.00
		EC0133.DAT	188.0	6.30
	Sediment Core	ASR10.0m	32.8	6.27
		ASR21.25m	69.7	7.03
		ASR33.75m	110.7	6.67
		ASR50.0m	164.0	6.55
		ASR57.3m	188.0	8.18
Gowton Soil Type Minimum Depth of Refusal				5.00
Gowton Soil Type Maximum Depth of Refusal				8.18
Gowton Soil Type Average Depth of Refusal				6.64
Surface distance measured relative to southern end of ERI line AS1.25C1				

In general the EC derived electrical resistivity data from both EC logs were observed to decrease with increasing depth. Considerable variability in the electrical properties of the sediments is observed in both EC logs. Several major resistive or conductive peaks observed in one EC log appears absent or inverted in the other EC log. The considerable electrical variability observed in both EC logs would make correlating sedimentary horizons between the two locations difficult. The differences observed near the surface in the EC data may be due in part to local variations in soil moisture content. The differences observed near the surface may also be an indication of past disturbance at the site. The Hatch EC resistivity data from both locations appear to correlate well with the corresponding ERI data (Figures A1 and A2).

Nine EC logs were collected at the Spears Ranch site (Table 6). The EC derived electrical resistivity data show values ranged between 0.1 and 8,300 ohm-m. Total depths of refusal for the EC logs ranged between 0.2 and 4.4 feet. The range in total depths of refusal appears to suggest that the thickness of the soil mantle is highly variable across the site.

In general the EC derived electrical resistivity data from the Spears Ranch EC logs were observed to increase with increasing depth. Considerable variability in the electrical properties of the sediments is observed in the EC logs. Similar electrical features are observed with depth across several of the Spears Ranch EC logs. In general the Spears Ranch EC resistivity data appears to correlate fairly well with the corresponding ERI data (Figures A14 thru A22).

Five EC logs were collected at the Arbuckle-Simpson site (Table 7). The EC derived electrical resistivity data show values ranged between 3.9 and 500 ohm-m. Total depths of refusal for the EC logs ranged between 5.0 and 7.6 feet. The range in total depths of refusal appears to suggest that the thickness of the soil mantle is variable across the site.

In general the EC derived electrical resistivity values from the EC logs were observed to increase to the depth of approximately three feet and then begin to decrease with increasing depth below three feet (figures A23 thru A27). Considerable variability in the electrical properties is observed in the upper one to three feet of the EC derived electrical resistivity data which do not appear to correlate well across the field site. Several features observed below three feet of depth in the EC derived electrical resistivity data appear to correlate well across

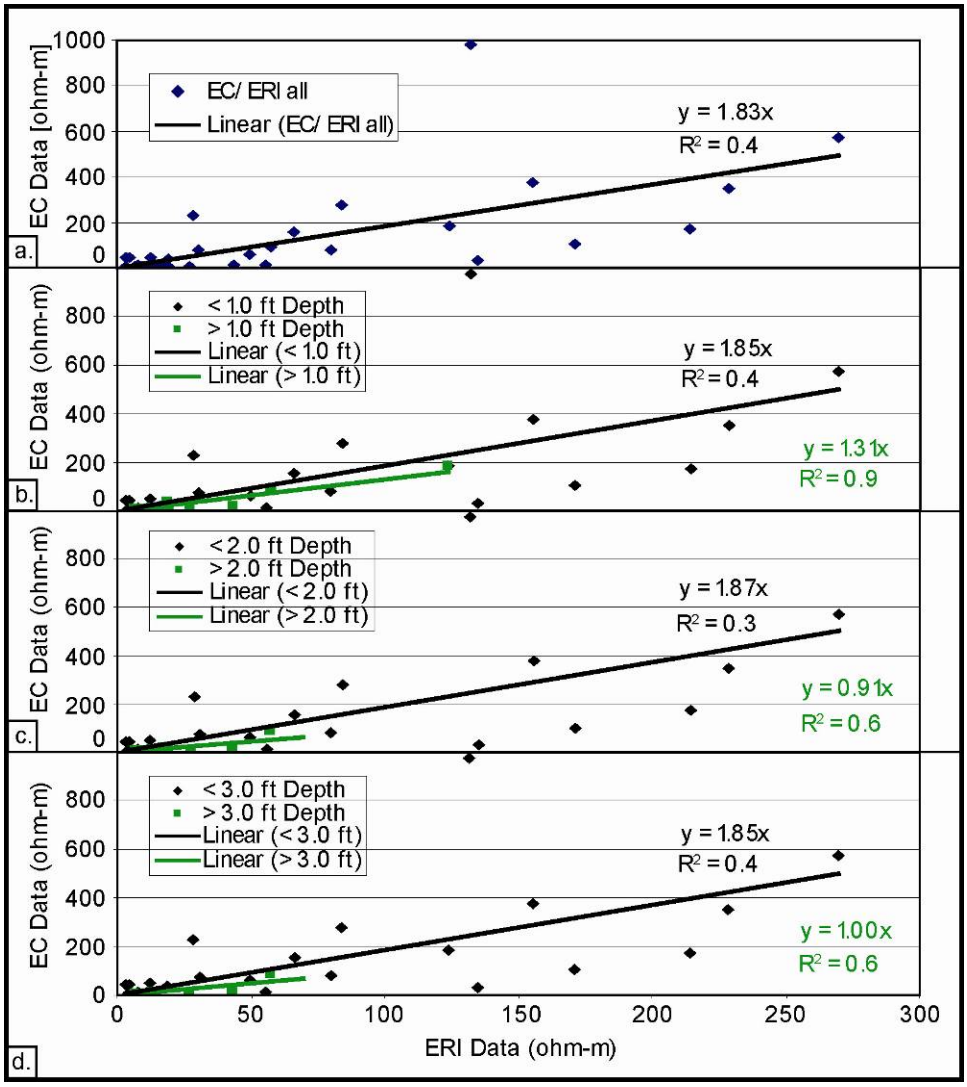

Figure 5.7. Surface and direct push electrical resistivity data versus the depth of the measurement analysis (a) overall relationship (b) relation of data collected above and below one foot of depth (c) relation of data collected above and below two feet of depth (d) relation of data collected above and below three feet of depth.

the field site. In general the Arbuckle-Simpson Ranch EC resistivity data appears to correlate fairly well with the corresponding ERI data.

The EC resistivity data were plotted against the corresponding ERI resistivity data to determine how well the two datasets correlated overall (Figure 5.7a). A linear trend line added to the plot with the intercept set at zero shows an

R^2 value of 0.4 suggesting that a relationship does exist. The slope of the trend line suggests that overall an almost 2:1 relationship appears to exist between the resistivity data.

Several plots of same data were constructed to analyze for any possible effects the depth of the measurements may have on the EC vs. ERI relationship. The electrical resistivity data above and below 1, 2, and 3 feet of depth were plotted separately (Figure 5.7b-d). The apparent relationship between the EC and ERI data appears to be stronger for the deeper data (R^2 = 0.6 – 0.9) in each of the depth intervals examined than the near surface data (R^2 = 0.3 – 0.4). The results appear to suggest that for the near surface data an overall ~2:1 relationship is reasonable. The results appear to suggest that for the deeper data the EC vs. ERI relationship may approach a 1:1 relationship.

In general the overall trends observed in EC data were observed to be mirrored in the ERI data. In general the values of the larger scale ERI data were not observed to vary significantly between adjacent data points (APPENDIX). In contrast the potential for variation between data points in the smaller scale EC data was observed to be significant. The majority of the observed differences between the two electrical resistivity datasets appear most likely due to the differences in the scale of the measurements.

In general the EC data collected in the drier conditions in the upper about one foot showed considerable variation while the ERI data collected in the same interval showed relatively little variation (APPENDIX). The EC vs. ERI relationship over the same interval appeared to be ~2:1. Over intervals where

the EC data showed relatively little variation the EC vs. ERI relationship approached a 1:1 ratio. The EC vs. ERI relationship appears to be largely controlled by the degree of electrical variation in the EC data. The expected relationship between the EC and ERI data would be weaker in intervals with a significant amount of variation within the EC data than in intervals with a lesser degree of variation in the EC data.

5.4 Direct Push Sediment Coring

Twenty seven direct push sediment cores were collected from the field sites. The observed sediment core total depths of refusal ranged between 0.2 and 12.8 feet. The observed range in total depths of refusal from the direct push sediment cores varied significantly between the field sites.

The locations of the direct push investigations were plotted as vertical bars on the ERI images for each field site (Figures 5.6, 5.8, and 5.9). At each location the total depths of refusal for the direct push sediment cores and EC logs were somewhat different. The length of the bars at the direct push locations in the ERI images indicate the maximum total depth of refusal that was achieved from both methods.

Thirteen sediment cores were collected at the Hatch site in March, 2007 (Table 5). Three sediment cores were also collected at the site in September, 2006 but not used in the analysis. Analysis of the 2006 sediment cores would have duplicated sediment core data collected at the same locations in 2007. Total depths of refusal for the thirteen sediment cores ranged between 0.9 and

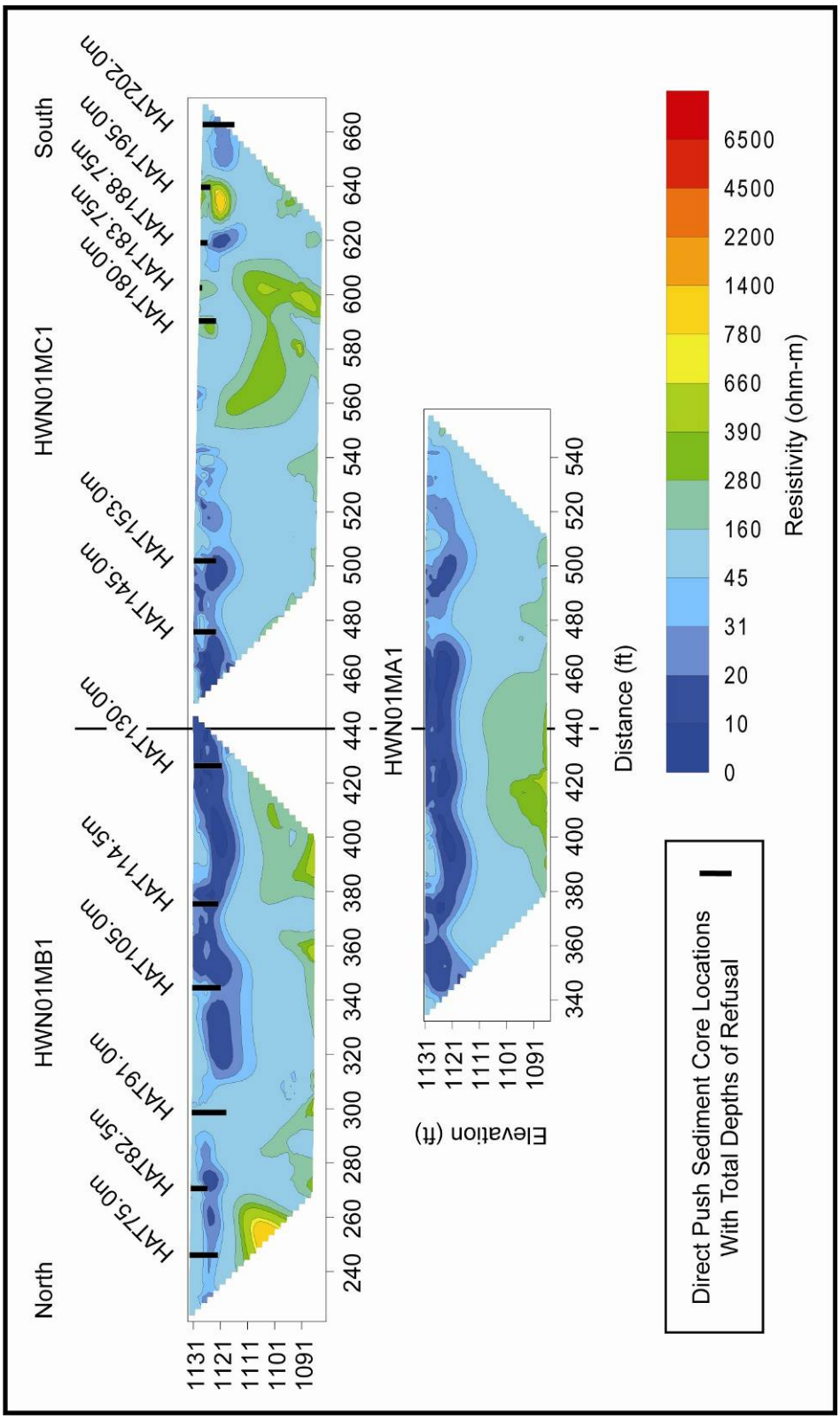

Figure 5.8. Hatch site ERI results with direct push locations and final depths of refusal. All ERI data images are aligned horizontally in space and to scale.

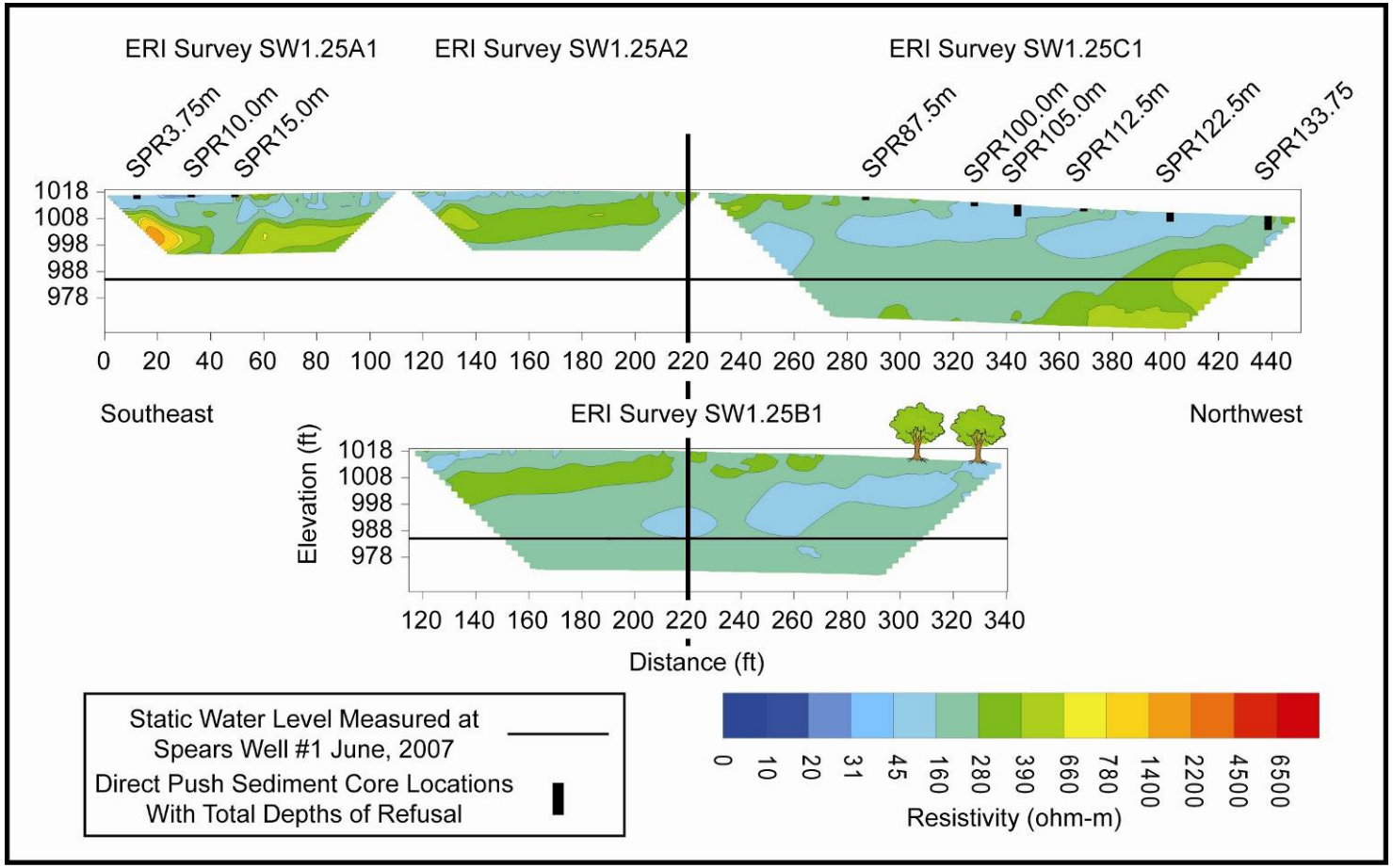

Figure 5.9. Spears Ranch site ERI results with direct push locations and final depths of refusal. All ERI data images are aligned horizontally in space and to scale.

12.8 feet. The range in total depths of refusal appears to suggest that the thickness of the soil mantle is highly variable across the site. In general the total depths of refusal were deeper in areas where the observed electrical resistivity values were relatively low and the total depths of refusal were shallower in areas where the observed electrical resistivity values were higher (Figure 5.8). The total depths of refusal from the Hatch site sediment cores do not appear to correspond well to any specific range of electrical resistivity values.

Nine sediment cores were collected at the Spears Ranch site (Table 6). Total depths of refusal for the sediment cores ranged between 0.6 and 3.5 feet. The range in total depths of refusal appears to suggest that the thickness of the soil mantle is variable across the site. In general the total depths of refusal were deeper in areas where the observed electrical resistivity values were relatively low and the total depths of refusal were shallower in areas where the observed electrical resistivity values were higher (Figure 5.9). The total depths of refusal from the Spears Ranch site sediment cores do not appear to correspond well to any specific range of electrical resistivity values.

Five sediment cores were collected at the Arbuckle-Simpson Ranch site (Table 7). Total depths of refusal for the sediment cores ranged between 6.3 and 8.2 feet. The range in total depths of refusal appears to suggest that the thickness of the soil mantle is somewhat uniform across the test site. In general the total depths of refusal appear to correspond fairly well to locations where the observed electrical resistivity values were between 10 and 30 ohm-m in the Arbuckle-Simpson Ranch ERI image (Figure 5.6).

5.5 Infiltration Tests

Twenty four infiltration experiments were accomplished at the field sites. Saturated hydraulic conductivity values estimated for each location from the infiltration experiment results ranged between 0.34 and 16.24 μm/s (Table 8). The saturated hydraulic conductivity values estimated from the infiltration experiment results were plotted along with the empirically derived hydraulic conductivity results from the sediment core analyses (APPENDIX).

Ten infiltration experiments were run at the Hatch site. The calculated hydraulic conductivity values for the Hatch site were highly variable across the field site. The calculated hydraulic conductivity values for the Hatch site ranged between 0.53 and 16.24 μm/s with a site geometric mean value of 2.99 μm/s (Table 8).

Nine infiltration experiments were run at the Spears Ranch site. The calculated hydraulic conductivity values for the Spears Ranch site were slightly less variable than at the Hatch site and ranged between 0.93 and 12.72 μm/s (Table 8). The geometric mean infiltration rate for the Spears Ranch site was 3.70 μm/s which was the highest average infiltration rate of the three field sites.

Five infiltration experiments were run at the Arbuckle-Simpson Ranch site. The calculated hydraulic conductivity values for the Arbuckle-Simpson Ranch site were the least variable of all of the sites and ranged between 0.34 and 1.67 μm/s (Table 8).Two of the infiltration experiments at the Arbuckle-Simpson Ranch site (ASRCCI10.0m and ASRCCI21.25m) were conducted on a dirt road crossing the site which may have affected the experiment results. The saturated hydraulic

Table 8. Infiltration test results summary.

Site Name	Filename	Distance Along ERI Line (ft)*	Calculated Infiltration Rate (μm/s)
Hatch	HATCCI75.0m	246.1	9.58
	HATCCI82.5m	270.7	16.24
	HATCCI91.0m	298.6	2.28
	HATCCI105.0m	344.5	1.91
	HATCCI114.5m	375.7	0.53
	HATCCI130.0m	426.5	3.97
	HATCCI145.0m	475.7	1.55
	HATCCI153.0m	502.0	3.13
	HATCCI180.0m	590.6	1.67
	HATCCI183.75m	602.9	5.00
		Site Minimum	**0.53**
		Site Maximum	**16.24**
		Site Geometric Mean	**2.99**
* Surface distance measured relative to north end of ERI line HWN05MA1			
Spears Ranch	SPRCCI3.75m	12.3	0.93
	SPRCCI10.0m	32.8	0.97
	SPRCCI15.0m	49.2	2.10
	SPRCCI87.5m	287.1	8.32
	SPRCCI100.0m	328.1	3.33
	SPRCCI105.0m	344.5	2.67
	SPRCCI112.5m	369.1	12.72
	SPRCCI122.5m	401.9	6.14
	SPRCCI133.75m	438.8	11.99
		Site Minimum	**0.93**
		Site Maximum	**12.72**
		Site Geometric Mean	**3.70**
* Surface distance measured relative to southern end of ERI line SW2.50A			
Arbuckle-Simpson Ranch	ASRCCI10.0m	32.8	0.34
	ASRCCI21.25m	69.7	Bad data
	ASRCCI33.75m	110.7	0.49
	ASRCCI50.0m	164.0	1.24
	ASRCCI57.3m	188.0	1.67
		Site Minimum	**0.34**
		Site Maximum	**1.67**
		Site Geometric Mean	**0.77**
* Surface distance measured relative to southern end of ERI line AS1.25C1			

conductivity value for the ASRCCI21.25m infiltration experiment could not be determined from the results. The geometric mean infiltration rate for the Arbuckle-Simpson Ranch site was 0.77 μm/s (Table 8), which was the lowest average infiltration rate of the three field sites. The infiltration experiment results will be further examined in the hydraulic conductivity calculation section at the end of this chapter.

5.6 Direct Push Sediment Core Descriptions

Each of the twenty seven sediment cores was analyzed one core segment at a time. Each core segment was extracted from its core sleeve, measured, split lengthwise, examined and described, and divided into intervals based upon apparent changes in the color, texture, or moisture content observed in the sediment cores. A total of 176 core intervals were identified and described from the 27 sediment cores. One core sample was extracted from each of 167 of the core intervals for analysis. No core samples were extracted from the remaining nine core intervals which consisted entirely of weathered rock. Images of the sediment cores can be seen in the APPENDIX.

The Hatch site sediment cores were the first to be analyzed. Ninety seven core intervals were identified from the thirteen sediment cores collected at the Hatch site (Figures A1 thru A13). The core intervals ranged from 0.02 to 5.35 feet in length. Ninety seven core samples were extracted from core intervals for analysis. Core diameter and initial field moist core sample volume measurements were not collected for Hatch site core samples 001-048 which

made volumetric water content calculations on those core samples impossible. The core diameter and initial field moist core sample volume measurements were collected for all the remaining core samples. Weathered rock fragments from the sediment core intervals, present at the bottom of the sediment cores, or retrieved from the cutting shoe and saved for examination if any were examined and identified as dolomite, chert, or dolomite with chert inclusions.

Twenty seven core intervals were identified from the nine sediment cores collected at the Spears Ranch site (Figures A14 thru A22). The core intervals ranged from 0.05 to 1.55 feet in length. Eighteen core samples were extracted from core intervals for analysis. The remaining nine core intervals essentially consisted entirely of weathered rock. Weathered rock from the sediment core intervals, present at the bottom of the sediment cores, or retrieved from the cutting shoe and saved for examination if any were identified as dolomite, chert, or dolomite with chert inclusions.

Fifty two core intervals were identified from the five sediment cores collected at the Arbuckle-Simpson Ranch site (Figures A23 thru A27). The core intervals ranged from 0.08 to 3.03 feet in length. Fifty two core samples were extracted from core intervals for analysis. Weathered rock fragments from the sediment core intervals, present at the bottom of the sediment cores, or retrieved from the cutting shoe and saved for examination if any were identified as dolomite, chert, or dolomite with chert inclusions.

5.7 Particle Size Distribution

Particle size analysis was accomplished on 165 of 167 core samples. The remaining two core samples were from the Hatch site and were lost prior to the particle size analysis. The particle size analysis results from each of the three field sites were very different.

The distribution of clay, silt, sand, and gravel in each sediment core sample was determined from the particle size analyses results using the USDA soil particle size classification scheme (Figure 4.3a). The experimentally determined particle size distribution in the sediment core samples were assumed to be representative of the particle size distribution of the entire sediment core intervals the core samples were extracted from. Vertical profiles of the percent distribution of clay, silt, sand, and gravel were constructed for each sediment core. The vertical particle size distribution profiles for each sediment core location can be seen in the APPENDIX.

The effective grain size, d_{10} [μm], was calculated for each sediment core sample from the particle size analysis results. Vertical d_{10} profiles were constructed for each sediment core to observe changes in the effective grain size with depth. The vertical d_{10} profiles can be seen in the APPENDIX.

The soil types present in the area of investigation at each field site were identified from the “sa_miads_soils” layer in the Arbuckle-Simpson Hydrology Study GIS dataset. The specific soils sampled by the sediment cores were determined by comparing the textural properties of the sediment core samples with the textural properties of the soil types in the NRCS soils database (Soil

Survey Staff, 2005). The soil type in the NRCS soils database with properties most closely matching the experimentally derived properties of the sediment core material was selected as the soil type sampled by the sediment core at the field site.

Particle size analysis was accomplished on 95 of 97 sediment core samples from the thirteen Hatch site sediment cores. Hatch site core samples 033 and 037 were lost before particle size analysis could be accomplished. Silt loam as defined by the USDA soil textural classification scheme (Figure 4.3b) was the dominant soil textural type in Hatch site sediment cores HAT75.0, 82.5, 91.0, 145.0, 180.0, 183.75, 188.75, and 195.0m. The dominant soil textural types in Hatch site sediment cores HAT105.0, 114.5, 130.0, 153.0, and 202.0m were sandy loam and loamy sand as defined by the USDA soil textural classification scheme.

Two soil types the Verdigris Silty Clay Loam and the Stephenville-Darnel Complex were indicated as present in the area of investigation at the Hatch field site (Figure 5.10). The sediment cores dominated by silt loam most closely fit the properties ascribed to the Verdigris silt loam. The remaining sediment cores dominated by sandy loam and loamy sand most closely fit the properties ascribed to the Stephenville member of the Stephenville-Darnel Complex.

The calculated d_{10} values for the Hatch core samples ranged in size from 0.93 to 46.77 μm. In general the vertical d_{10} profiles indicated that particle size tended to decrease with depth across the field site (Figures A1 thru A13). Several locations experienced an increase in effective grain size near the bottom

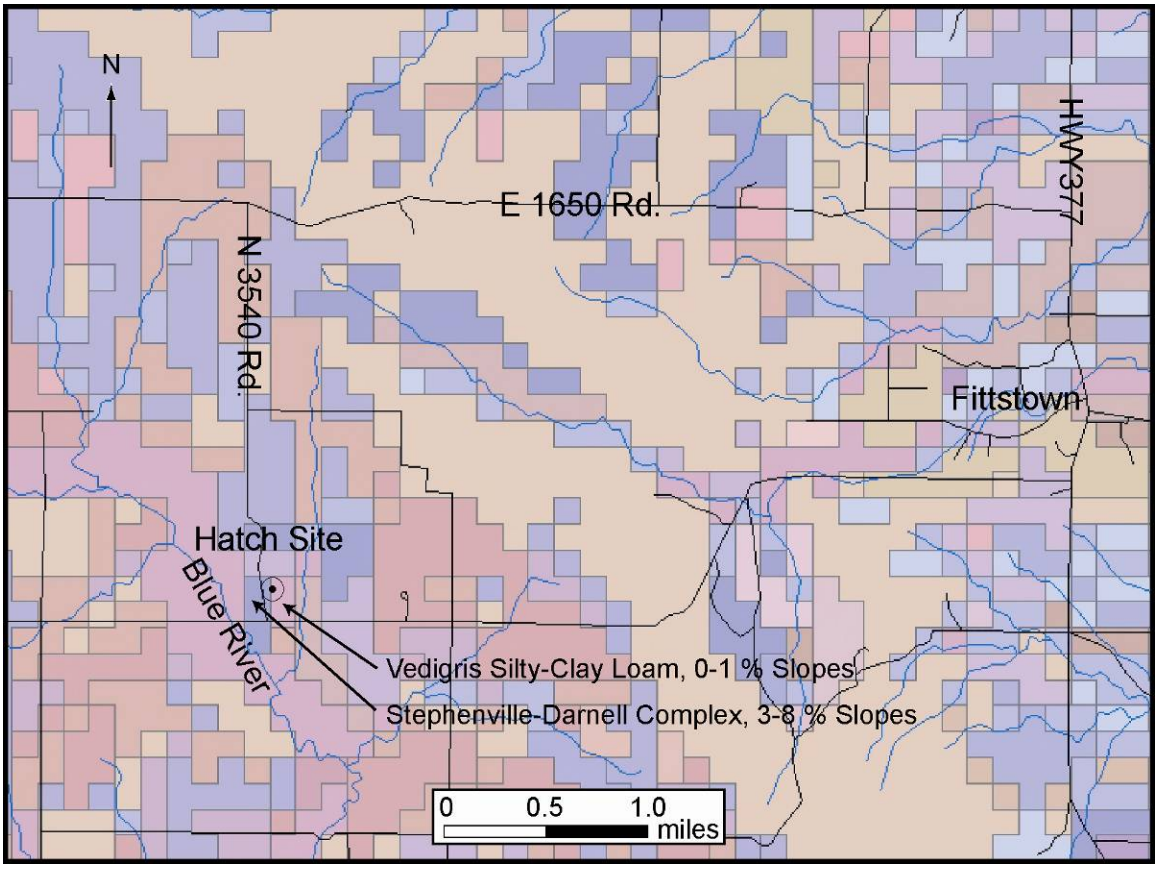

Figure 5.10. Hatch site soil types from the "sa_miads_soils" layer in the Arbuckle-Simpson Hydrology Study GIS dataset.

of the sediment cores especially in the cores consisting of the Stephenville soil type.

The observed electrical resistivity values exhibited by the two soil types represented at the Hatch site as constrained by the final direct push depths of refusal appear to be highly variable but are generally less than 55 ohm-m. The differences between the electrical properties of the two soil types appear to be significant enough to be observed in the ERI image (Figure 5.6). The more conductive feature near the surface at the distance of from around 315 to 510 feet appears to coincide with the presence of the sandy loam and loamy sand characteristic of the Stephenville soil type whereas the silt loams more

characteristic of the Verdigris soil type appear limited to areas that are generally less conductive.

Particle size analysis was accomplished on all eighteen sediment core samples from the nine Spears Ranch site sediment cores. Silt loam as defined by the USDA soil textural classification scheme (Figure 4.3b) was the dominant soil textural type in the majority of the sediment cores at the Spears Ranch site. Sandy loam as defined by the USDA soil textural classification scheme (Figure 4.3b) was dominant at the surface in the SPR133.75m sediment core.

One soil type, the Kiti-Rock Outcrop Complex, was indicated as present in the area of investigation at the Spears Ranch field site (Figure 5.11). With the exception of the sandy loam present in the SPR133.75m sediment core, the soil textures present in the Spears Ranch core samples were consistent with the properties ascribed to the Kiti member of the Kiti-Rock Outcrop Complex. The sandy loam present at the surface in the SPR133.75m sediment core may be an artifact resulting from recent drilling activities when the Spears Ranch wells #1 and 2 were installed. The presence of the remains of a cigarette filter found in sediment core SPR105.0m at a depth of between 0.35 and 0.90 feet is evidence that the surface of the site has experienced some relatively recent disturbance.

The calculated effective grain size, d_{10}, for the Spears Ranch core samples ranged in size from 1.55 to 10.00 μm (Figures A14 thru A22). The Spears Ranch cores were generally too shallow to indicate any significant trend in grain size distribution with depth across the site. The few vertical d_{10} profiles

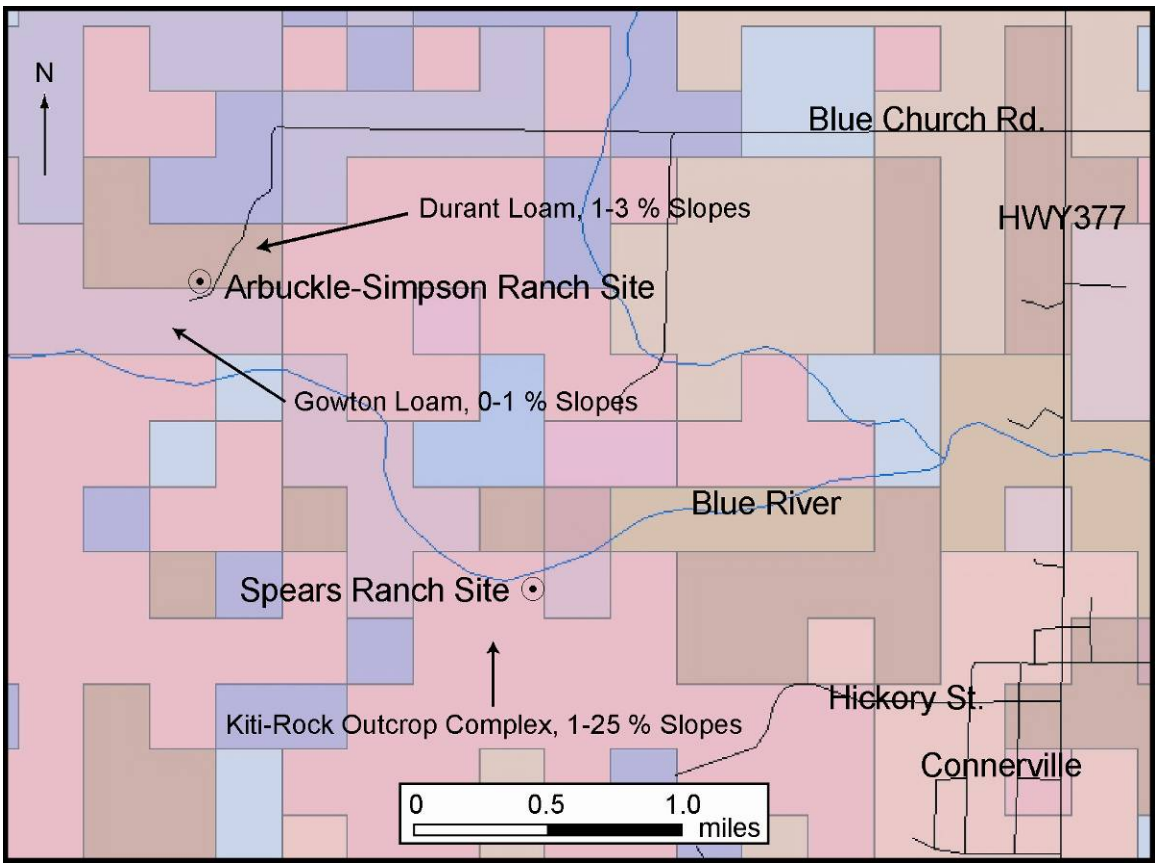

Figure 5.11. Arbuckle-Simpson and Spears Ranch sites soil types from the "sa_miads_soils" layer in the Arbuckle-Simpson Hydrology Study GIS dataset.

with any observable trend in the data appeared to suggest that in general particle size tended to decrease with depth across the field site.

Particle size analysis was accomplished on all 52 sediment core samples from the five Arbuckle-Simpson Ranch site sediment cores. Silt loam and silt as defined by the USDA soil textural classification scheme (Figure 4.3b) were the dominant soil textural types in the sediment cores at the Arbuckle-Simpson Ranch site. Sediment cores (ASR 10.0 and 21.25m) contained an interval of sandy loam below about a depth of about 4.6 feet.

Two soil types, the Gowton and the Durant Loams, were indicated as present in the area of investigation at the field site (Figure 5.11). With the exception of the sandy loam present in the ASR 10.0 and 21.25m sediment cores the soil textures present in the Arbuckle-Simpson Ranch core samples were mostly consistent with the properties ascribed to the Gowton Loam. The properties ascribed to the Durant Loam did not appear to fit well with the particle size distribution results from any of the sediment core samples.

The calculated effective grain size, d_{10}, for the Arbuckle-Simpson Ranch core samples ranged in size from 1.45 to 11.00 μm (Figures A23 thru A27). The larger d_{10} values were restricted to the core samples containing sandy loam or were classified as gravelly. In general the d_{10} values indicated that the effective grain size tended to be coarser at the surface and to fine downward to a depth of about four feet across the field site. Below the depth of about four feet the effective grain size tended to increase and became highly variable across the field site.

In general the electrical resistivity of earth materials typically decreases with increasing clay content (Reynolds, 1997). A plot of the clay content versus the corresponding electrical resistivity values for the core samples was constructed to determine if a similar inverse relationship exists in the data (Figure 5.12a). A linear trend line added to the plot shows an R^2 value of 0.05 suggesting that overall no clear relationship exists.

The electrical resistivity values in the plot appear to be highly variable when clay content is very low and appear to become less variable and more

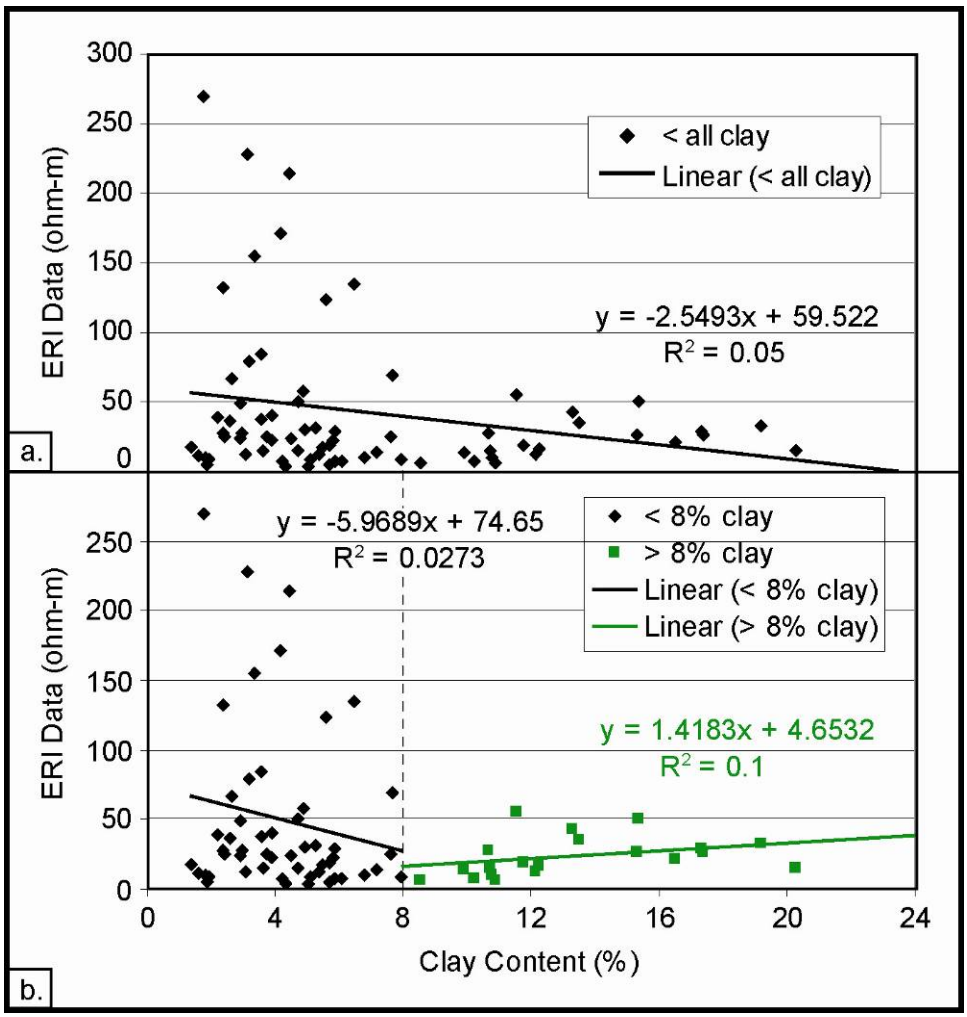

Figure 5.12. Relationship between surface ERI data and clay content (a) overall relation (b) relation at clay content < 8% and > 8% clay.

conductive as clay content increases. The electrical resistivity values appear to converge rapidly as clay content increases to about 8% and then appear to become more consistent as clay content increases above 8%. A second plot was constructed to look for a relationship between electrical resistivity and clay content when the clay content is either below or above 8% (Figure 5.12b). The trend line for the data with clay content < 8% with an R^2 value of 0.03 suggests

that no relationship exists. The trend line for the data with clay content > 8% with an R^2 value of 0.1 appears to suggest that a weak relationship may exist.

5.8 Porosity

Total porosities were calculated for 165 of 167 core samples using equation 4.15. The data from the remaining two core samples were from the Hatch site and were lost prior to the porosity analysis. Vertical profiles of the calculated total porosities with depth were constructed for each sediment core. The vertical profiles of the calculated total porosity versus depth for each sediment core can be seen in the APPENDIX.

The calculated bulk densities for all of the sediment core samples ranged from 1.09 to 2.20 g/cm^3. The calculated bulk densities for the Hatch site sediment core samples 001-048 ranged from 1.09 to 1.61 g/cm^3 with an average calculated bulk density of 1.34 g/cm^3. The calculated bulk densities for all of the remaining core samples from the three field sites ranged from 1.10 to 2.20 g/cm^3 with an average calculated bulk density of 1.62 g/cm^3.

The majority of the calculated bulk densities fell within the expected bulk density range for common earth materials (Table 9). Four calculated bulk density values from the Hatch site and one bulk density value from the Spears Ranch site were below the expected minimum bulk density value of 1.20 g/cm. The anomalously low calculated bulk density values from the Hatch site were derived from sediment core sample volumes that were measured using manually packed oven-dry sediment core material as is described for Hatch site sediment core

Table 9. Bulk density ranges of common earth materials [Modified from Telford et al., 1990; Reynolds, 1997].

Earth Materials	Density Range (g/cm^3)
Alluvium	1.96-2.00
Loess	1.40-1.93
Soil	1.20-2.40
Clay	1.63-2.60
Silt	1.80-2.20
Sand	1.70-2.30
Gravel	1.70-2.40

samples (001 – 048) in chapter 4. It was expected that the bulk densities of highly disturbed oven dry soils that had been manually packed into containers for measurement would be somewhat lower than the bulk densities of the same soils in undisturbed and field moist conditions. The anomalously low calculated bulk density value from the Spears Ranch site was derived from a sediment core sample volume that was measured using the immersion method (chapter 4). The anomalously low bulk density could have resulted from a volume measurement that was too large. The volume of a sediment core sample measured by the immersion method as described in chapter 4 could be too large if air bubbles became trapped in the container with the sediment core sample and were not removed prior to the volume measurement.

The calculated particle densities for the Hatch site core samples 001-048 ranged from -44.2 to 40.9 g/cm^3 which indicated that there were errors in the volume measurements for those core samples. The calculated particle densities for remainder of the core samples from all three field sites ranged from 1.77 to 2.99 g/cm^3 and averaged 2.56 g/cm^3. The calculated particle density values for

Table 10. Porosity ranges of unconsolidated sediments [Modified after Fetter, 2001; Weight and Sonderegger, 2001].

Unconsolidated Materials	Φ%
Clay	33-70
Silt	35-50
Sand	25-50
Gravel	20-50
Sand and gravel, mixed	15-35
Glacial till	10-20

the three field sites excepting those derived for Hatch core samples 001-048 would be considered reasonable particle density values.

The total porosity calculations for all the sediment core samples were normalized by assuming a particle density of 2.65 g/cm^3. The percentage difference between the assumed particle density value of 2.65 g/cm^3 and the average calculated particle density value of 2.56 g/cm^3 was 3.45%. The relatively small percentage difference between the calculated and assumed particle densities suggested that the assumed particle density was reasonable to use.

Based upon the published porosity ranges for common earth materials (Table 10) and the types of earth materials observed in the sediment cores the expected calculated total porosity range for the core samples was 15.0 to 50.0%. The maximum expected calculated total porosity value was 54.2% based upon a minimum bulk density of 1.20 g/cm^3 and the assumed particle density of 2.65 g/cm^3. The calculated total porosities from all three field sites using the calculated bulk densities and the assumed particle density ranged from 16.9 to

Table 11. Calculated total porosity results summary.

Site Name	Soil Type Encountered	Sediment Core Filename	Minimum Total Porosity (%)	Maximum Total Porosity (%)	Average Total Porosity (%)
Hatch	Verdigris silty clay loam	HAT75.0m	41.9	58.7	51.0
		HAT82.5m	46.1	54.1	49.5
		HAT91.0m	45.9	53.7	50.4
		HAT145.0m	20.9	55.8	41.2
		HAT180.0m	35.3	45.7	39.9
		HAT183.75m	39.4	39.4	39.4
		HAT188.75m	35.2	48.1	41.6
		HAT195.0m	31.0	41.3	36.3
	Average Total Porosity for Verdigris Soil Type				**45.0**
	Stephenville fine sandy loam	HAT105.0m	40.8	56.0	48.3
		HAT114.5m	34.9	53.7	46.9
		HAT130.0m	39.1	55.4	49.4
		HAT153.0m	34.5	50.4	42.1
		HAT202.0m	31.5	50.8	43.9
	Average Total Porosity for Stephenville Soil Type				**45.7**
Spears Ranch	Kiti very flaggy silt loam	SPR3.75m	51.8	51.8	51.8
		SPR10.0m	37.3	45.1	41.2
		SPR15.0m	34.0	34.0	34.0
		SPR87.5m	54.2	54.2	54.2
		SPR100.0m	47.7	52.6	50.1
		SPR105.0m	32.6	58.5	48.2
		SPR112.5m	31.4	36.3	33.9
		SPR122.5m	19.1	47.9	37.7
		SPR133.75m	16.9	16.9	16.9
	Average Total Porosity for Kiti Soil Type				**42.3**
Arbuckle-Simpson Ranch	Gowton loam	ASR10.0m	29.9	40.7	35.7
		ASR21.25m	22.6	48.5	35.5
		ASR33.75m	29.3	36.3	33.3
		ASR50.0m	29.5	47.6	36.4
		ASR57.3m	29.5	38.6	35.6
	Average Total Porosity for Gowton Soil Type				**35.1**

58.7% (Table 11). The core samples with calculated total porosity values greater than 50.0% all had relatively low calculated bulk densities associated with them. Anomalously high calculated total porosities could result if the true particle densities were less than the assumed particle density of 2.65 g/cm^3 or if the calculated bulk densities were anomalously low. The calculated total porosities could also be too low if the true particle densities were greater than the assumed particle density of 2.65 g/cm^3 or if the calculated bulk densities were too high.

The calculated total porosity values for the Hatch site ranged between 20.9 and 58.7% (Table 11). The calculated total porosity range for Hatch core samples 001-048 (34.9 to 58.7%) was higher than the calculated total porosity range for Hatch core samples 049-097 (20.9 to 55.8%). The higher calculated porosities for the Hatch core samples 001-048 were reflected in the average total porosities calculated for each Hatch site sediment core (Table 11). The average total porosities for the Hatch site sediment cores generally fell within the expected range of porosities for unconsolidated earth materials and were consistent with the types of earth materials observed in the sediment cores (Table 10 and Figures A1 thru A13).

The calculated total porosities for the Spears Ranch site displayed the highest range of variability of the three field sites. The calculated total porosity values for the Spears Ranch site ranged between 16.9 and 58.5% (Table 11). The anomalously high porosity value of 58.5% came from sediment core sample 008 from the Spears Ranch sediment core SPR105.0m and was associated with an anomalously low bulk density value of 1.10 g/cm^3. The average total

porosities for the Spears Ranch site sediment cores generally fell within the expected range of porosities for unconsolidated earth materials and while some seemed high, they were generally consistent with the types of earth materials observed in the sediment cores (Table 10 and Figures A14 thru A22).

The calculated total porosity values for the Arbuckle-Simpson Ranch site ranged between 22.6 and 48.5% (Table 11). The calculated total porosity values for the Arbuckle-Simpson Ranch site displayed the lowest range of variability of the three field sites (Table 10 and Figures A23 thru A27).

5.9 Water Content

Water content analysis was accomplished on all 167 core samples. Gravimetric water content was calculated for all core samples using equation 11. Volumetric water content (eq. 12) and saturation ratios (eq. 13) were calculated for all core samples except for Hatch core samples 001-048 due to the absence of initial sample volume measurements.

The calculated gravimetric water contents for all the field sites ranged from 3.3 to 52.0%. In general, the gravimetric water contents increased with depth. An increase in gravimetric water content with depth in the vadose zone was expected in intervals with similar effective grain size. The gravimetric water content in the vadose zone was expected to decrease in intervals with an increase in effective grain size due to gravity drainage in such intervals. The calculated gravimetric water content versus depth for each sediment core can be seen in the APPENDIX.

The calculated gravimetric water contents from the Hatch site sediment cores ranged from 3.8 to 52.6% (Figures A1 thru A13). The calculated gravimetric water content for Hatch site core sample 008 of 52.6% seems somewhat high and may have resulted from measurement error. The remaining calculated gravimetric water contents from the Hatch site display values were < 40.1% which would be considered reasonable. The observed gravimetric water content generally increased with depth and correlated with changes in the grain size distribution.

The calculated gravimetric water contents from the Spears Ranch site ranged from 3.30 to 31.4% (Figures A14 thru A22). The observed gravimetric water content generally increased with depth and correlated with changes in the grain size distribution. Gravimetric water content values from core samples at the surface with values that were equal to or greater than from core samples at depth may have been influenced by the lingering effects of spotty precipitation experienced at the field site during the period of investigation.

The calculated gravimetric water contents from the Arbuckle-Simpson Ranch site ranged from 7.69 to 36.7% (Figures A23 thru A27). The observed gravimetric water content generally increased with depth and correlated with changes in the grain size distribution. The calculated water content values near the bottom of at least one of the Arbuckle-Simpson Ranch sediment cores may be lower than conditions in the field appeared to indicate. A significant amount of water was observed to be pouring from the bottom of the ASR57.3m sediment core location as the sediment core was being extracted which would indicate that

saturated or near saturated conditions were present at the total depth of refusal. Water was not noted as pouring from any of the remaining sediment core bottoms in any significant amount although the bottoms of all of the sediment cores from the site appeared wet as they were extracted.

The volumetric water contents calculated for all sediment core samples except for Hatch core samples 001-048 ranged from 5.5 to 52.2%. The observed variations in volumetric water content with depth in general appeared similar to the variations observed in the gravimetric water content results over the same intervals. In general the observed variations in volumetric water content with depth appeared to respond to relative changes in both the gravimetric water content and porosity.

The calculated volumetric water contents for several of the sediment core samples were observed to be greater than the corresponding calculated porosity values yielding calculated water saturations that were as high as 152%. The anomalous water saturation values suggest the presence of errors in the volumetric water content and/or porosity calculations. Volumetric water contents that were too high and/or total porosities that were too low could have caused the anomalous water saturations.

The calculated volumes of the sediment core samples were relatively small (< 80 cm^3). Errors in the calculation of such relatively small sediment core sample volumes would have translated into errors in the volumetric water contents and associated water saturations that were potentially significant. Uncertainties surrounding the sediment core sample volume calculations appear

the most likely cause of errors in the volumetric water content and associated water saturation calculations. The uncertainties with the volume calculations and the observed anomalous water saturation values suggest that the water saturations calculated from the volumetric water content results may not be reliable.

An alternative to using the volumetric water content to calculate water saturation would be to use the gravimetric water content. The gravimetric water contents calculated on a mass basis would be considered a more accurate measure of relative water content than the volumetric water contents. A saturation ratio using the gravimetric water content (gravimetric saturation) would not provide an absolute measure of water saturation but would provide a relative and more reliable measure of water saturation in the sediment cores. Gravimetric saturation ratios were calculated for all of the sediment cores.

The specific retention of sediments increases with decreasing particle size (Fetter, 2001) thus a relationship between clay content and water saturation would be expected. The volumetric and gravimetric water saturations were plotted against clay content to determine the nature of the expected relationship (Figure 5.13a). The plots were also used to compare the volumetric and gravimetric water saturation results.

Similar patterns in the distribution of the data points can be seen in the plots of both saturation method results. The volumetric water saturation results (Figure 5.13a) show a weak direct relationship with clay content with an R^2 value of 0.2 for the trend line. Figure 5.13a also illustrates the uncertainties with the

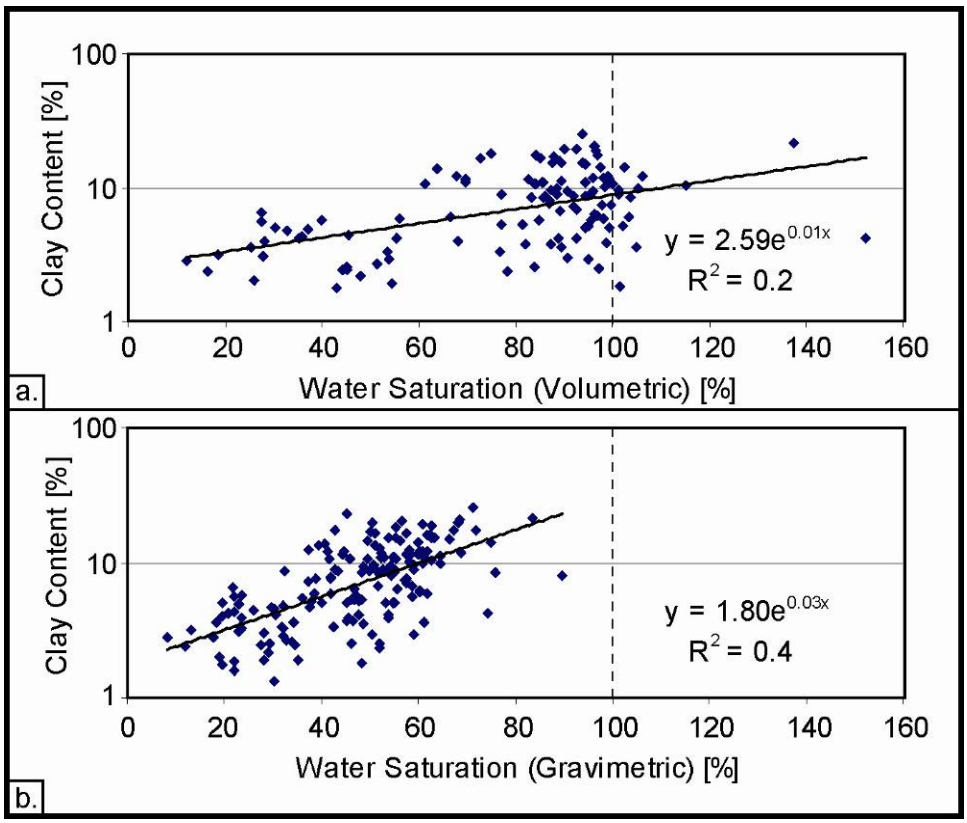

Figure 5.13. Relationship between clay content and water saturation (a) volumetric saturation relation (b) gravimetric saturation relation.

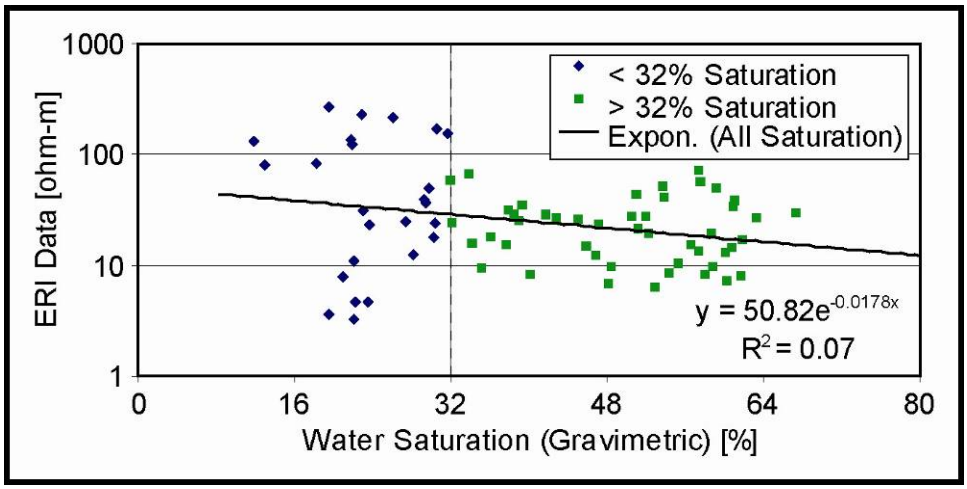

Figure 5.14 Relationship between surface ERI results and gravimetric water saturation.

volumetric results with the calculated water saturation values exceeding 100%. The plot of the gravimetric water saturation values in Figure 5.13b shows a stronger relationship with clay content with an R^2 value of 0.4 for the trend line.

The gravimetric water saturation values were plotted against the ERI results to determine if there was any observable relationship between water saturation and the electrical properties of the earth materials (Figure 5.14). The R^2 value of 0.07 for the trend line suggests that no relationship exists between water saturation and the electrical properties of the earth materials. The observed electrical resistivity values at water saturations < 32% appear relatively variable and range in value over about two orders of magnitude. The observed electrical resistivity values at water saturations > 32% appear to be less variable and range in value over about one order of magnitude.

5.10 Hydraulic Conductivity Calculations

Hydraulic conductivity, *K* [μm/s], values were empirically derived for 165 of 167 sediment core samples from the porosity and particle size analysis results using the Carmen-Kozeny and Fair-Hatch equations. The remaining two sediment core samples were from the Hatch site and were lost prior to the porosity and particle size analyses. Vertical hydraulic conductivity profiles were constructed for each sediment core (APPENDIX). Gaps observed in the vertical hydraulic conductivity profiles represent core intervals with no data due to the loss of data (Hatch site) or intervals of weathered rock in the sediment cores (Spears Ranch site). The range of *K* values from each method was observed to

Table 12. Hydraulic conductivity values of common earth materials [Modified after Weight and Sonderegger, 2001].

Material Type	Material	Hydraulic Conductivity Range (μm/s)
Unconsolidated	Unweathered marine clay	$8 \times 10^{-7} – 2 \times 10^{-3}$
	Clay	$1 \times 10^{-7} – 4.7 \times 10^{-3}$
	Silt, loess	$1 \times 10^{-3} – 20$
	Fine sand	0.2 – 200
	Medium sand	0.9 – 500
	Coarse sand	0.9 – 6000
	Gravel	300 – 30000
	Till	$8 \times 10^{-6} – 2$
Sedimentary rocks	Shale	$1 \times 10^{-7} – 2 \times 10^{-3}$
	Siltstone	$1 \times 10^{-5} – 1.4 \times 10^{-2}$
	Sandstone	$3 \times 10^{-4} – 6$
	Limestone, dolomite	$1 \times 10^{-3} – 6$
	Karst and reef limestone	1 – 20000

vary significantly between the field sites. All of the calculated hydraulic conductivity values fall within the range of values expected for the Earth materials encountered (Table 12).

The Hatch field site had the greatest observed range of *K* values of the three field sites for both methods. The Hatch site Carmen-Kozeny *K* values ranged from 0.006 to 38.7 μm/s and the Fair-Hatch *K* values ranged from 0.05 to 26.0 μm/s (Figures A1 thru A13). The Carmen-Kozeny *K* value of 38.7 μm/s calculated for Hatch core sample S047 from the HAT130.0m sediment core was the highest calculated hydraulic conductivity value from all of the sites. Hatch core sample S047 was from an interval that was composed of 90% sand with minor clay and silt components. The corresponding Fair-Hatch *K* value was 12.7 μm/s. The remaining Carmen-Kozeny *K* values from the Hatch site were < 8.0

μm/s. The Hatch sediment core sample S047 was the only sediment core sample from all three field sites to have a Carmen-Kozeny *K* value that was equal to or greater than the corresponding Fair-Hatch *K* value.

The Fair-Hatch *K* value of 26.0 μm/s calculated for Hatch core sample S026 from the HAT105.0m sediment core was the highest Fair-Hatch calculated hydraulic conductivity value from all of the sites. Hatch core sample S026 was from an interval that was composed of 70% sand with 28% silt and a minor clay component. The corresponding Carmen-Kozeny *K* value was 8.0 μm/s. The remaining Fair-Hatch *K* values from the Hatch site were ≤ 12.7 μm/s.

The observed range of *K* values from both methods at the Spears Ranch field site was significantly narrower than was observed at the Hatch site but broader than was observed at the Arbuckle-Simpson Ranch site. The Spears Ranch site Carmen-Kozeny *K* values ranged from 0.007 to 1.6 μm/s. The Spears Ranch site Fair-Hatch *K* values ranged from 0.05 to 5.2 μm/s (Figures A14 thru A22).

The observed range of *K* values from both methods at the Arbuckle-Simpson Ranch field site was the narrowest of the three field sites. The Arbuckle-Simpson Ranch site Carmen-Kozeny *K* values ranged from 0.008 to 0.5 μm/s. The Arbuckle-Simpson Ranch site Fair-Hatch *K* values ranged from 0.07 to 1.2 μm/s (Figures A23 thru A27). In general the observed K values from both methods were observed to be greater at the surface than at depth at each of the field sites. Trends, if any, observed with depth in the typical range of *K* values for

the soil types sampled by the sediment cores were also generally observed in the corresponding Carmen-Kozeny and Fair-Hatch results.

The Carmen-Kozeny and Fair-Hatch *K* results for each of the soil types encountered were plotted together along with the typical range of *K* values for the specific soil type encountered and the corresponding infiltration *K* results to facilitate the comparison of the hydraulic conductivity results from all three sources. In general the Carmen-Kozeny, Fair-Hatch, and infiltration experiment hydraulic conductivity values each varied over about one order of magnitude for each soil type. While some overlap was observed, the results from the Carmen-Kozeny and Fair-Hatch methods were observed to group separately.

In general, the Fair-Hatch *K* values corresponding to the Stephenville soil type from the Hatch site were generally observed to be on average about one order of magnitude less than would fall within the typical range of values associated with the Stephenville soil type (Figure 5.15). The Carmen-Kozeny *K* values were generally observed to be on average about two orders of magnitude less than would fall within the typical range of values associated with the Stephenville soil type. The infiltration experiment *K* results were observed to be on average about one order of magnitude less than the typical range of values associated with the Stephenville soil type at the surface and appeared to correspond more closely to the Fair-Hatch results than the Carmen-Kozeny results.

In general the Fair-Hatch *K* values corresponding to the Verdigris soil type from the Hatch site were observed to be about one order of magnitude less than

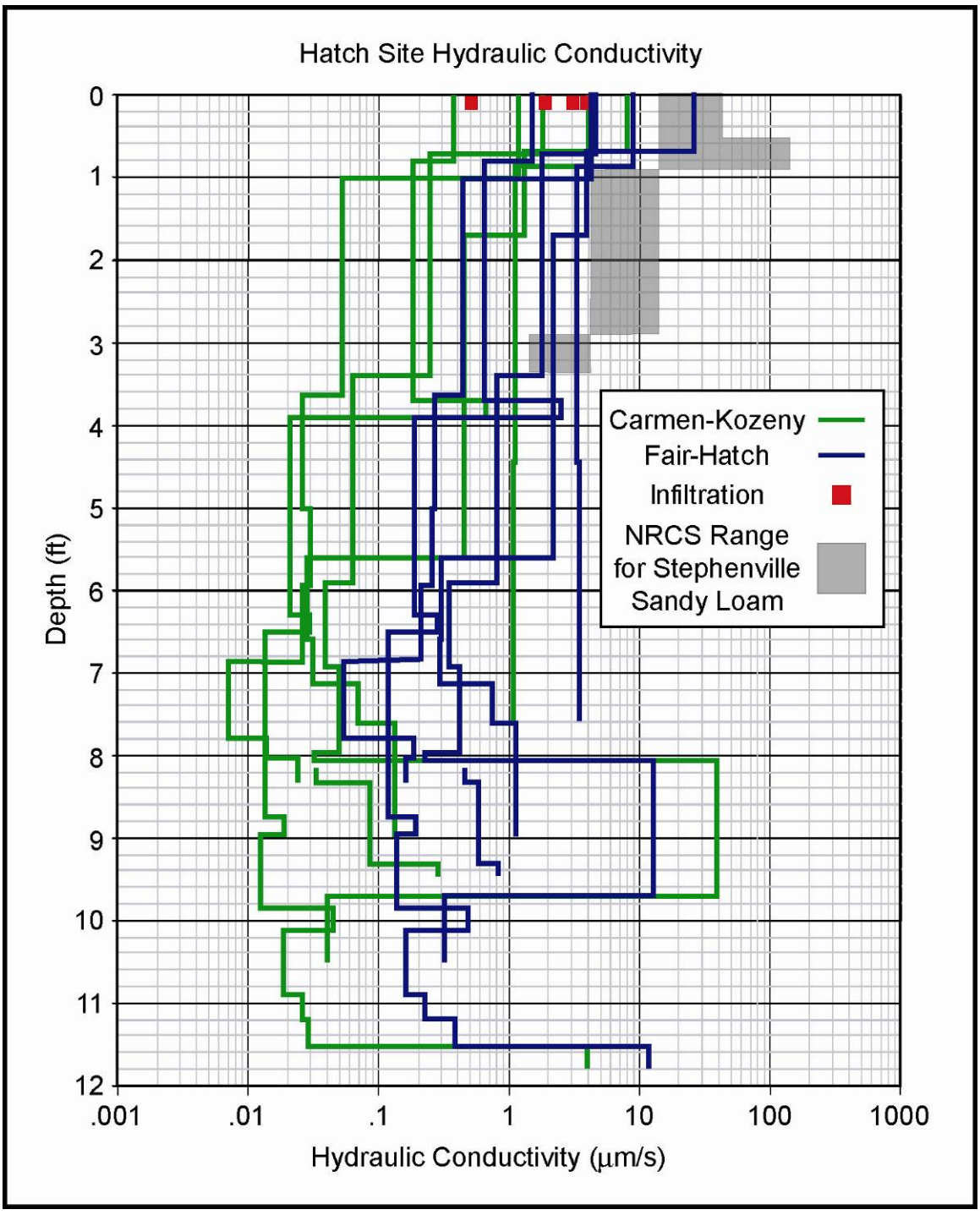

Figure 5.15. Hatch site hydraulic conductivity results from all methods for the Stephenville soil type.

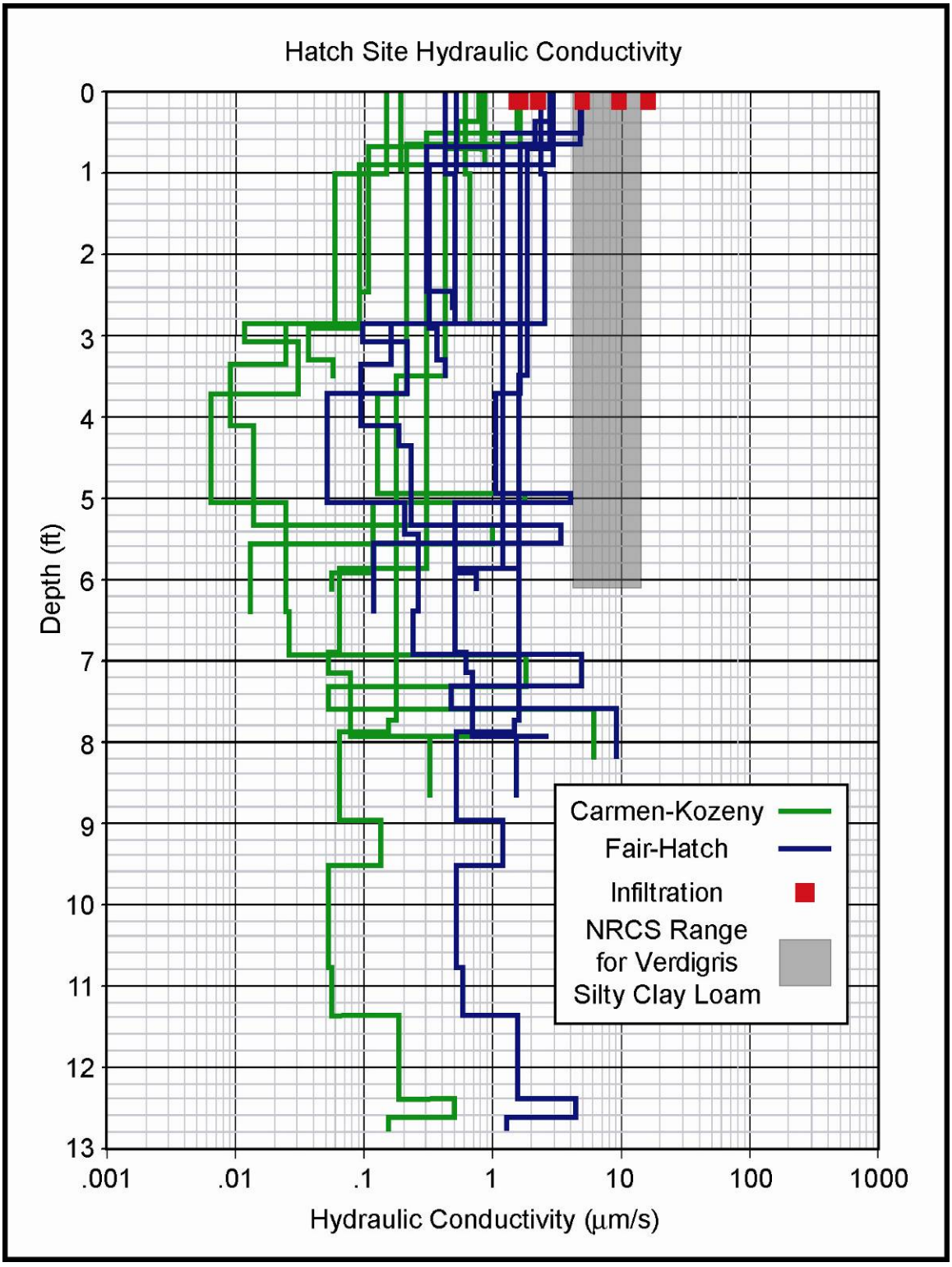

Figure 5.16. Hatch site hydraulic conductivity results from all methods for the Verdigris soil type.

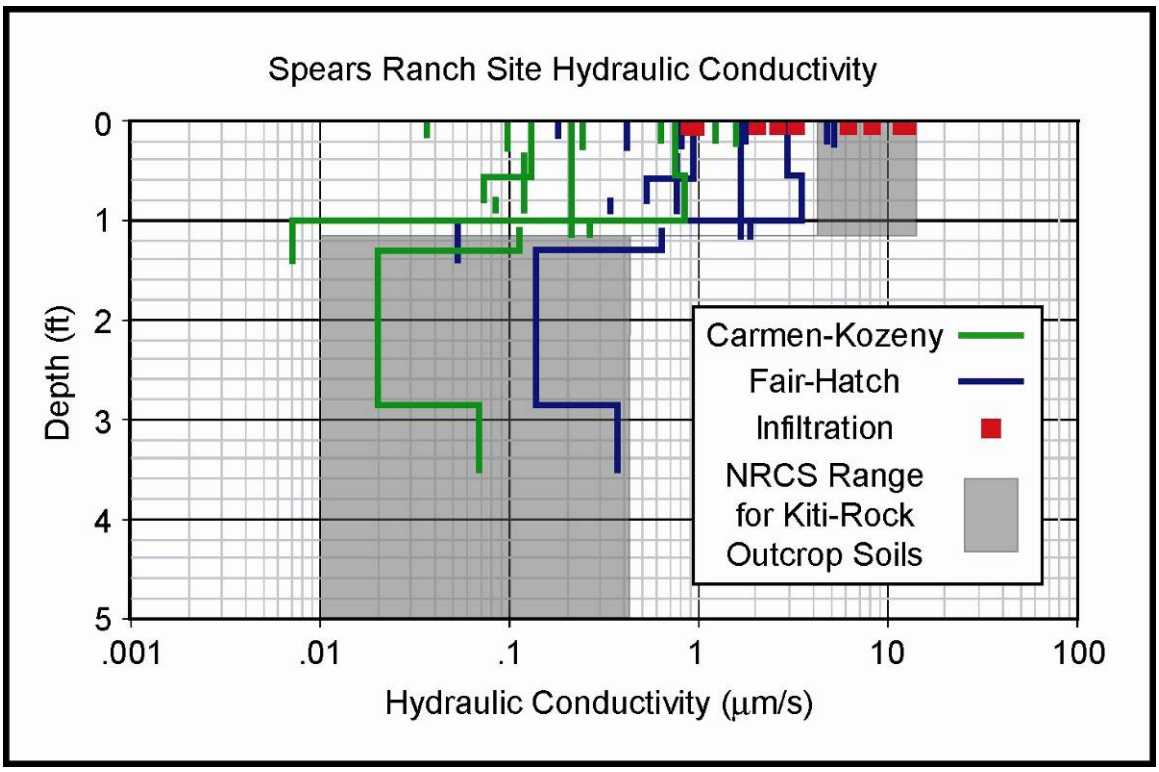

Figure 5.17. Spears Ranch site hydraulic conductivity results from all methods for the Kiti-Rock outcrop soil type.

the typical range of values associated with the Verdigris soil type (Figure 5.16). The Carmen-Kozeny *K* values were observed to be on average two orders of magnitude less than the typical range of values associated with the Verdigris soil type. The infiltration experiment *K* results agree fairly well with the typical range of values associated with the Verdigris soil type at the surface. Two of the infiltration experiment *K* values fell within the range of Fair-Hatch values.

In general the Fair-Hatch *K* values corresponding to the Kiti-Rock Outcrop soil type from the Spears Ranch site were about one order of magnitude less than the typical range of values associated with the soil type (Figure 5.17).

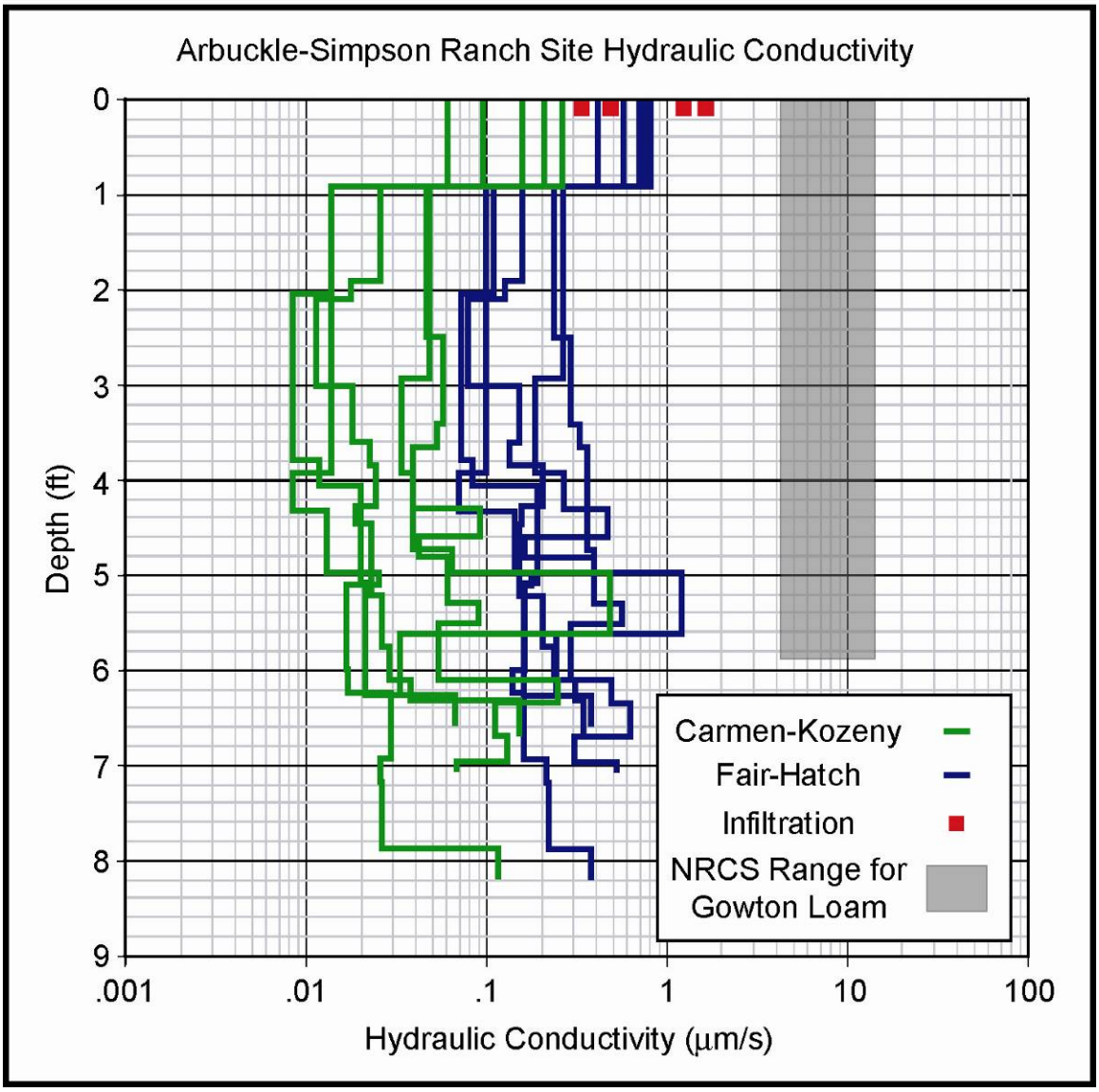

Figure 5.18. Arbuckle-Simpson Ranch site hydraulic conductivity results from all methods for the Gowton soil type.

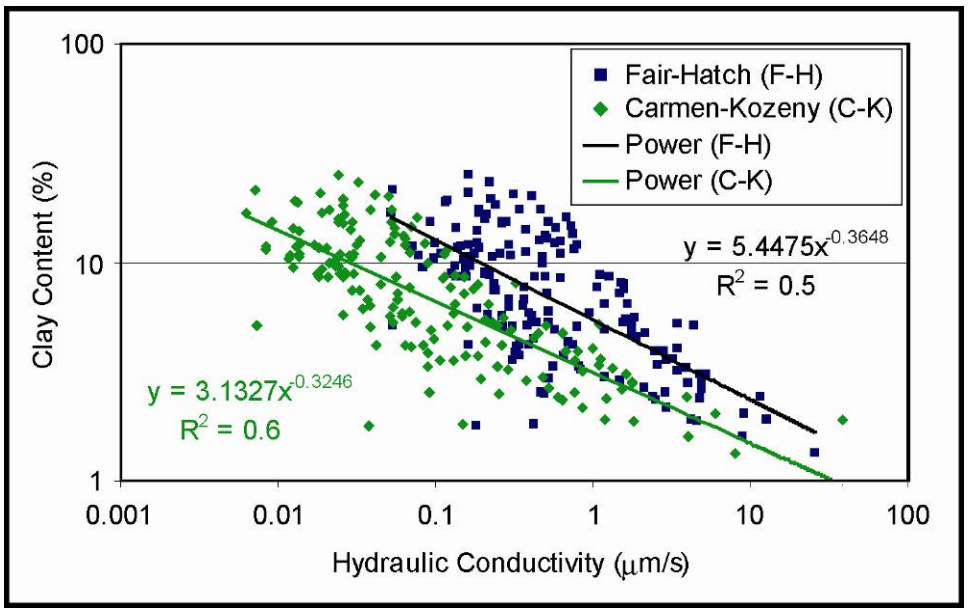

Figure 5.19. The relationship between the Fair-Hatch and Carmen-Kozeny hydraulic conductivity results and clay content.

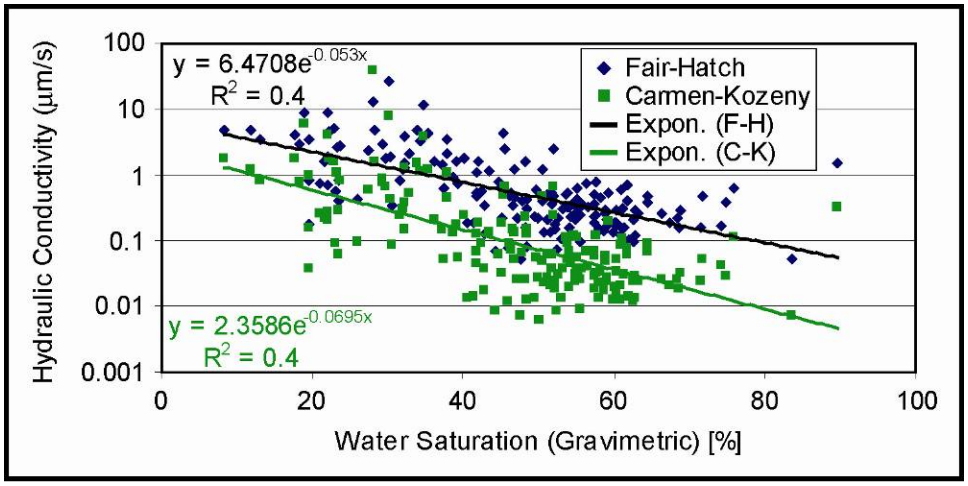

Figure 5.20. The relationship between the Fair-Hatch and Carmen-Kozeny hydraulic conductivity results and gravimetric water saturation.

The Carmen-Kozeny *K* values were about two orders of magnitude less than the typical range of values associated with the soil type. Three of the infiltration experiment *K* results were observed to agree well with the typical range of values associated with the Kiti-Rock Outcrop soil type at the surface. The remaining five infiltration experiment *K* values fell within the Fair-Hatch range of values.

The Fair-Hatch *K* values for the Gowton loam soil type from the Spears Ranch site were on average a little more than one order of magnitude less than the typical range of values associated with the Gowton loam soil type (Figure 5.18). The Carmen-Kozeny *K* values were a little more than two orders of magnitude less than the typical range for the soil type. The infiltration experiment *K* results were about one order of magnitude less than the typical range of values and corresponded more closely to the Fair-Hatch results than the Carmen-Kozeny results.

The hydraulic conductivity values from each method were expected to have an inverse relationship with increasing clay content (Figure 5.19). The Carmen-Kozeny method exhibited the stronger relationship of the two with an R^2 value of 0.6 for the trend line versus the R^2 value of 0.5 for the Fair-Hatch method. The Carmen-Kozeny method was expected to have the stronger relationship versus the clay content due to the differences in the way that each method accounts for grain size distribution in the equations. The hydraulic conductivity values for each method were compared to the gravimetric water saturation (Figure 5.20). The R^2 value of 0.4 for the trend line of both methods suggests that an inverse relationship exists.

CHAPTER VI

DISCUSSION

The following chapter will address each of the primary goals of the study. The discussion will begin evaluating the thickness of the epikarst zone. The discussion will examine the hydraulic properties of hydraulic conductivity and storativity of the epikarst zone. Finally the relationships between the electrical and hydraulic properties of the epikarst zone will be addressed.

6.1 Epikarst Thickness

In order to characterize the thickness of the epikarst zone of the Arbuckle-Simpson aquifer the approximate depth from the land surface to the top and the bottom of the epikarst zone had to be determined. The approximate depth to the top of the epikarst zone from the land surface was estimated from the direct push depth of refusal results. The depth to the bottom of the epikarst zone from the land surface was estimated from the ERI results.

Because direct push methods can only push pipe into unconsolidated earth materials, the direct push depth of refusal at each location would correspond to the approximate depth from the land surface to the top of the epikarst zone. The direct push depth of refusal would also correspond to the

approximate thickness of the soil zone. Considerable variation was observed in the direct push depths of refusal for each of the four soil types encountered (Tables 5 thru 7). The natural variability expected to be observed in soils could explain the variability observed in the soil mantle. The variability could also be due to the highly irregular weathering and solution features typical of karst topography. An anthropogenic component can also not be ruled out for each of the field sites. The average of the direct push depths of refusal for the four soil types encountered at the field sites ranged from 1.4 to 10.1 feet (Table 13).

A comparison was done in order to determine if the soil zone thickness estimations from the direct push depths of refusal results were comparable to the thicknesses of the soil types as defined in the NRCS Soil Survey database. The comparison was also done to determine whether it would be reasonable to use the soil thicknesses in the NRCS Soil Survey database for all of the soils mantling the epikarst over the aquifer. In general, the thicknesses of the soil types appear to correlate reasonably well with the average of the direct push depths of refusal.

An anomalous difference was observed between the published thickness of the Stephenville Fine Sandy Loam and corresponding average of the direct push depths of refusal at the Hatch site. Locally intense weathering of the epikarst could potentially account for the observed difference. A local thickening of the soil cover due to anthropogenic causes can not be ruled out due to a long history of dairy and beef cattle ranching at the Hatch site. The sediment core

Table 13. Summary epikarst thickness calculations.

Field Site	Soil Type	Average Direct Push Depth of Refusal (ft)	NRCS Thickness of Soils (ft)	Approximate Average Depth to Bottom of Epikarst (ft)	Approximate Epikarst Zone Thickness (ft)	Epikarst Zone/Soil Thickness Ratio (dim)	Depth to the Groundwater Table (ft)
Hatch	Verdigris Silty Clay Loam	6.5	6.0	53	47	7.8	80
	Stephenville Fine Sandy Loam	10.1	3.3	53	50	15.1	80
Spears Ranch	Kiti Very Flaggy Silt Loam	1.4	1.3	17	16	12.1	25
Arbuckle-Simpson Ranch	Gowton Loam	6.6	5.8	29	23	4.0	9

material identified as Stephenville Fine Sandy Loam may also be from a different soil type not identified as present in the area in the “sa_miads_soils” layer from the Arbuckle-Simpson Hydrology Study GIS dataset.

The ERI results were used in conjunction with the direct push depth of refusal results to electrically constrain the base of the soil zone at the field sites. The base of the soil zone at the Hatch and Arbuckle-Simpson Ranch field sites as constrained by the direct push depths of refusal correlate well with the 45 ohm-m contour line in the ERI data. The base of the soil zone at the Spears Ranch field site as constrained by the direct push depths of refusal generally correlated with the 160 ohm-m contour line. The discrimination of the electrical properties at the base of the soil zone would be problematic without the direct observations made possible by the direct push methods.

The approximate average depth to the bottom of the epikarst zone at each field site was estimated from the results of the ERI surveys. The electrical resistivity value that most closely approximated the transition from weathered to competent rock at the base of the epikarst zone was estimated from vertical 1-D profiles of the ERI data with elevation (depth) at each site (Figure 5.3). The approximate average depth from the land surface to the bottom of the epikarst zone was determined from the contour line corresponding to the electrical resistivity value.

At all three field sites the bottom of the epikarst was estimated as corresponding to the electrical resistivity value of 280 ohm-m (Figures 5.1, 5.4, and 5.5). The approximate average depth from the land surface to the bottom of

the epikarst zone estimated from the 280 ohm-m contour was observed to be highly variable between the field sites and ranged from 17 to 53 feet (Table 13). At the Hatch site the approximate average depth to the bottom of the epikarst was estimated to range between 9 and 139 feet with an average value of 53 feet. The approximate average depth to the bottom of the epikarst at the Spears Ranch site was estimated to range between 9 and 29 feet with an average value of 17 feet. The approximate average depth to the bottom of the epikarst at the Arbuckle-Simpson Ranch site was estimated to range between 22 and 43 feet with an average value of 29 feet.

The approximate thickness of the epikarst zone was calculated for the area under each soil type (Table 13). The typical thicknesses of the soil types as defined in the NRCS soil survey dataset were used in the calculations (Soil Survey Staff, 2005). The thickness of the epikarst zone was determined by subtracting the thickness of the soil type from the average depth to the bottom of the epikarst zone. At the Hatch site the approximate thickness of the epikarst was estimated to range between about 6 and 133 feet with an average value of 47 feet for the epikarst under the Verdigris soil type and 50 feet for the epikarst under the Stephenville soil type. The approximate thickness of the epikarst at the Spears Ranch site was estimated to range between 8 and 28 feet with an average value of 16 feet. The approximate thickness of the epikarst at the Arbuckle-Simpson Ranch site was estimated to range between 16 and 37 feet with an average value of 23 feet.

Because the formation of the epikarst and the soil mantle are controlled by the same environmental factors (Klimchouk, 2004) it would be reasonable to expect that a relationship might exist between the resulting thicknesses of each. The ratios of the approximate epikarst zone thicknesses to the typical thicknesses the soil types were calculated (Table 13). The calculated geometric mean value of the thickness ratios is 8.7, indicating that for a given soil thickness, the epikarst zone would be expected to be about nine times larger. In the absence of additional data, it would be reasonable to consider using the geometric mean value of the thickness ratios for the purpose of estimating the epikarst zone thickness under soils across the Hunton Anticline.

It would not however be reasonable to expect that in areas where the soil cover is negligible or absent that the epikarst is also negligible or absent. It would be more reasonable to expect that the epikarst thickness would not be significantly less than 9.0 feet thick when the soil thickness is less than one foot. As the soil thicknesses in the NRCS soils range from 0.0 to 7.2 feet for the area, the epikarst zone would then range in thickness from about 9.0 to over 60 feet.

The measured depth to the static water level ranged from 9.0 to about 80 feet at the field sites (Table 13). The static water level measured from wells at the Hatch and Spears Ranch sites was generally below the depth to the bottom of the epikarst zone. The static water level measured from each well represents an integrated measurement of the range of head over the total open interval within the well and thus may not accurately reflect the depth to the water table in the shallow subsurface.

The static water level estimated from the surface water elevation of the pond at the Arbuckle-Simpson Ranch site was close to the top of the epikarst zone. The presence of the static water level well within the epikarst at the Arbuckle-Simpson Ranch site may suggest that the processes responsible for the formation of epikarst in the unsaturated zone can persist into the phreatic zone. The pond at the Arbuckle-Simpson Ranch site was formed by the retention of spring water behind an embankment dam. The pond has been present at the site since at least 1967 as suggested by its presence on the USGS "Connerville, OK" quadrangle map. The proximity of the pond to the field site suggests that the artificially maintained water surface elevation of the pond may have exerted an anthropogenic influence on the local static water level.

6.2 Hydraulic Conductivity

Hydraulic conductivity values were estimated from the infiltration measurements and empirically derived from the direct push sediment core porosity and grain size distribution analyses results using the Fair-Hatch (Todd, 1959) and Carmen-Kozeny (Bear, 1988, c1972) equations. The experimentally derived *K* results were collectively compared along with the typical ranges of *K* values established for the soil types in the NRCS Soil Survey database (Soil Survey Staff, 2005). The comparison was accomplished in order to evaluate the reasonableness of the experimentally derived *K* results and to determine whether it would be reasonable and appropriate to use the established typical *K* ranges in

the NRCS Soil Survey database for all of the soil types represented in the Arbuckle-Simpson study area.

The hydraulic conductivity of soils is highly variable and can vary by more than a factor of ten within an area smaller than a square meter (Soil Survey Division Staff, 1993). The replication of hydraulic conductivity measurements (10 to 20 or more) would be required to achieve an adequate statistical distribution to arrive at a mean hydraulic conductivity for an area the size of an average plot (Reynolds et al., 2002b). In general the experimentally derived *K* results from each method and for each soil type encountered were observed to range in value over about one order of magnitude which would be considered reasonable given the natural variability of soils.

Several of the infiltration *K* results fell within the expected range for the identified soil types but the majority of the infiltration tests produced hydraulic conductivity values that were below the expected range by, on average, one order of magnitude (Figures 5.15 thru 5.18). Several of the Fair-Hatch *K* results fell within the expected range for the identified soil types but the majority of the Fair-Hatch calculations produced hydraulic conductivity values that were below the expected range by, on average, one order of magnitude. None of the Carmen-Kozeny *K* results fell within the expected range for the identified soil types. Several of the Carmen-Kozeny *K* results fell within the same range of values as the Fair-Hatch *K* results but the majority of the Carmen-Kozeny calculations produced hydraulic conductivity values that were below the expected range by, on average, two orders of magnitude.

The differences between the Fair-Hatch and Carmen-Kozeny hydraulic conductivity values are attributable to the differences in the way that each method accounts for grain size distribution in the equations. The effect of the particle size distribution on the value of hydraulic conductivity in the Carmen-Kozeny equation (Eq. 16) is represented by the effective grain size, d_e, which for this study is defined as d_{10} [μm] which is the size fraction that is 10% finer by mass (Weight and Sonderegger, 2001; Fetter, 2001). The choice of d_{10} as the effective grain size for the analyses may have been too small given the dominance of silt size particles in the majority of the sediment core samples. The use of a larger effective grain size would have resulted in *K* values that were more in agreement with the infiltration test and Fair-Hatch results.

Hydraulic conductivity measurements are scale dependent and increase with the scale of the measurement regardless of the method used (Rovey and Cherkauer, 1995). Both the infiltration tests and sediment core laboratory methods used in the analyses are very small scale measurements and were not expected to have sampled the full range of hydraulic properties at any of the field locations. Very small scale laboratory and infiltration measurements such as the methods used for this study can produce hydraulic conductivity values as much as two orders of magnitude less than the values produced by small scale field measurements like slug tests, and values that are as much as three orders of magnitude less than regional scale hydraulic conductivity values (Rovey and Cherkauer, 1995). Given the effect of scale on the hydraulic conductivity measurements, the experimentally derived *K* results appear to be in relatively

good agreement with the typical range of *K* values from the NRCS Soil Survey database for the soil types investigated. These results appear to suggest that it would be reasonable to apply the NRCS Soil Survey hydraulic conductivity values to all of the soil types in the study area.

6.3 Storativity

Storativity, *S* [dim], is a measure of the amount of water that can be stored by an aquifer (Fetter, 2001; Weight and Sonderegger, 2001). Storativity is defined by the equation

$$S = S_y + bS_s \qquad \text{(Eq. 19)}$$

where S_y [dim], is the specific yield, S_s [L^{-1}], is the specific storage, and *b* [L], is the saturated thickness of the aquifer. The specific or elastic storage component is a measure of the volume of water that an aquifer will yield from the compression of the aquifer skeleton. The specific storage component in an unconfined aquifer is usually very small compared to the specific yield and can be neglected. When the specific storage component is negligible, the storativity is commonly taken as equal to the specific yield. For this study the storativity of each of the soil types mantling the epikarst was taken as equal to the average calculated total porosity, Φ [dim], for each of the individual soil types (Table 14). The average total porosities were multiplied by the NRCS thicknesses of the soil types to provide an estimate of the storage potential in the soil mantle. The storage potential would be roughly equivalent to the depth of a lake storing the water in that zone, and ranges from 0.55-2.7 feet for the soil types studied.

Table 14. Storage property estimates for various components of the Arbuckle-Simpson Aquifer.

Field Site	Soil Type	NRCS Thickness of Soils (ft)	Average Porosity of Soils (dim)	Storage Potential of Soils (ft)	Approximate Epikarst Zone Thickness (ft)	Estimated Storativity of Epikarst (dim)	Storage Potential of Epikarst (ft)	Storage Potential of Mantled Epikarst (ft)
Hatch	Verdigris Silty Clay Loam	6.0	0.45	2.7	47	0.05	2.4	5
	Stephenville Fine Sandy Loam	3.3	0.46	1.5	50	0.05	2.5	4
Spears Ranch	Kiti Very Flaggy Silt Loam	1.3	0.42	0.55	16	0.05	0.8	1
Arbuckle-Simpson Ranch	Gowton Loam	5.8	0.35	2.0	23	0.05	1.2	3
							Approximate Arbuckle-Simpson Aquifer Thickness (ft)	3,500
							Approximate Arbuckle-Simpson Aquifer Storativity (dim)	0.002 - 0.014
							Approximate Arbuckle-Simpson Aquifer storage potential (ft)	7 - 49

The storativity of the bulk rock mass of the Arbuckle-Simpson aquifer has been estimated as between 0.002 and 0.014 (Christenson et al., 2007) (Table14). The average saturated thickness of the Arbuckle-Simpson aquifer has been estimated as ~3,500 feet. (Fairchild et al., 1990). The storage potential for the saturated thickness of the aquifer was estimated by multiplying the storativity of the bulk rock mass of the Arbuckle-Simpson aquifer by the average saturated thickness. The storage potential for the saturated thickness of the aquifer was estimated as approximately between 7 and 49 feet.

The storativity of the epikarst zone has been conservatively estimated as 0.05. This would be an order of magnitude above the storativity estimate of the primary aquifer. No studies that quantified this value better than estimating it as 1-2 orders of magnitude higher than the bedrock are known. Additionally, as a conservative estimate, it is an order of magnitude below the storage in the soil zone. The storage potential for the epikarst zone was estimated by multiplying the storativity of the epikarst zone by the epikarst zone thickness for each soil type (Table 14).

Using conservative estimates for storage in the soil and epikarst domains, the total storage in these areas was estimated to be the same order of magnitude as the entire remainder of the aquifer. The true values may be 2-5 times higher depending on the variability of determining storage in the epikarst zone. This would make storage in the shallow epikarst zone similar to the aquifer storage parameters and may influence the functioning of the aquifer.

6.4 Electrical and Hydraulic Property Relationships

The electrical resistivity and hydraulic conductivity values were analyzed to determine if a relationship could be determined. The electrical resistivity and hydraulic conductivity values were each observed to generally vary within about one order of magnitude at each field site. Both direct and inverse apparent relationships were observed in the vertical electrical resistivity and hydraulic conductivity profiles constructed for each sediment core (APPENDIX).

The ERI data were compared to the hydraulic conductivity data to observe if any relationship could be determined to exist between the two properties (Figure 6.1a). The data from the Carmen-Kozeny and Fair-Hatch methods provided very similar and overlapping results and for clarity only the Fair-Hatch results are plotted. The R^2 value of 0.03 for the trend line through the points appears to suggest that no clear relationship exists between the electrical and hydraulic properties for the core materials extracted from the field sites. The ERI versus *K* results were analyzed with respect to clay content and water saturation to determine if either factor exerted a control on the results. No data was collected on the water or soil chemistry so those factors could not be analyzed.

The ERI versus Fair-Hatch hydraulic conductivity results were plotted with respect to clay contents of < 8% and > 8% (Figure 6.1b). No apparent relationship (R^2 = 0.004) was observed between electrical resistivity and hydraulic conductivity for the 53% of the sediment core samples with clay content < 8%. A direct relationship (R^2 = 0.4) was observed between electrical resistivity and hydraulic conductivity for the 47% of the sediment core samples with clay

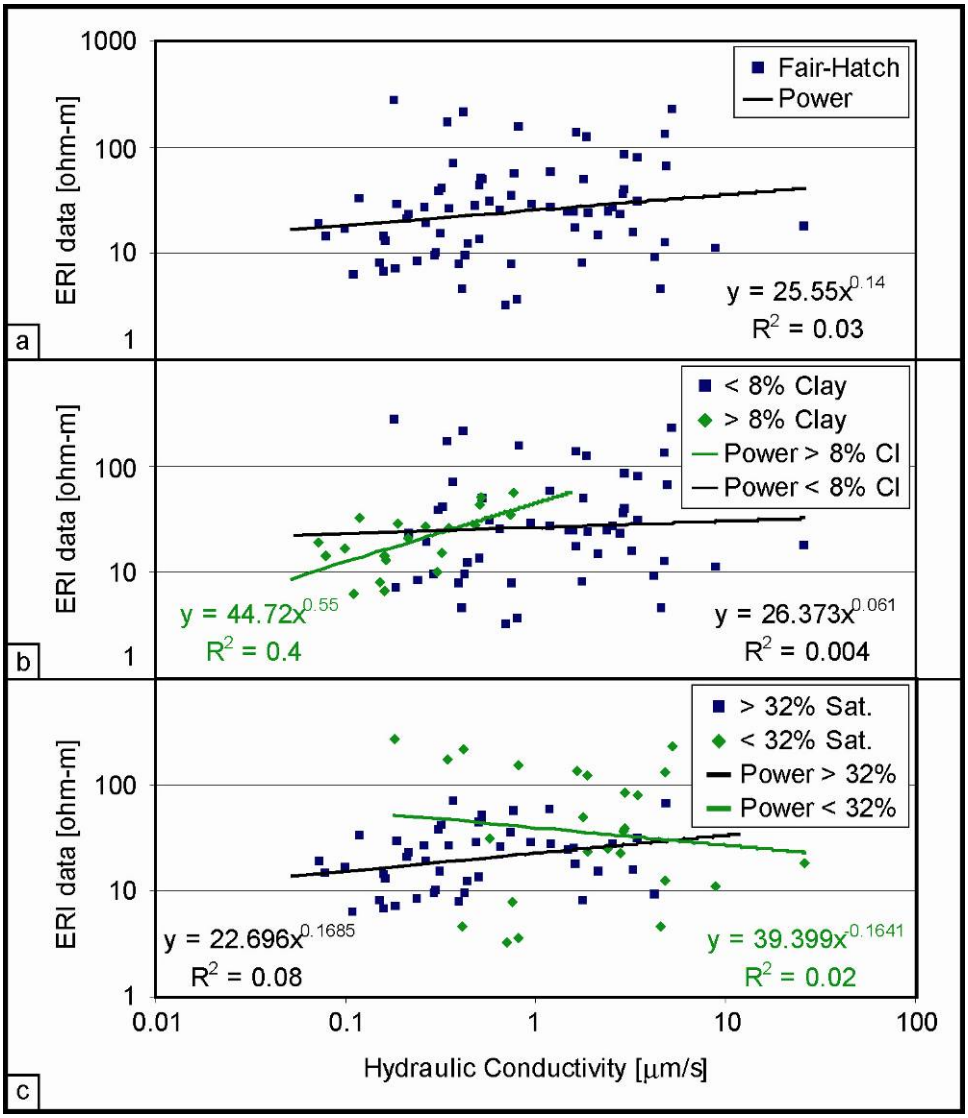

Figure 6.1. The relationship between the Surface electrical resistivity and Fair-hatch hydraulic conductivity results (a) overall relation (b) relation with respect to clay content (c) relation with respect to gravimetric water saturation.

content > 8%. Clay content was shown to have an inverse relationship with hydraulic conductivity (Figure 5.19) and a weak direct relationship with electrical resistivity when clay content was > 8% (Figure 5.12b) so a direct relationship between electrical resistivity and hydraulic conductivity was expected.

The ERI versus Fair-Hatch hydraulic conductivity results were plotted with respect to water saturations of < 32% and > 32% (Figure 6.1c). No apparent relationship was observed between the electrical resistivity and hydraulic conductivity values with respect to water saturation. Gravimetric water saturation was shown to have an inverse relationship with hydraulic conductivity (Figure 5.20). The ERI data did not show a relationship with water saturation although the electrical resistivity values did appear to be somewhat constrained for water saturation values > 32% (Figure 5.14). The decrease in electrical variability at water saturations > 32% observed in Figure 5.14 may indicate that dielectric conduction is significant in sediments when water saturation is < 32% but when water saturation is > 32% electrolytic conduction becomes more important.

The properties of moisture content, porosity, and particle size distribution including clay content were observed to be highly variable within each soil type and could be equally variable within each sediment core. The degree of variability observed in the soils mantling the epikarst may have been too great to permit the discrimination of a quantifiable relationship given the methods used for the analysis. The determination of water and soil chemistry parameters on the sediment core samples may have provided the additional information necessary to quantify a relationship.

The apparent absence of a quantifiable relationship between the electrical resistivity and hydraulic conductivity values of the sediment core material may also be the result of the effects of the different scales of the measurements. The ERI data were collected at a much larger scale than either the direct push EC

data or the sediment core sampling. Each data point in the ERI data reflects the effective electrical resistivity value of an area that is large relative to the other datasets and does not capture the variability observed in the smaller scale datasets.

6.5 Future work

The results from this study provide information on the thickness of the mantled epikarst of the Arbuckle-Simpson aquifer which suggest that the epikarst thickness is approximately 9 times thicker than the soil zone. The data for this study were collected from locations possessing a variety of soil landscapes. The underlying geology at every location was the West Spring Creek Formation. Future work would include the investigation of the mantled epikarst in areas underlain by other formations within the Arbuckle and Simpson Groups to determine if the observed epikarst/ soil zone thickness relationship holds true for other geologic units within the aquifer.

An apparent fault zone was observed to be crossed by the ASE5.00B ERI survey from the Arbuckle-Simpson Ranch site (Figure 5.5). No direct push or infiltration data was collected over the apparent fault zone. Future work would include the investigation of the electrical and hydraulic properties of the mantled epikarst across a fault zone.

CHAPTER VII

CONCLUSIONS

The mantled epikarst of the Arbuckle-Simpson aquifer in south central Oklahoma was characterized in terms of thickness, the hydraulic properties of hydraulic conductivity and storativity, and electrical resistivity at three field sites. A summary table of the major findings has been provided for each field site (Tables 15 – 17). The properties of hydraulic conductivity and electrical resistivity were also evaluated to determine any relationship existed.

The thickness of the soil zone at each of the field sites was estimated from the direct push results. The thicknesses of the four soil types examined at the field sites were derived from direct push depths of refusal and were found to correlate with the soil thicknesses available from the NRCS Soil Survey database (Tables 15 – 17). This finding indicates that it would be reasonable to apply the NRCS soil thicknesses to all of the soil types mantling the epikarst in the study area.

The thickness of the epikarst zone at each field site was estimated from the ERI and direct push results (Tables 15 – 17). The bottom of the epikarst zone was estimated to coincide with the electrical resistivity value of 280 ohm-m at all three field sites and the depth to the bottom of the epikarst zone was

Table 15. Summary of the Hatch site findings

HATCH FIELD SITE	
GEOPHYSICS	
Electrical Resistivity Imaging	
Scale of measurement (electrode spacing)	16.4 ft (5.0 m)
Total range	4.3 – 7,300 ohm-m
ERI range: soil zone	< 45 ohm-m
ERI range: epikarst zone	45 – 280 ohm-m
Eri range: bedrock	> 280 ohm-m
Direct Push Electrical Conductivity	
Total range	0.1 – 7,100 ohm-m
HYDRAULICS BY SOIL TYPE	
Verdigris Soil Type	
Direct push depth of refusal range	0.9 – 12.8 ft
Direct push depth of refusal average	6.5 ft
NRCS soil thickness	6.0 ft
Porosity value range	20.9 – 58.7%
Porosity value average	45.0%
Hydraulic conductivity: infiltration tests	1.6 – 16.2 µm/s
Hydraulic conductivity: Fair-Hatch	0.05 – 9.1 µm/s
Hydraulic conductivity: NRCS	4.2 – 14.1 µm/s
ERI epikarst zone thickness range	6 – 133 ft
ERI epikarst zone thickness average	47 ft
Epikarst zone/ soil zone thickness ratio	7.8
Estimated epikarst zone storativity	0.05
Mantled epikarst storage potential	5 ft
Stephenville Soil Type	
Direct push depth of refusal range	8.3 – 11.8 ft
Direct push depth of refusal average	10.1 ft
NRCS soil thickness	3.3 ft
Porosity value range	31.5 – 56.0%
Porosity value average	45.7%
Hydraulic conductivity: infiltration tests	0.5 – 4.0 µm/s
Hydraulic conductivity: Fair-Hatch	0.05 – 26.0 µm/s
Hydraulic conductivity: NRCS	1.4 – 141.1 µm/s
ERI epikarst zone thickness range	6 – 133 ft
ERI epikarst zone thickness average	50 ft
Epikarst zone/ soil zone thickness ratio	15.2
Estimated epikarst zone storativity	0.05
Mantled epikarst storage potential	4 ft

Table 16. Summary of the Spears Ranch site findings

SPEARS RANCH FIELD SITE	
GEOPHYSICS	
Electrical Resistivity Imaging	
Scale of measurement (electrode spacing)	8.2 ft (2.5 m)
Total range	61 – 569 ohm-m
ERI range: soil zone	< 160 ohm-m
ERI range: epikarst zone	160 – 280 ohm-m
ERI range : bedrock	> 280 ohm-m
Direct Push Electrical Conductivity	
Total range	0.1 – 8,300 ohm-m
HYDRAULICS BY SOIL TYPE	
Kiti Soil Type	
Direct push depth of refusal range	0.2 – 4.4 ft
Direct push depth of refusal average	1.4 ft
NRCS soil thickness	1.3 ft
Porosity value range	16.9 – 58.5%
Porosity value average	42.3%
Hydraulic conductivity: infiltration tests	0.9 – 12.7 μm/s
Hydraulic conductivity: Fair-Hatch	0.05 – 5.2 μm/s
Hydraulic conductivity: NRCS	0.01 – 14.1 μm/s
ERI epikarst zone thickness range	8 – 28 ft
ERI epikarst zone thickness average	16 ft
Epikarst zone/ soil zone thickness ratio	12.3
Estimated epikarst zone storativity	0.05
Mantled epikarst storage potential	1 ft

estimated from the 280 ohm-m electrical contour line. The thickness of the epikarst zone was found to vary considerably across and between the field sites. The epikarst thickness at the Hatch site ranged between 6 and 133 feet with an average thickness of 47 feet for the Verdigris soil type and 50 feet for the Stephenville soil type. At the Spears Ranch site, the epikarst ranged in thickness from 8 to 28 feet with an average thickness of 16 feet for the Kiti soil type. The epikarst thickness at the Arbuckle-Simpson Ranch site ranged from16 to 37 feet

Table 17. Summary of the Arbuckle-Simpson Ranch site findings

ARBUCKLE-SIMPSON RANCH FIELD SITE	
GEOPHYSICS	
Electrical Resistivity Imaging	
Scale of measurement (electrode spacing)	16.4 ft (5.0 m)
Total range	8.6 – 3,500 ohm-m
ERI range: soil zone	< 45 ohm-m
ERI range: epikarst zone	45 – 280 ohm-m
ERI range: bedrock	> 280 ohm-m
Direct Push Electrical Conductivity	
Total range	3.9 – 500 ohm-m
HYDRAULICS BY SOIL TYPE	
Gowton Soil Type	
Direct push depth of refusal range	5.0 – 8.2 ft
Direct push depth of refusal average	6.6 ft
NRCS soil thickness	5.8 ft
Porosity value range	22.6 – 48.5%
Porosity value average	35.1%
Hydraulic conductivity: infiltration tests	0.3 – 1.7μm/s
Hydraulic conductivity: Fair-Hatch	0.1 – 1.2 μm/s
Hydraulic conductivity: NRCS	4.2 – 14.1 μm/s
ERI epikarst zone thickness range	16 – 37 ft
ERI epikarst zone thickness average	23 ft
Epikarst zone/ soil zone thickness ratio	4.0
Estimated epikarst zone storativity	0.05
Mantled epikarst storage potential	3 ft

with an average thickness of 23 feet. The epikarst zone was highly variable in thickness across the aquifer.

Ratios, constructed between the thickness of the epikarst zone and the thickness of the soil zone, were used to evaluate the relationship between the epikarst and the soil (Tables 15 – 17). The epikarst zone/ soil thickness ratios for the soil types at the Hatch site were 7.8 for the Verdigris soil type and 15.1 for the Stephenville soil type. The ratio for the Kiti soil type at the Spears Ranch site was 12.1 and the ratio for the Gowton soil type at the Arbuckle-Simpson Ranch

site was 4.0. The geometric mean of the epikarst zone/ soil thickness ratios was 8.7 which implies that the epikarst zone across the Arbuckle-Simpson aquifer is approximately nine times thicker than the soil zone for all of the soil types mantling the epikarst. These results indicate that the average epikarst zone ranges in thickness from approximately 9 to 60 feet, but deeper depths are expected in local areas.

The hydraulic conductivity results from the infiltration test and Fair-Hatch methods are consistent with the expected values for the earth materials present at the field sites (Tables 15 – 17). The hydraulic conductivity results for the Verdigris soil type ranged from 1.6 to 16.2 μm/s for the infiltration tests and from 0.05 to 9.0 μm/s for the Fair-Hatch results. The hydraulic conductivity results for the Stephenville soil type ranged from 0.5 to 4.0 μm/s for the infiltration tests and from 0.05 to 26.0 μm/s for the Fair-Hatch results. The hydraulic conductivity results for the Kiti soil type ranged from 0.9 to 12.7 μm/s for the infiltration tests and from 0.05 to 5.2 μm/s for the Fair-Hatch results. The hydraulic conductivity results for the Gowton soil type ranged from 0.3 to 1.7 μm/s for the infiltration tests and from 0.1 to 1.2 μm/s for the Fair-Hatch results. The analysis methods used resulted in hydraulic conductivity values that were smaller than larger scale field scale measurements. The results indicate that it would be reasonable to apply the hydraulic conductivity values available NRCS Soil Survey database for the soils mantling the epikarst. The hydraulic conductivity of the soil zone is important for understanding the recharge potential.

The storativity of the epikarst zone was conservatively estimated as 0.05 which is an order of magnitude above the storativity estimate of the primary aquifer and an order of magnitude below the storage in the soil zone (Tables 15 – 17). The results indicate that the storage potential of the mantled epikarst ranges from 1 to 5 feet for the areas investigated. The storage potential for the saturated thickness of the aquifer was estimated as between 7 and 49 feet. These results indicate that the storage potential for the mantled epikarst is on the same order of magnitude as in the aquifer. These results characterizing the epikarst in terms of thickness, hydraulic conductivity, and storage may influence transient hydrologic models of the Arbuckle-Simpson aquifer.

The results did not find a clear overall relationship between the electrical resistivity and hydraulic conductivity values of the unsaturated soil zone material. The results indicate that a direct relationship between the electrical resistivity and hydraulic conductivity values does exist when the clay content of the soil material analyzed was greater than 8%. No relationship was observed for the 53% of the sediment core samples analyzed where clay content was less than 8%. These results imply that for the unsaturated materials examined significant clay content may be required to establish a relationship between electrical resistivity and hydraulic conductivity. These results may also imply that the degree of variability in the electrical and hydraulic properties of the unsaturated sediments in a fractured karst setting is too great for the establishment of a meaningful relationship.

REFERENCES

Allen, T., 1981, Particle size measurement, third edition: Chapman and Hall, New York, 678 p.

Archie, G. E., 1942, The electrical resistivity log as an aid in determining some reservoir characteristics: Trans. AIME, v. 146, pp. 54-62. Reprinted in SPE Reprint Series, 1986, v. 21, pp. 310-4.

Asquith, G., and D. Krygowski, 2004, Basic relationships of well log interpretation: in G. Asquith and D. Krygowski, Basic well log analysis: AAPG Methods in Exploration, no. 16, pp. 1-20.

Bear, J., 1988, c1972, Dynamics of fluids in porous media: Dover Pub., Inc., New York, 764 p.

Beuselinck, L., G. Govers, J. Poesen, G. Degraer, and L. Froyen, 1998, Grain-size analysis by laser diffractometry: comparison with the sieve-pipette method: Catena Giessen, v. 32, no. 3-4, pp. 193-208.

Biella, G., A. Lozej, and I. Tabacco, 1983, Experimental study of some hydrogeophysical properties of unconsolidated porous media: Ground Water, v. 21, no. 6, pp. 741-51.

Blott, S. J., D. J. Croft, K. Pye, S. E. Saye, and H. E. Wilson, 2004, Particle size analysis by laser diffraction: In K. Pye and D. J. Croft (Eds.), Forensic Geoscience; Principles, Techniques and Applications, Geological Society of London, Special Publications, v. 232, pp. 63-73.

Bodhinayake, W., C. S. Bing, and K. Noborio, 2004, Determination of hydraulic properties in sloping landscapes from tension and double-ring infiltrometers: Vadose Zone Journal, v. 3, no. 3, pp. 964-970.

Bosak, P., and V. Benes, 2003, Geophysical characteristics of epikarst: case studies from Zagros Mts. (Iran) and the Koneprusy region (Czech Republic): Acta Carsologica, v. 32, no. 2, pp. 255-67.

Charbeneau, R. J., 2000, Groundwater hydraulics and pollutant transport: Prentice – Hall, Inc., Upper Saddle River, New Jersey, 593 p.

Christenson, S., N. Osborn, and C. R. Neel, 2007, Groundwater hydrology of the Arbuckle-Simpson aquifer, Oklahoma Water Research Symposium, Oklahoma City, OK, Oct 23-25, 2007.

Cilas, 2008, Laser particle size analyzer Cilas 1180 operating specifications [Online WWW]. Available URL: "http://www.cilasus.com/analyzers/f1180.html" [Accessed 05 February 2008].

Cilas, 2004, Particle size analyzer: Cilas 920, 930e, 1064 & 1180 user manual: version NT-1503192-31, issue September 2004, pp. 81.

Curtis, B., and W. E. Kelly, 1990, Resistivity-recharge relationships—field study: Journal of Hydrology, v. 118, no. 1-4, pp. 39-53.

Environmental Protection Agency, 1989, Arbuckle-Simpson aquifer of south central Oklahoma sole source aquifer; final determination: Federal Register, v. 54, no. 184, pp. 39230.

Eshel, G., G. J. Levy, U. Mingelgrin, and M. J. Singer, 2004, Critical evaluation of the use of laser diffraction for particle-size distribution analysis: Soil Science Society of America Journal, v. 68, no. 3, pp. 736-43.

Fairchild, R. W., R. L. Hanson, and R. E. Davis, 1990, Hydrology of the Arbuckle mountains area, south-central Oklahoma: Oklahoma Geological Survey, Circular 91, 112 p.

Fetter, C. W., 2001, Applied hydrogeology, 4th edition: Prentice-Hall, Upper Saddle River, New Jersey, 598 p.

Gee, G. W., and J.W. Bauder, 1986, Particle-size analysis: In R. Klute (ed.), Methods of soil analysis, Part 1. Physical and mineralogical methods: Agronomy Monograph no. 9, 2nd edition, SSSA Madison Wisconsin, pp. 383-411.

Geoprobe, 2006, Geoprobe DT22 dual tube soil sampling system: standard operating procedure, Technical Bulletin No. MK3140. Geoprobe Systems, Salina, Kansas.

Giancoli, D. C., 1995, Physics: principles with applications, 4th edition: Prentice Hall, Englewood Cliffs, New Jersey, 1020 p.

Gorman, T., and W. E. Kelly, 1990, Electrical-hydraulic properties of unsaturated Ottawa sands: Journal of Hydrology, v. 118, pp. 1-18.

Ham, W. E., 1969, Regional geology of the Arbuckle Mountains, Oklahoma: Guide book - Oklahoma Geological Survey, v. 17, 52 p.

Heigold, P. C., R. H. Gilkeson, K. Cartwright, and P. C. Reed, 1979, Aquifer transmissivity from surficial electrical methods: Ground Water, v. 17, no. 4, pp. 338-45.

Huntley, D., 1986, Relations between permeability and electrical resistivity in granular aquifers: Ground Water, v. 24, no. 4, pp. 466-74.

Jones, P. H., and T. B. Buford, 1951, Electric logging applied to ground-water exploration: Geophysics, v. 16, no. 1, pp. 115-39.

Keller, G. V., and F. C. Frischknecht, 1966, Electrical methods in geophysical prospecting: Pergamon, New York, p. 517.

Kelly, W. E., and P. F. Reiter, 1984, Influence of anisotropy on relations between electrical and hydraulic properties of aquifers: Journal of hydrology, v. 74, no. 3-4, pp. 311-21.

Klimchouk, A., 2004, Towards defining and delimiting and classifying epikarst: Its origin, and variants of geomorphic evolution: In W. K. Jones, D. C. Culver, and J. Herman (Eds.), Karst Waters Institute Special Publication, v. 9, pp. 13-35: Republished (modified), 2004, in Speleogenesis and Evolution of Karst Waters, v. 2, no. 1, pp. 1-13.

Kosinski, W. K., and W. E. Kelly, 1981, Geoelectric soundings for predicting aquifer properties: Ground Water, v. 19, no. 2, pp. 163-71.

Kwader, T., 1985, Estimating aquifer permeability from formation resistivity factors: Ground Water, v. 23, no. 6, pp. 762-6.

Lindsay, P. J., J. B. Percival, A. C. Tsai, and M. H. M. Wygergangs, 1998, Investigation of automated particle size analysis techniques: In Current Research 1998-E; Geological Survey of Canada, pp. 173-82.

Mazac, O., W. E. Kelly, and I, Landa, 1985, A hydrophysical model for relations between electrical and hydraulic properties of aquifers: Journal of Hydrology, v. 79, no. 1-2, pp. 1-19.

McCave, I. N., R. J. Bryant, H. F. Cook, and C. A. Coughanowr, 1986, Evaluation of a laser-diffraction analyzer for use with natural sediments: Journal of Sedimentary Petrology, c. 56, no. 4, pp. 561-4.

Oklahoma State Senate, 2003, Senate Bill 288: 82 Oklahoma Statutes.

Oklahoma Water Resources Board, 2008, Outcrop area of Arbuckle-Simpson aquifer in Oklahoma [jpeg]. [Online WWW]. Available URL: "http://www.owrb.ok.gov/studies/groundwater/arbuckle_simpson/outcrop.php" [Accessed 28 March 2008].

Perrin, J., P-Y. Jeannin, and F. Zwahlen, 2003, Epikarst storage in a karst aquifer: a conceptual model based on isotopic data, Milandre test site, Switzerland: Journal of Hydrology, v. 279, no. 1-4, pp. 106-24.

Reynolds, J. M., 1997, An introduction to applied and environmental geophysics: John Wiley & Sons Ltd., New York, 796 p.

Reynolds, W. D., D. E. Elrick, and E. G. Youngs, 2002a, The soil solution phase. Ring or cylinder infiltrometers (vadose zone): In J. H. Dane, and G. C. Topp (eds.), Methods of soil analysis, Part 4. Physical methods, Agronomy Monograph no. 5, SSSA Madison Wisconsin, p. 818-20.

Reynolds, W. D., D. E. Elrick, and E. G. Youngs, 2002b, The soil solution phase. Single-ring and double- or concentric-ring infiltrometers: In J. H. Dane, and G. C. Topp (eds.), Methods of soil analysis, Part 4. Physical methods, Agronomy Monograph no. 5, SSSA Madison Wisconsin, p. 821-24.

Reynolds, W. D., D. E. Elrick, E. G. Youngs, and A. Amoozegar, 2002c, The soil solution phase. Field methods (vadose and saturated zone techniques): In J. H. Dane, and G. C. Topp (eds.), Methods of soil analysis, Part 4. Physical methods, Agronomy Monograph no. 5, SSSA Madison Wisconsin, pp. 817.

Rovey, C. W.,and D. S. Cherkauer, 1995, Scale dependency of hydraulic conductivity measurements: ground Water, v. 33, No. 5, pp. 769-80.

Rust, W.M., 1938, A historical review of electrical prospecting methods: Geophysics, v. 3, no. 1, pp. 1-6.

Sample, M. A., and T. Halihan, 2004, A new method for electrical imaging of the Arbuckle-Simpson aquifer, Oklahoma: Geological Society of America Abstracts with Programs, v. 36, no. 5, pp. 571.

Singh, K. P., 2005, Nonlinear estimation of aquifer parameters from surficial resistivity measurements: Hydrology and Earth System Sciences Discussions, v. 2, pp. 917-38.

Soil Survey Staff, 2005, Natural Resources Conservation Service, United States Department of Agriculture. Soil surveys of Atoka, Carter, Coal, Garvin, Johnston, Marshall, Murray, and Pontotoc Counties, Oklahoma [Online WWW]. Available URL: "http://soildatamart.nrcs.usda.gov/Survey.aspx?State=OK" [Accessed 20 December 2005].

Soil Survey Division Staff, 1993, Soil survey manual: Soil Conservation Service, U.S. Department of Agriculture Handbook 18, 437 p.

Sperazza, M., J. N. Moore, and M. S. Hendrix, 2004, High-resolution particle size analysis of naturally occurring very vine-grained sediment through laser diffractometry: Journal of Sedimentary Research, v. 74, no. 5, pp. 736-43.

Sri Niwas, and O. A. L. de Lima, 2003, Aquifer parameter estimation from surface resistivity data: Ground Water, v. 41, no. 1, pp. 94-9.

Telford, W. M., L. P. Geldart, R. E. Sheriff, 1990, Applied geophysics, 2nd edition: Cambridge University Press, New York, 770 p.

Todd, D. K., 1959, Ground water hydrology: John Wiley & Sons, Inc., New York, 336 p.

U.S. Department of Agriculture; Natural Resources Conservation Service, 2007, National Soil Survey Handbook, title 430-VI: [Online] Available: http://soils.usda.gov/technical/handbook/.

U.S. Geological Survey, 2008, Overview of the state of Oklahoma with inset of the location of the Arbuckle-Simpson aquifer outcrop [jpeg]. [Online WWW]. Available URL: "http://ok.water.usgs.gov/arbsimp/" [Accessed 28 March 2008].

Weight, W. D., and J. L. Sonderegger, 2001, Manual of applied field hydrogeology: McGraw – Hill, New York, 608 p.

Williams, P. W., 1983, The role of the subcutaneous zone in karst hydrology: Journal of Hydrology, v. 61, no. 1-3, pp. 45-67.

Winsauer, W. O., H. M. Shearin Jr., P. H. Masson, and M. Williams, 1952, Resistivity of brine-saturated sands in relation to pore geometry: AAPG Bulletin, v. 36, no. 2, pp. 253-77.

APPENDIX

DATA COMPILATION FIGURES

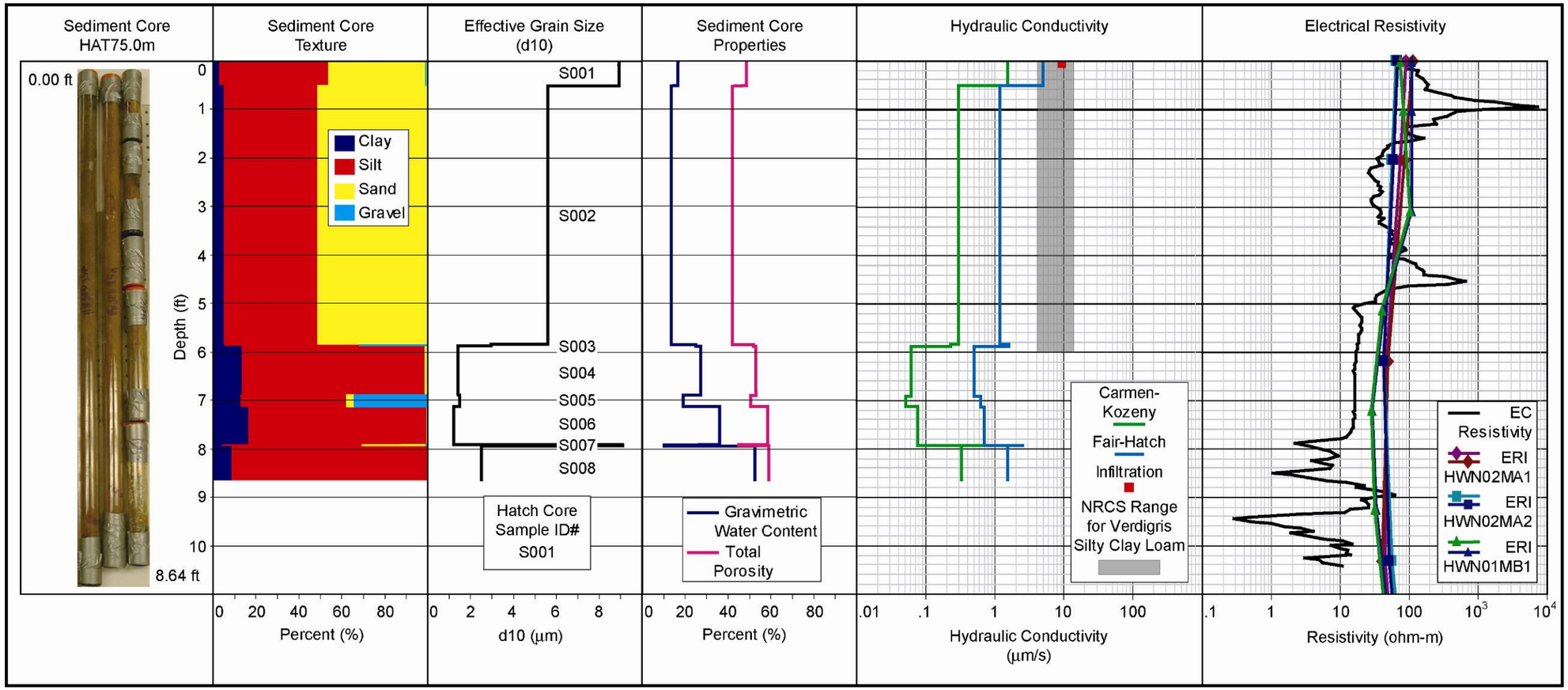

Figure A1. Hatch site data compilation for HAT75.0m location.

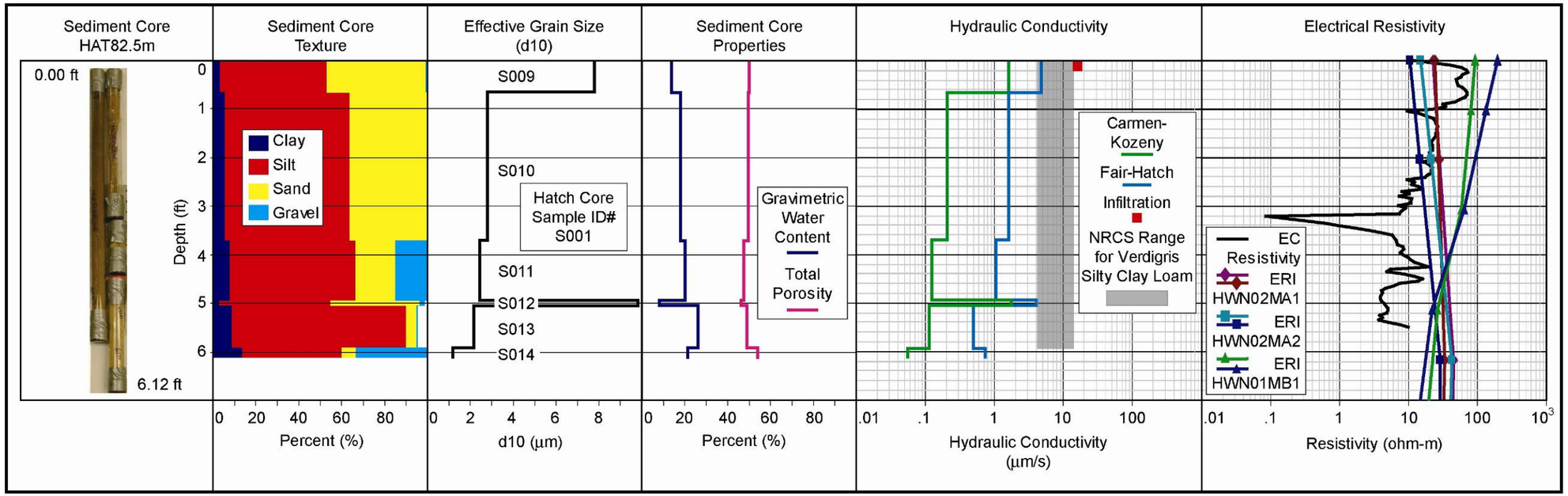

Figure A2. Hatch site data compilation for HAT82.5m location.

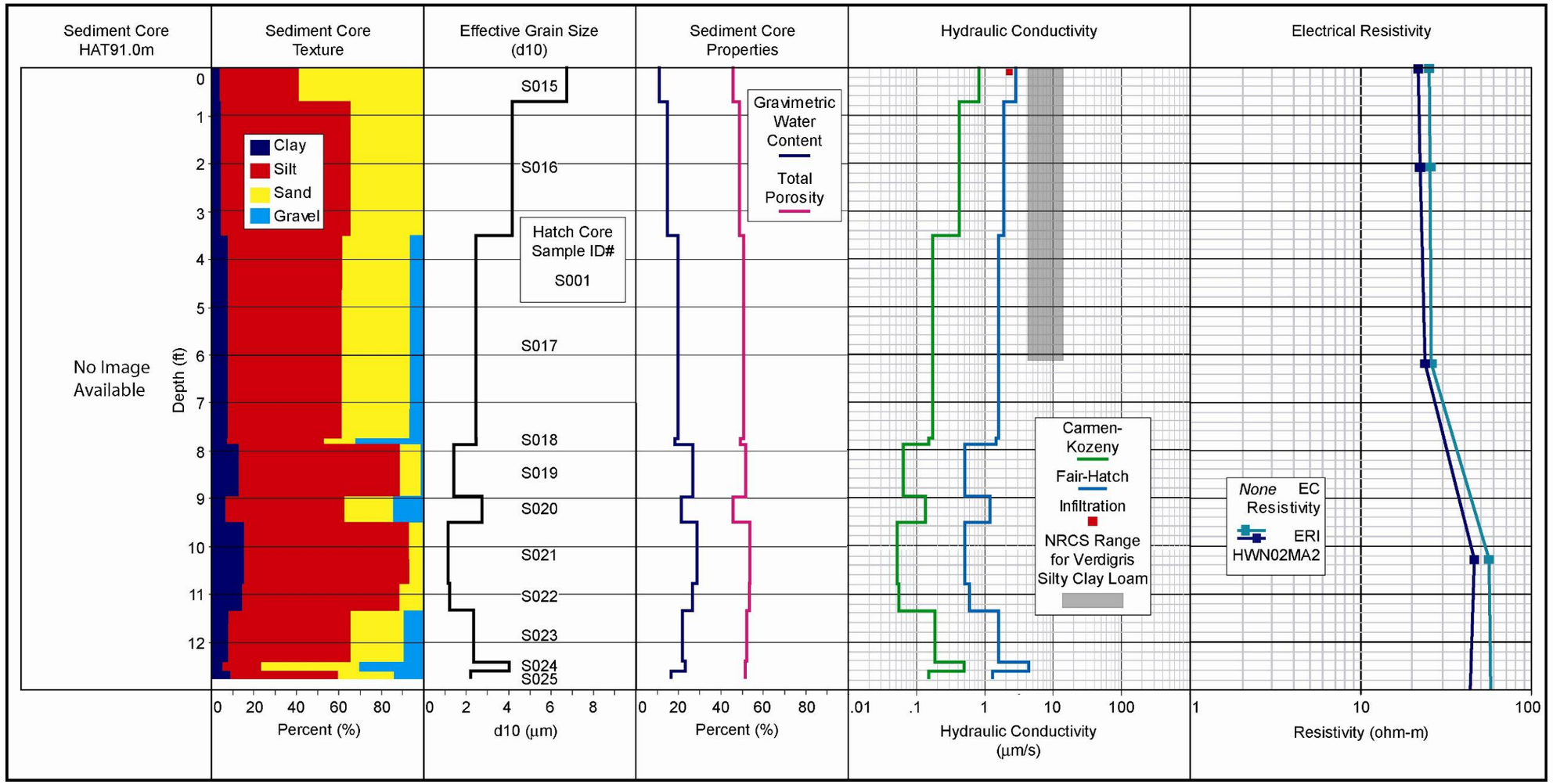

Figure A3. Hatch site data compilation for HAT91.0m location.

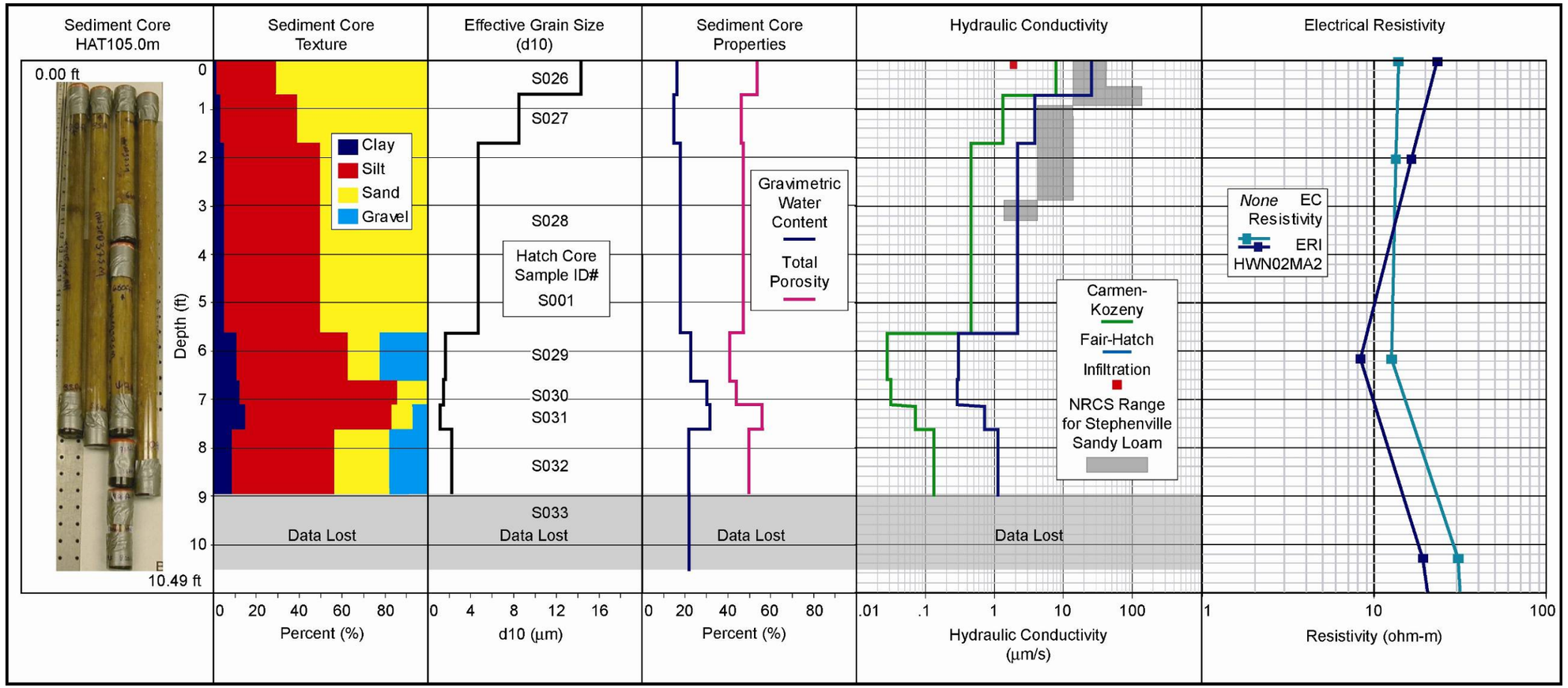

Figure A4. Hatch site data compilation for HAT105.0m location.

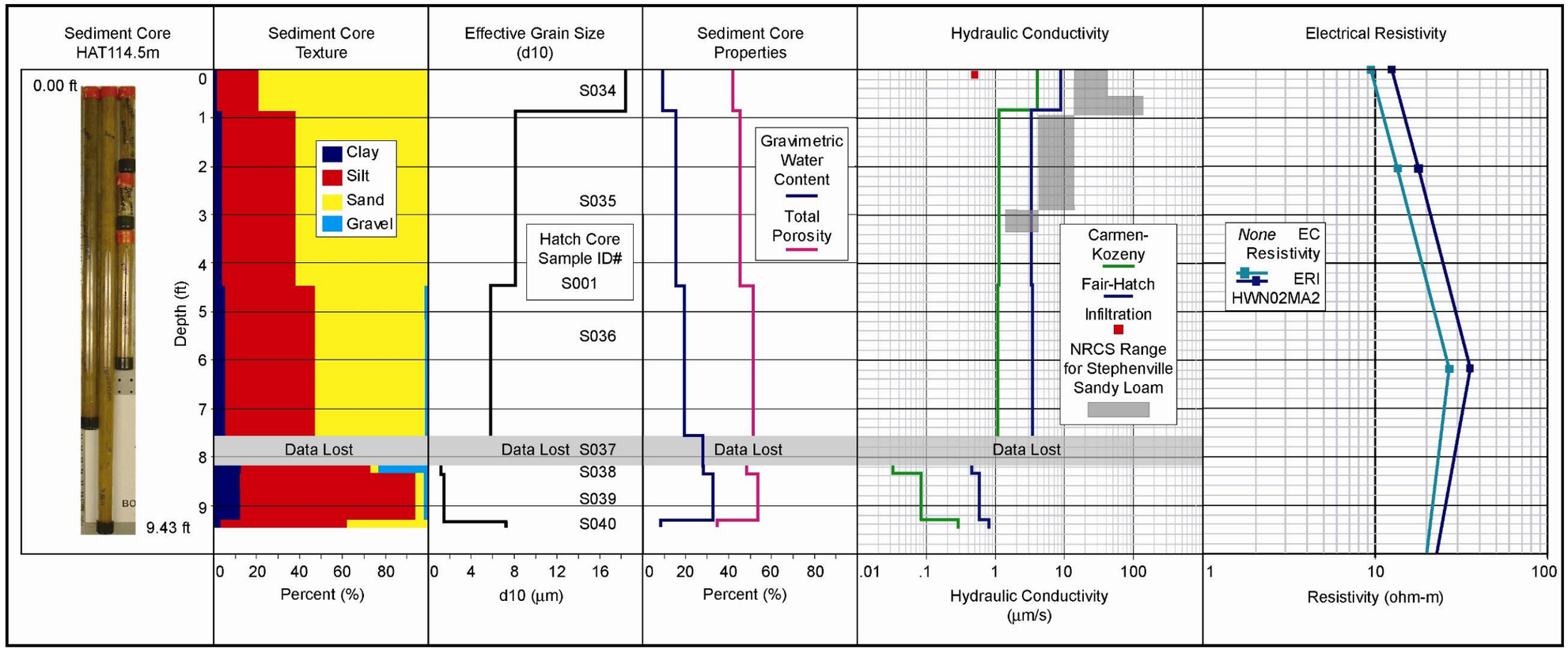

Figure A5. Hatch site data compilation for HAT114.5m location.

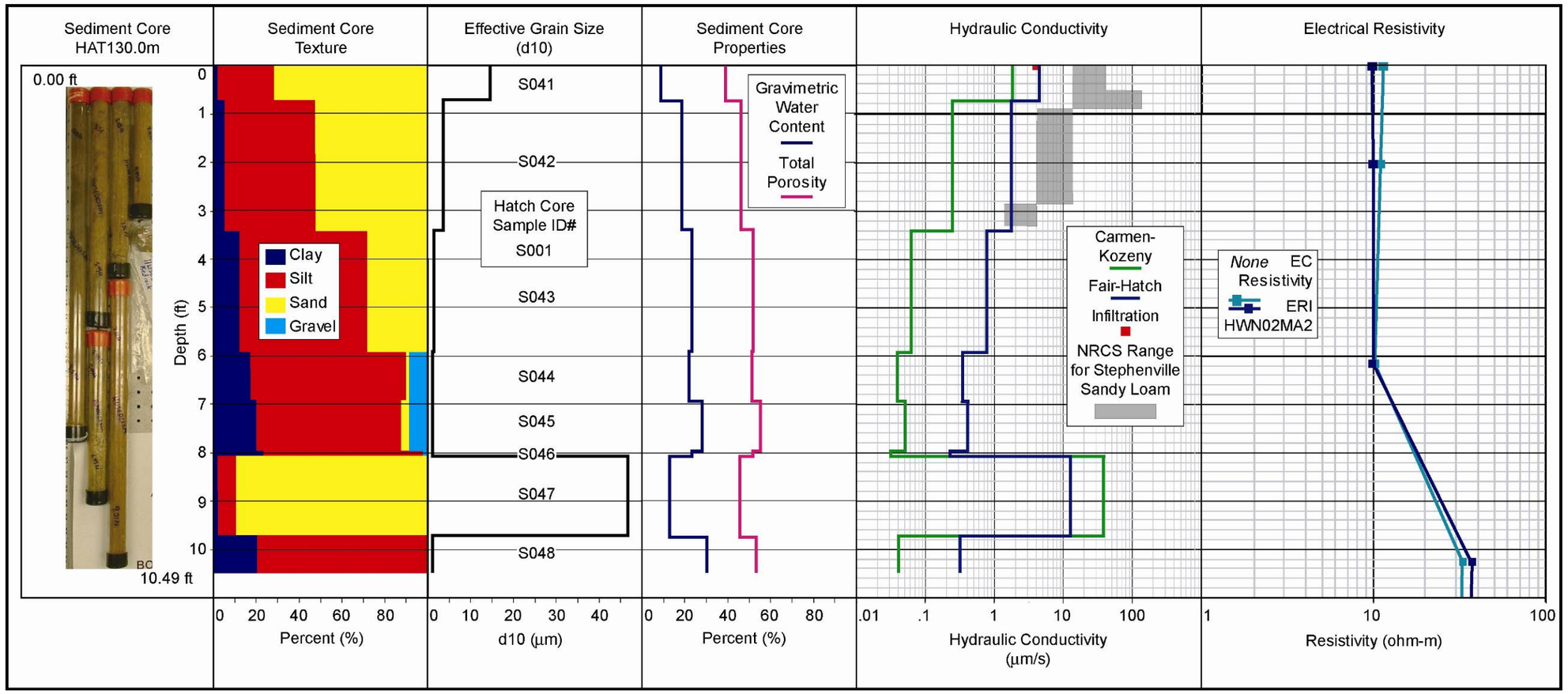

Figure A6. Hatch site data compilation for HAT130.0m location.

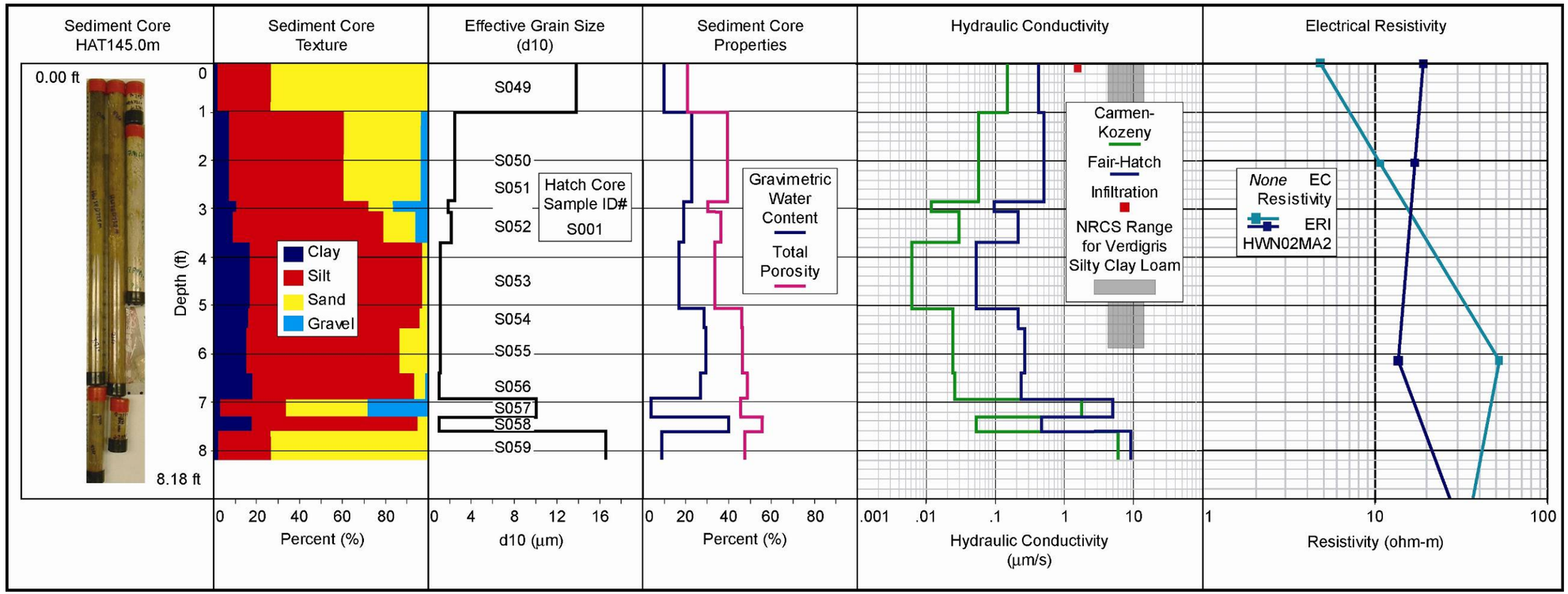

Figure A7. Hatch site data compilation for HAT145.0m location.

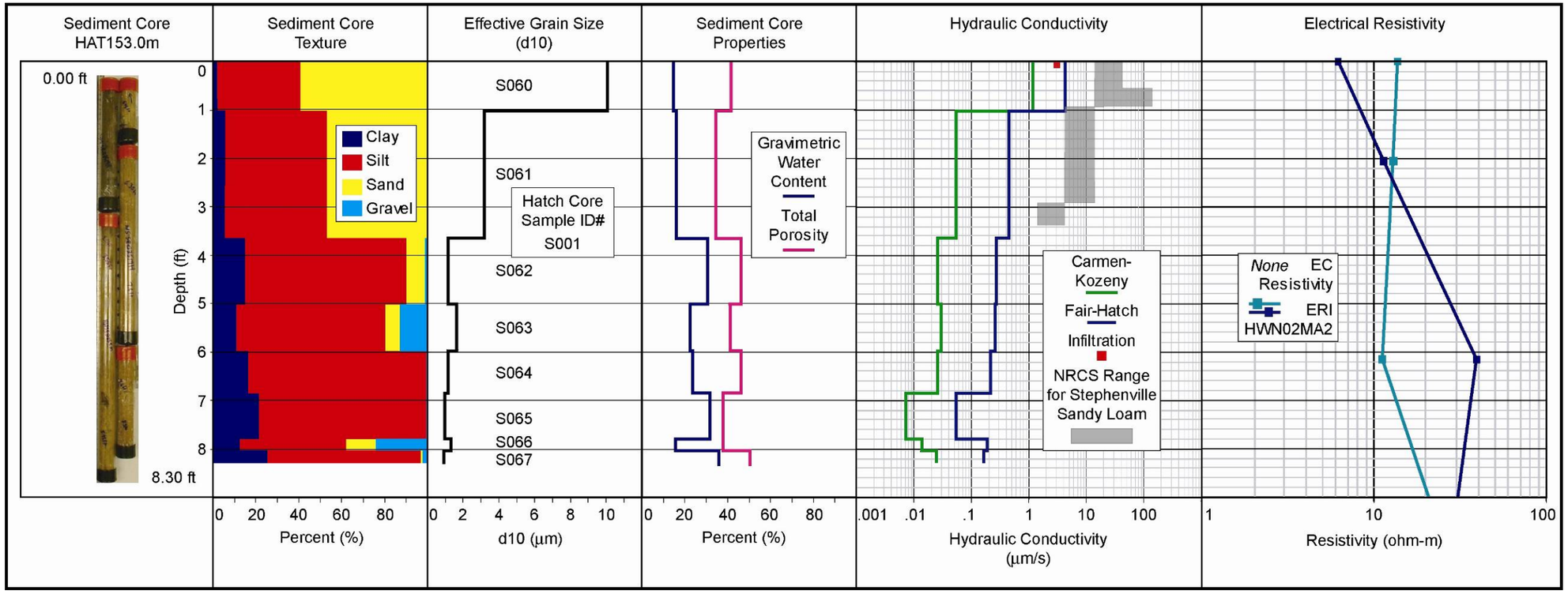

Figure A8. Hatch site data compilation for HAT153.0m location.

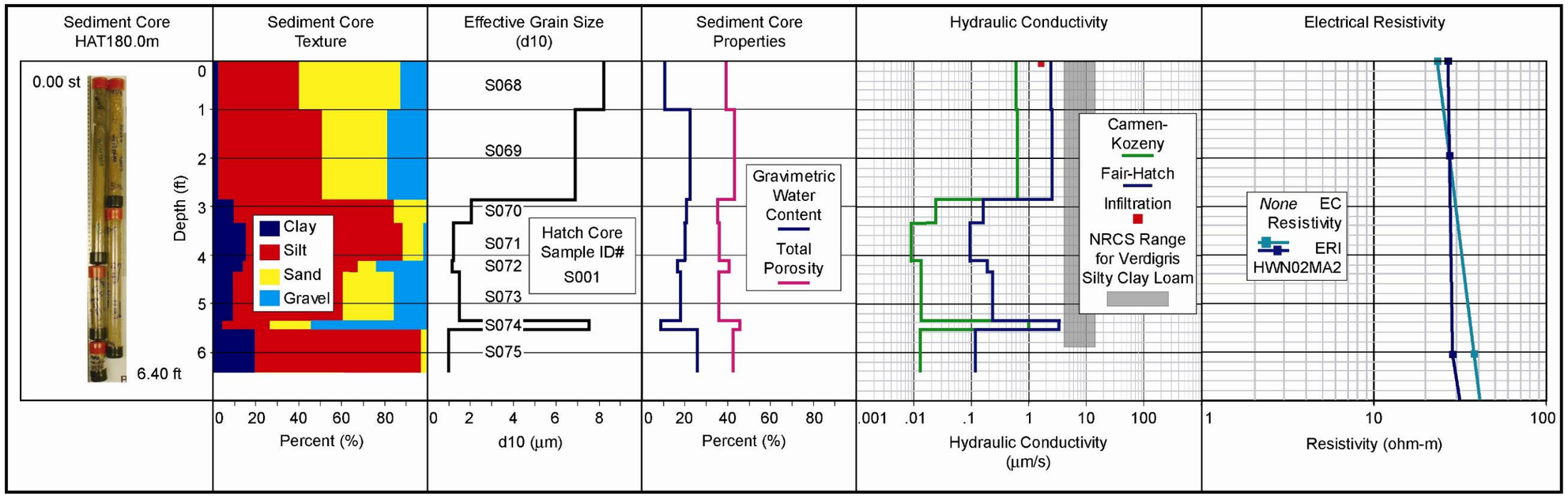

Figure A9. Hatch site data compilation for HAT180.0m location.

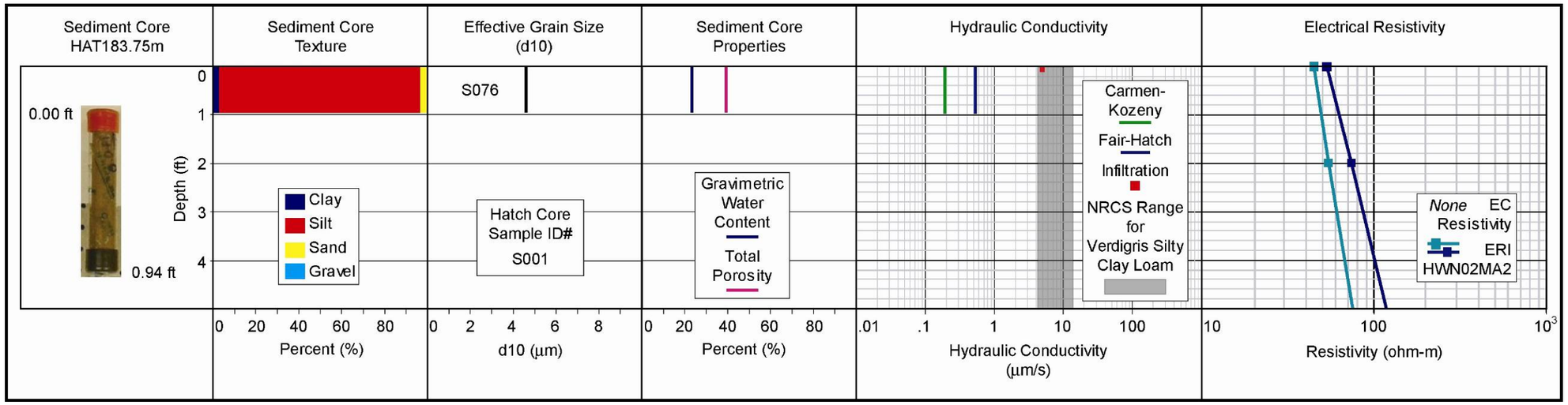

Figure A10. Hatch site data compilation for HAT183.75m location.

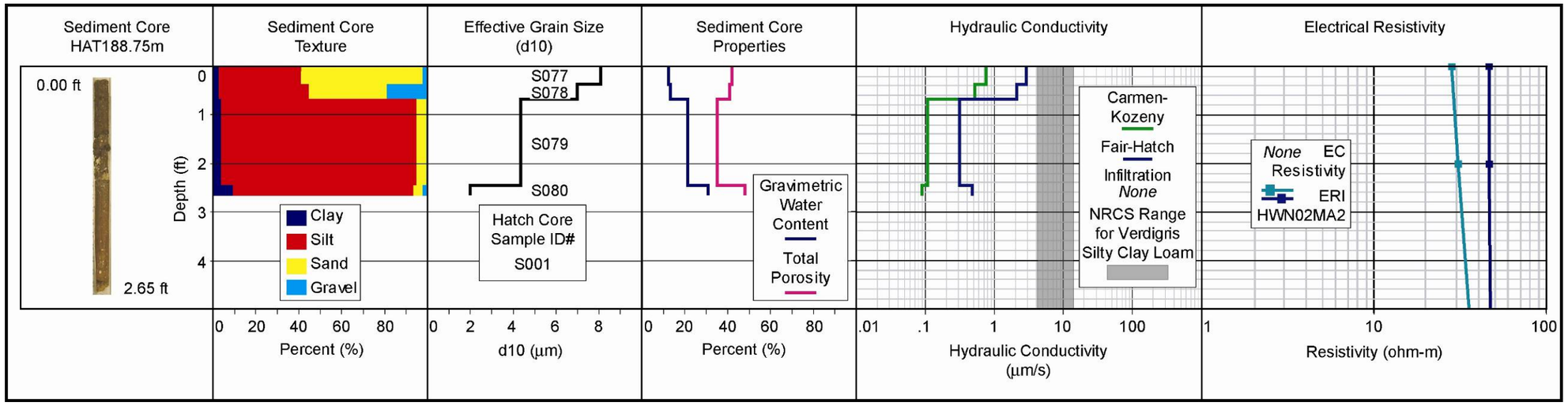

Figure A11. Hatch site data compilation for HAT188.75m location.

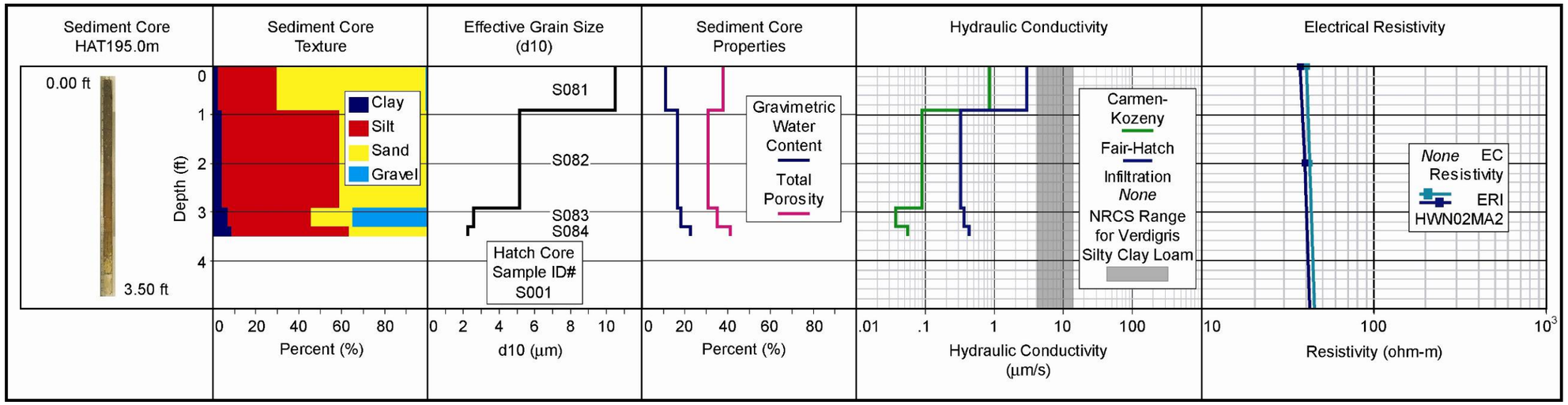

Figure A12. Hatch site data compilation for HAT195.0m location.

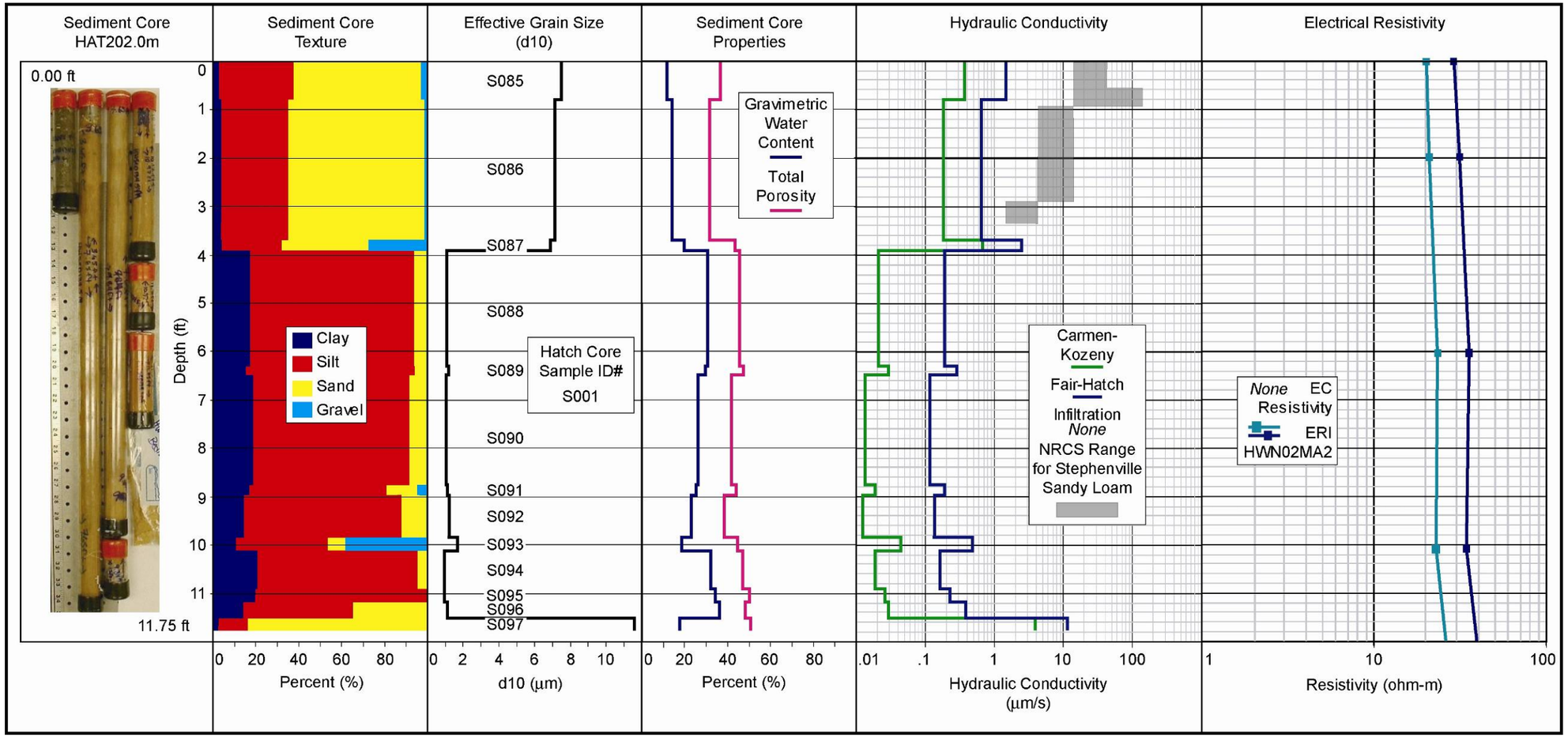

Figure A13. Hatch site data compilation for HAT202.0m location.

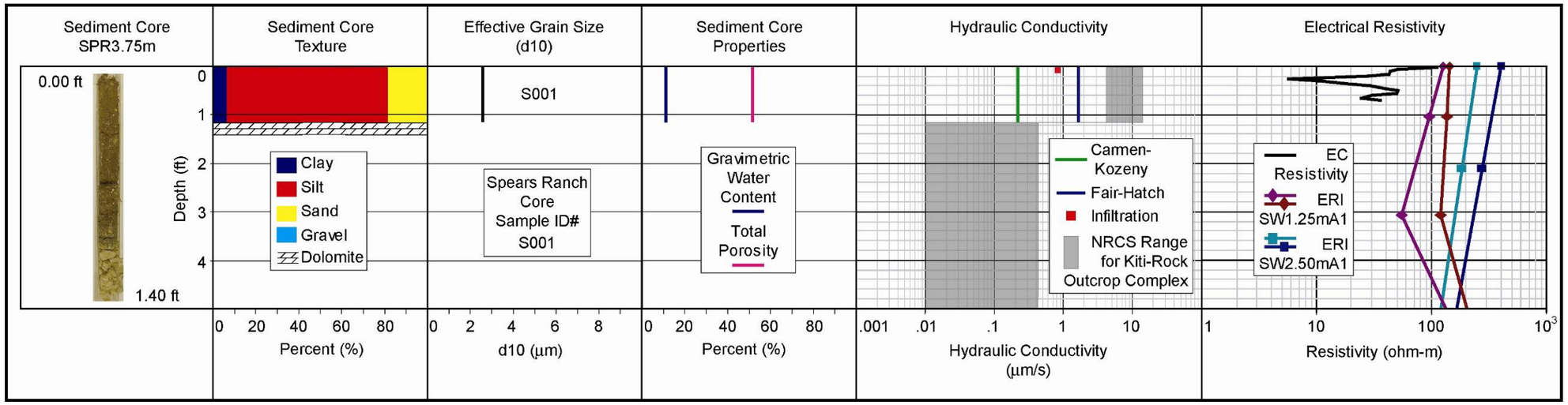

Figure A14. Spears Ranch site data compilation for SPR3.75m location.

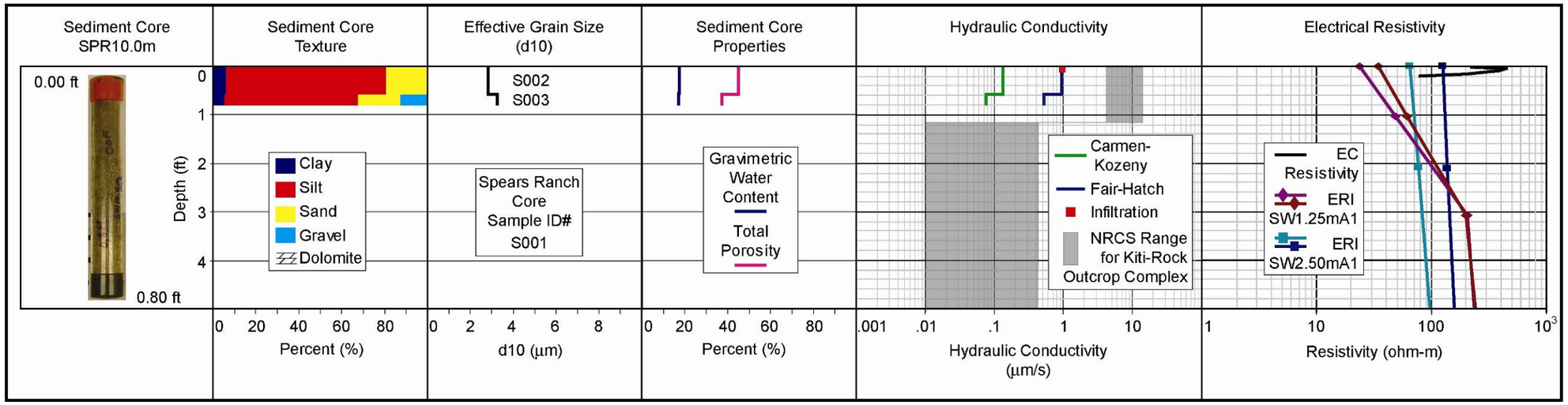

Figure A15. Spears Ranch site data compilation for SPR10.0m location.

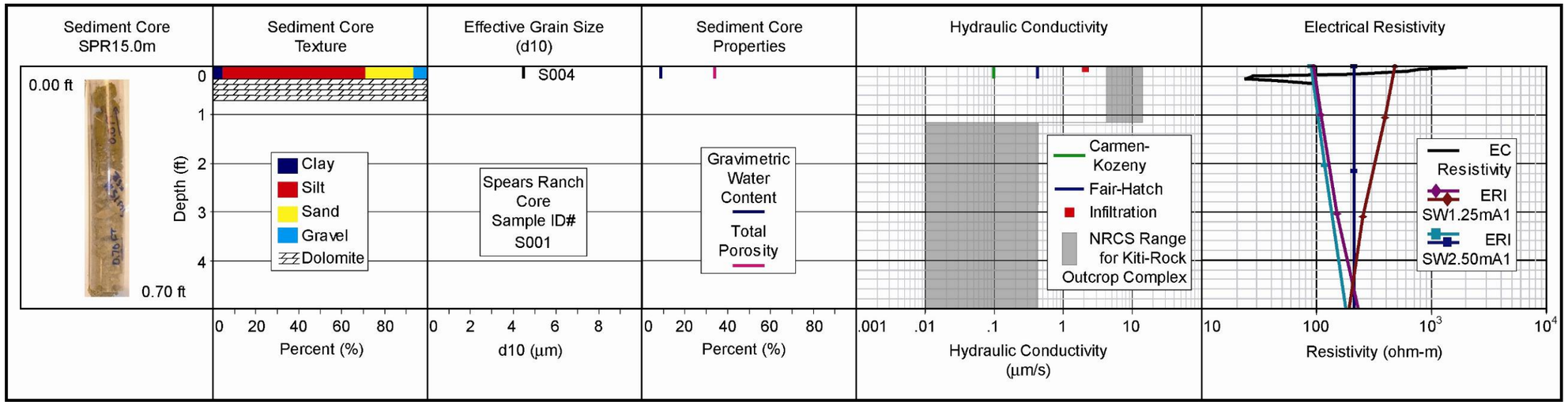

Figure A16. Spears Ranch site data compilation for SPR15.0m location.

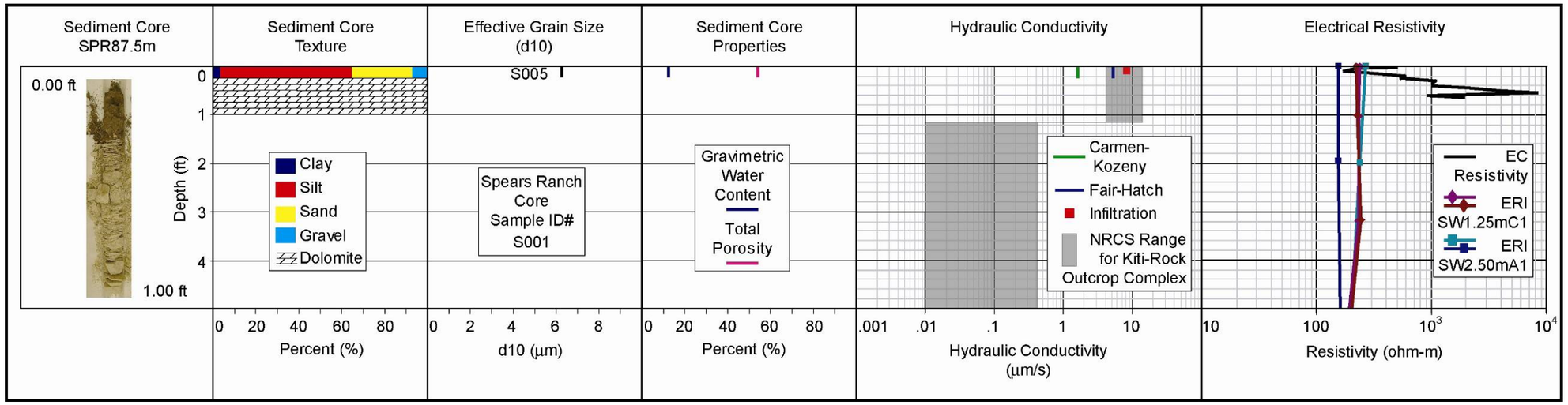

Figure A17. Spears Ranch site data compilation for SPR87.5m location.

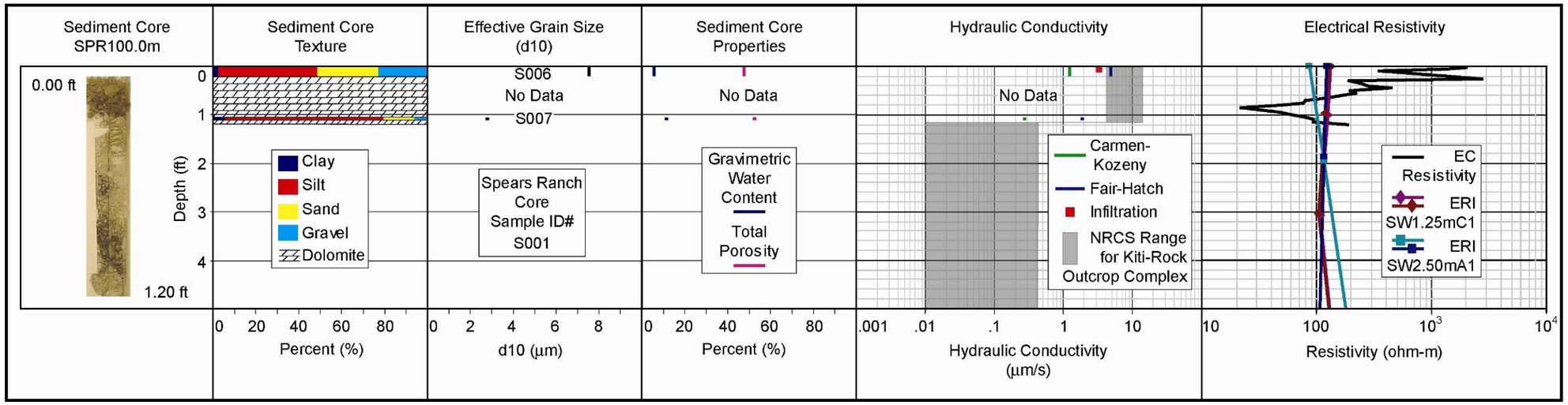

Figure A18. Spears Ranch site data compilation for SPR100.0m location.

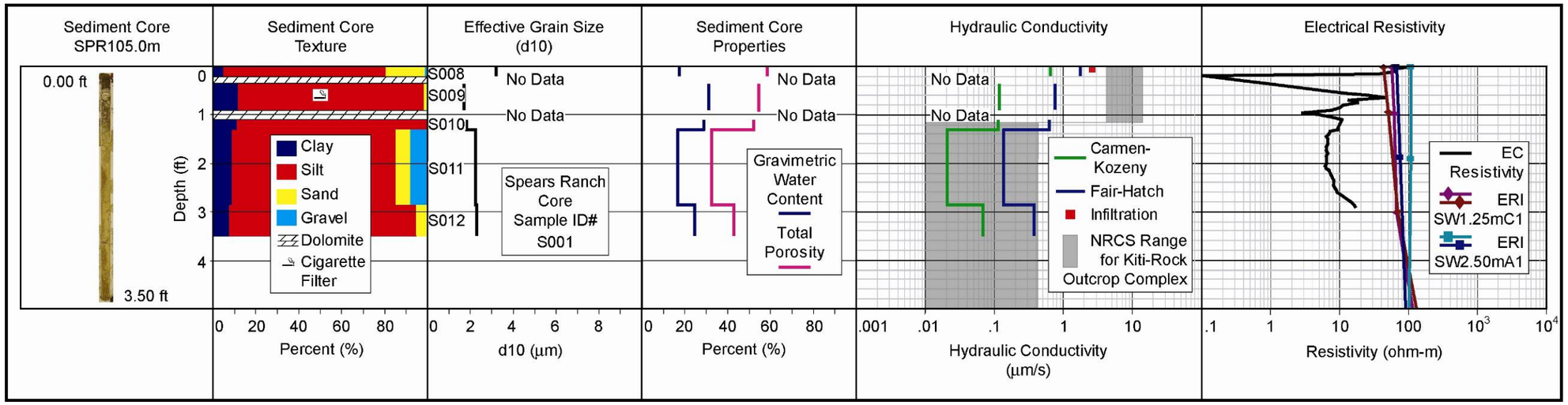

Figure A19. Spears Ranch site data compilation for SPR105.0m location.

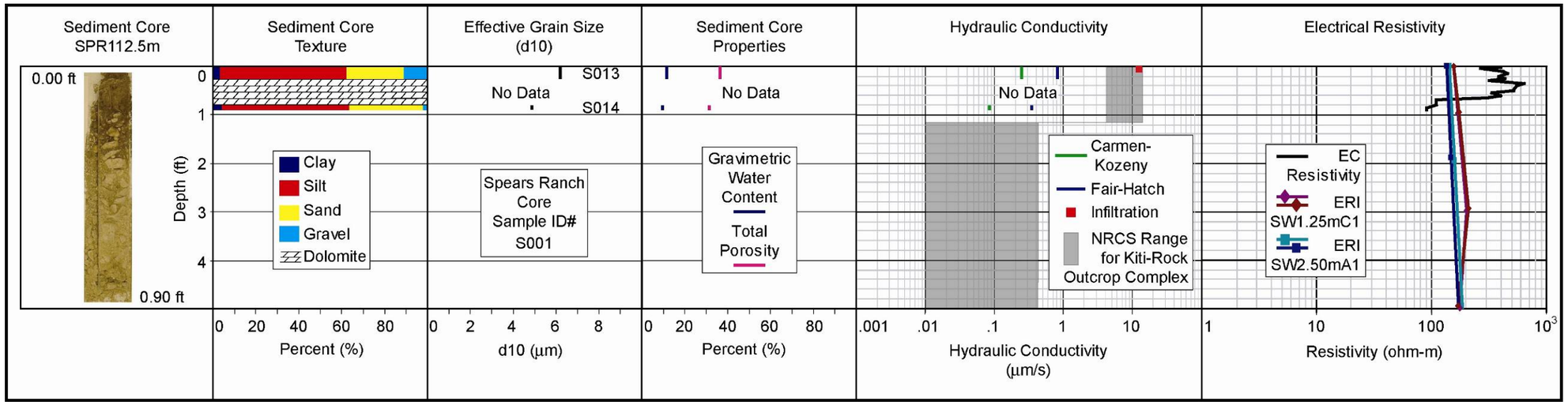

Figure A20. Spears Ranch site data compilation for SPR112.5m location.

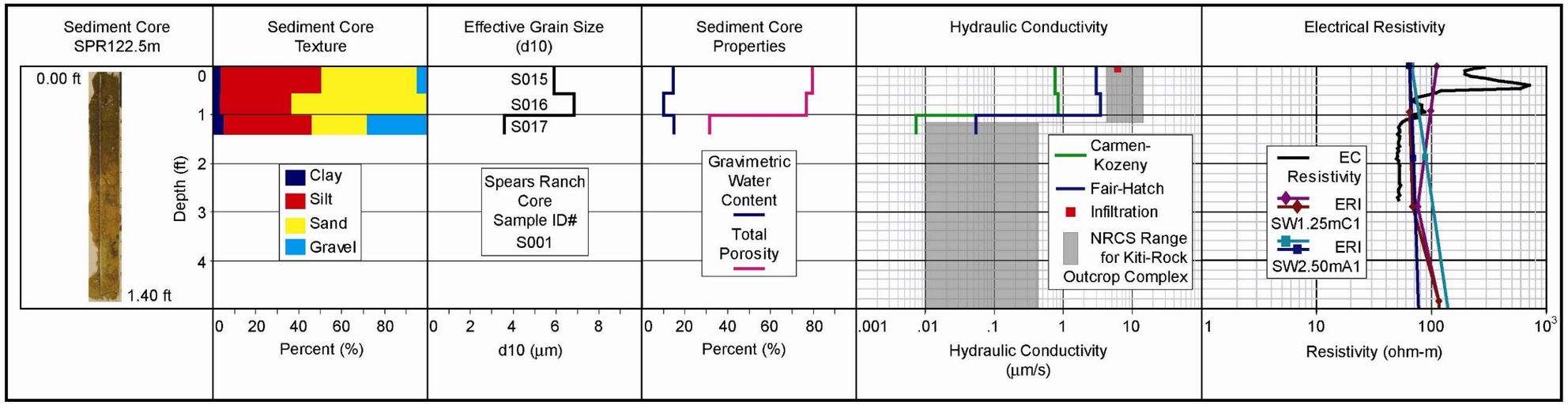

Figure A21. Spears Ranch site data compilation for SPR122.5m location.

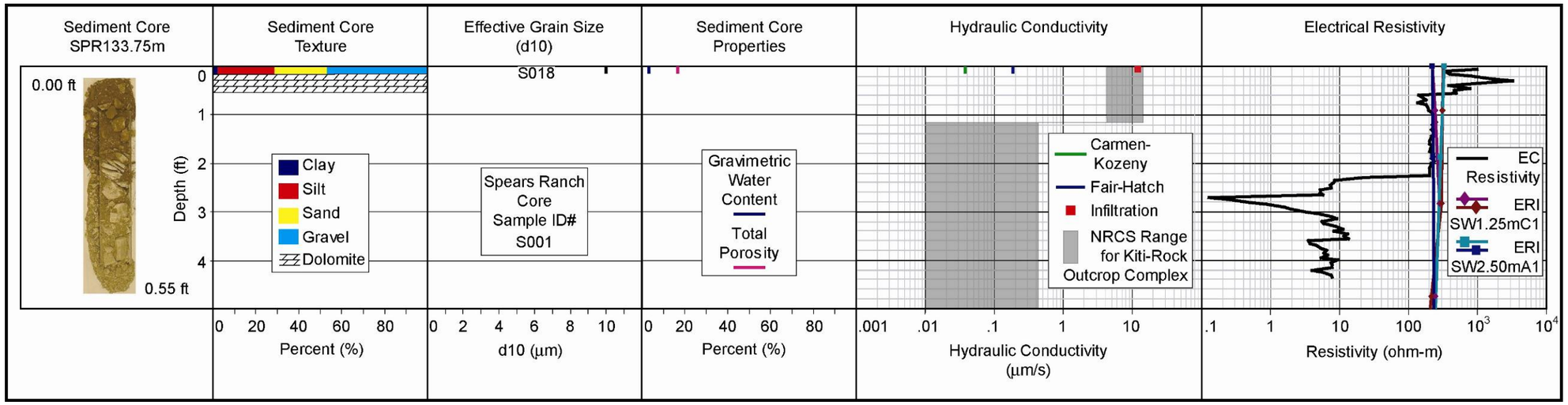

Figure A22. Spears Ranch site data compilation for SPR133.75m location.

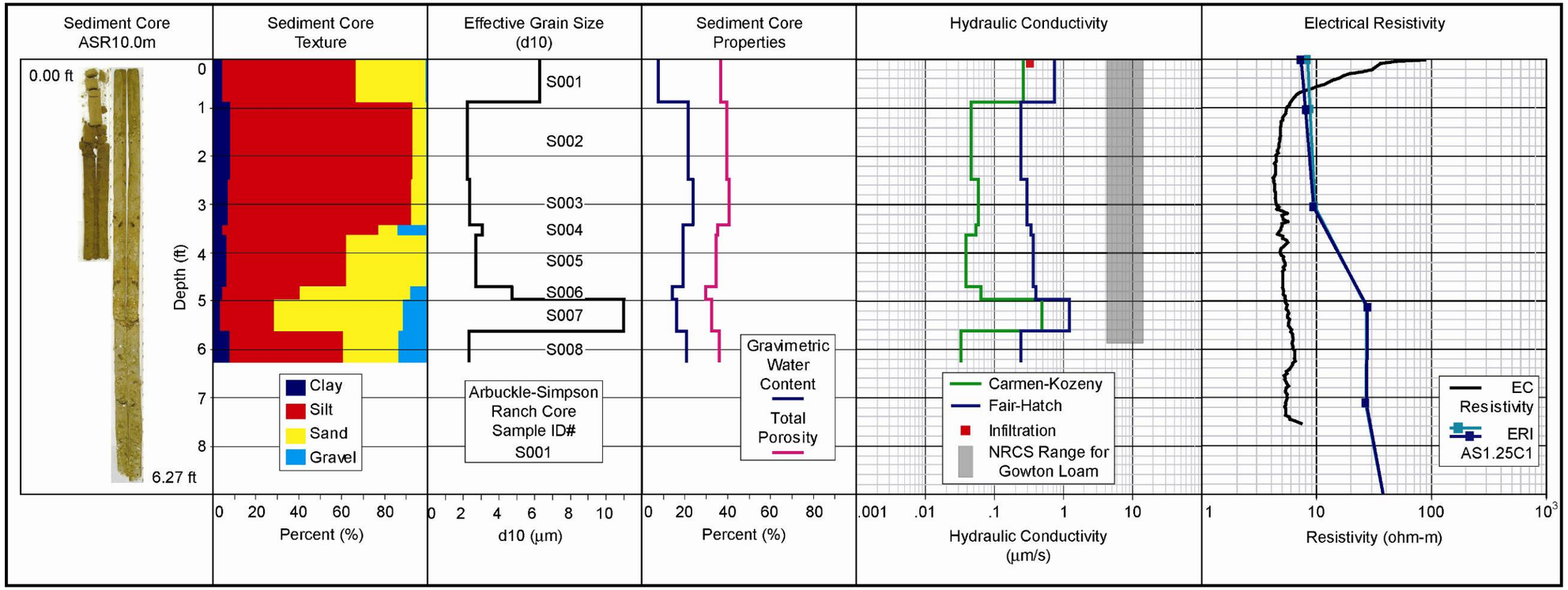

Figure A23. Arbuckle-Simpson Ranch site data compilation for ASR10.0m location.

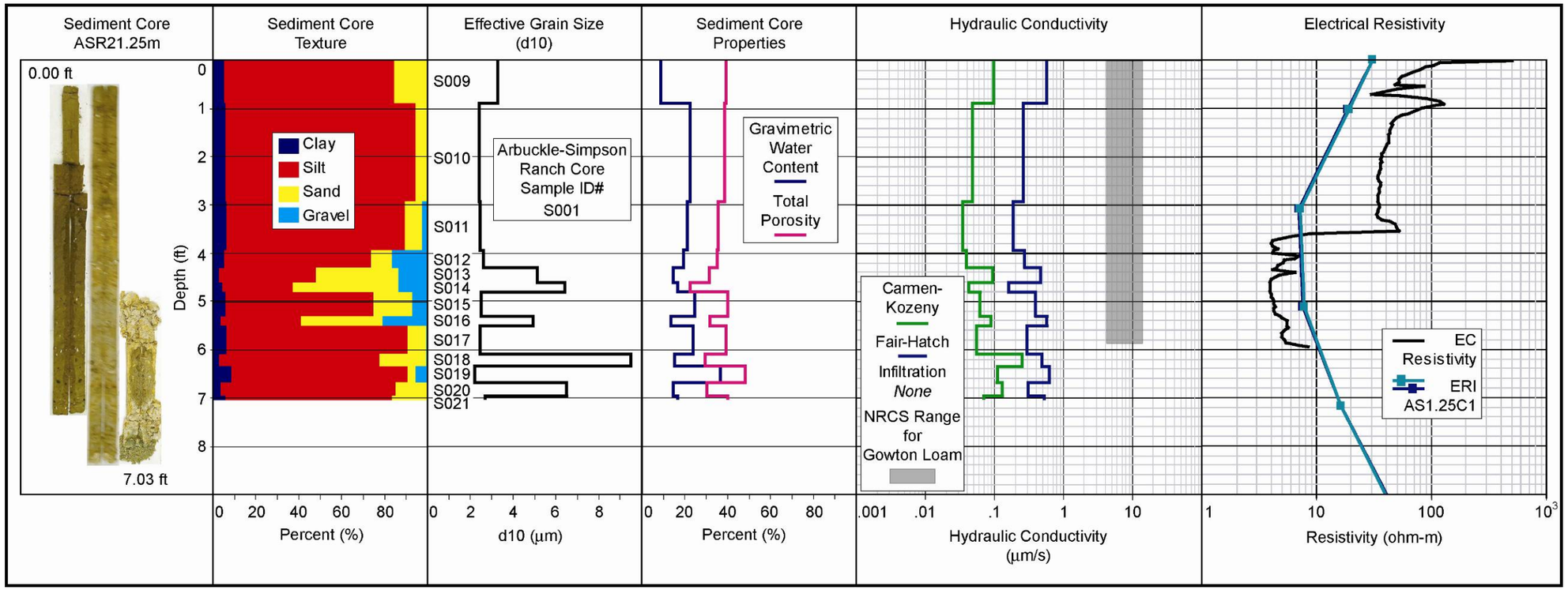

Figure A24. Arbuckle-Simpson Ranch site data compilation for ASR21.25m location.

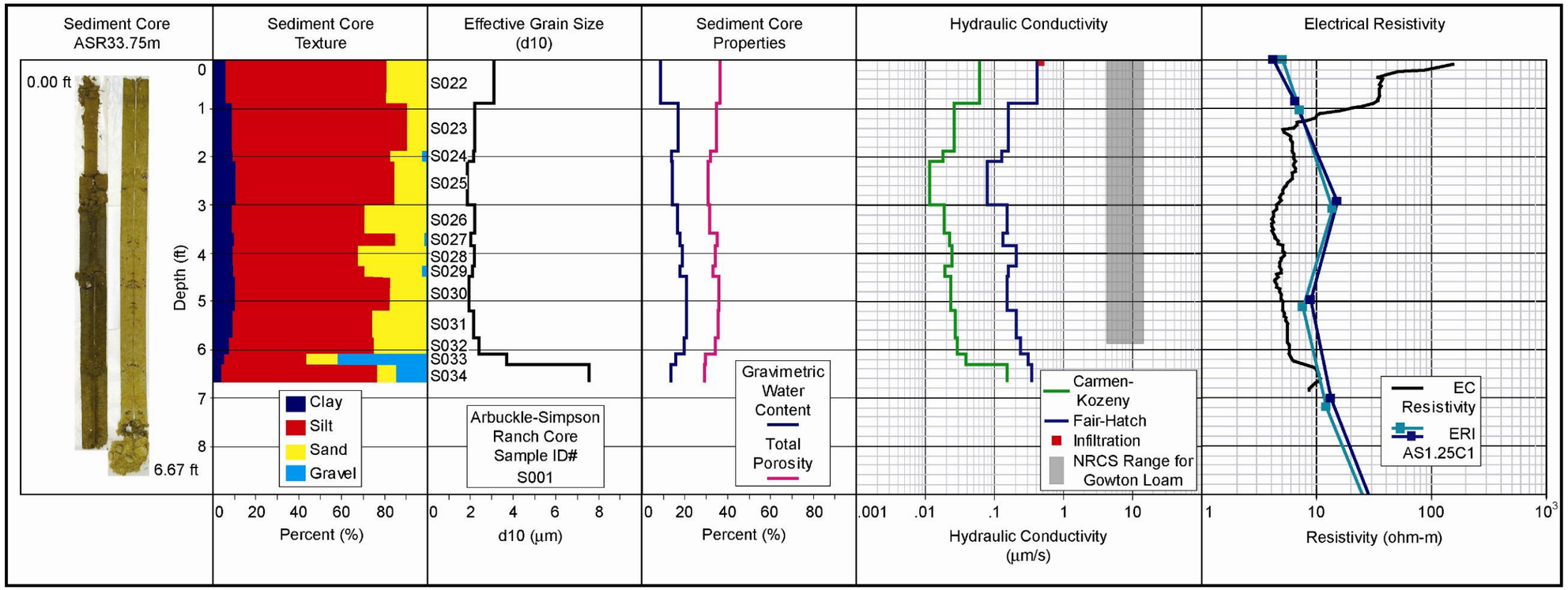

Figure A25. Arbuckle-Simpson Ranch site data compilation for ASR33.75m location.

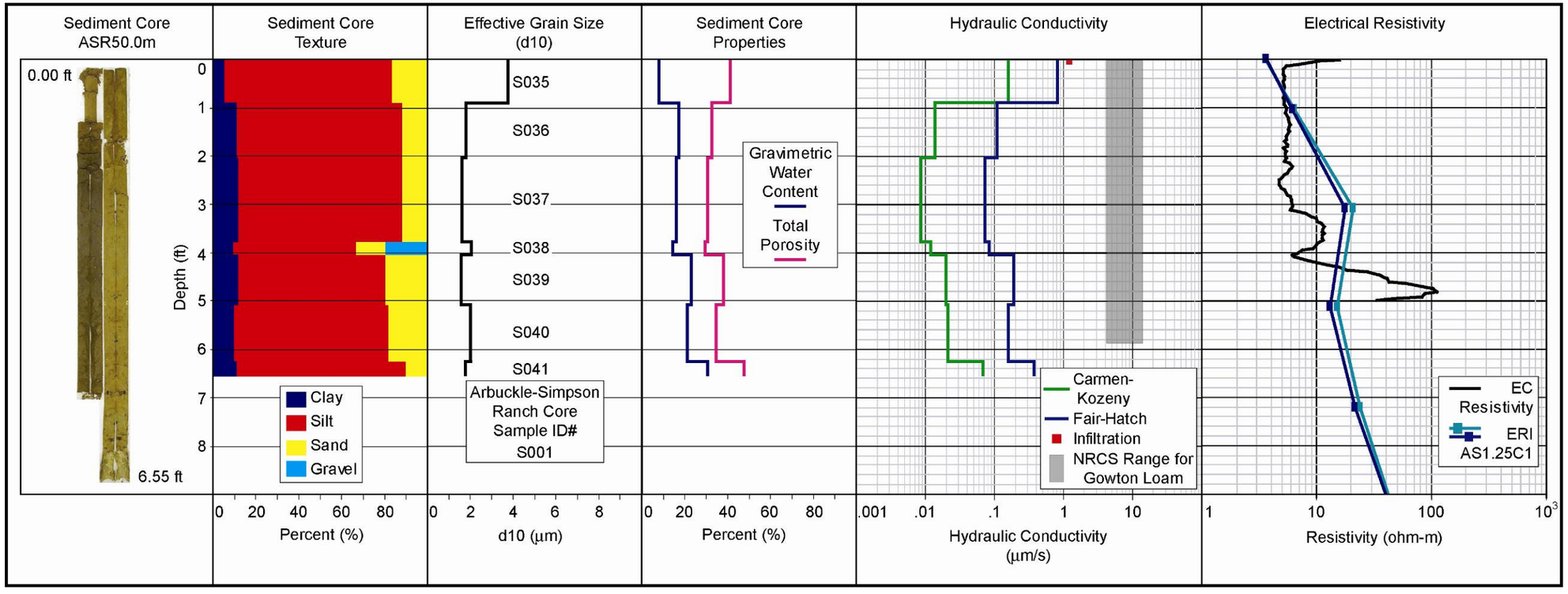

Figure A26. Arbuckle-Simpson Ranch site data compilation for ASR50.0m location.

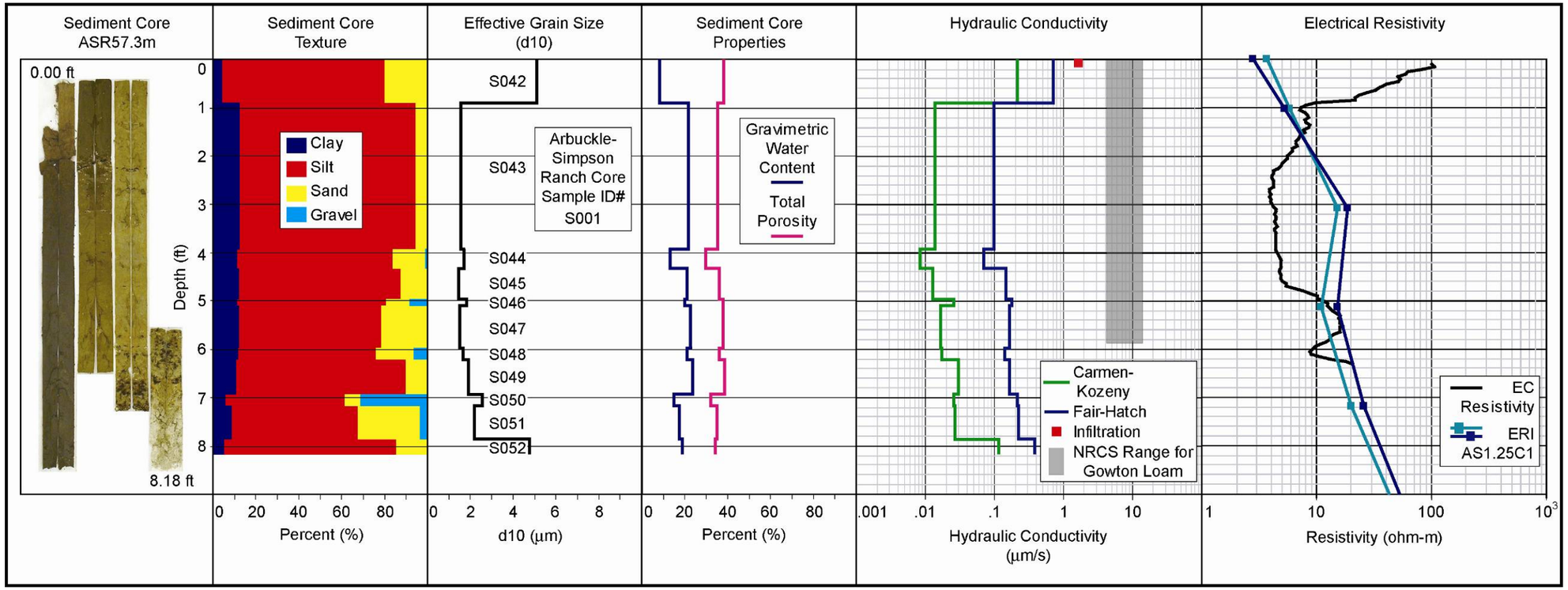

Figure A27. Arbuckle-Simpson Ranch site data compilation for ASR57.3m location.

VITA

Michael Andrew Sample

Candidate for the Degree of

Master of Science

Thesis: CHARACTERIZATION OF THE EPIKARST OVER THE HUNTON ANTICLINE, ARBUCKLE-SIMPSON AQUIFER, OKLAHOMA

Major Field: Geology

Biographical:

Personal Data: Born in Columbus, Ohio, on June 2, 1959, the son of William A. and Elizabeth A. R. Sample.

Education: Graduated from Bishop McGuiness High School, Oklahoma City, Oklahoma in May 1978; received Bachelor of Science degree in Geology from Oklahoma State University, Stillwater, Oklahoma in December 2005. Completed the requirements for the Master of Science degree with a major in Geology at Oklahoma State University in December 2007.

Experience: Graduate Research Assistant, School of Geology, Oklahoma State University, January 2005 to October 2007; Graduate Teaching Assistant, School of Geology, Oklahoma State University, August 2006 to December 2006; Undergraduate Research Assistant, School of Geology, Oklahoma State University, September 2003 to December 2005.

Professional Memberships: Geological Society of America; The National Honor Society for the Earth Sciences of Sigma Gamma Epsilon; The Honor Society of Phi Kappa Phi.

Name: Michael Andrew Sample Date of Degree: May, 2008

Institution: Oklahoma State University Location: Stillwater, Oklahoma

Title of Study: CHARACTERIZATION OF THE EPIKARST OVER THE HUNTON ANTICLINE, ARBUCKLE-SIMPSON AQUIFER, OKLAHOMA

Pages in Study: 207 Candidate for the Degree of Master of Science

Major Field: Geology

Scope and Method of Study: Three field sites were examined using surface and direct push electrical methods, direct push sediment cores, and infiltration tests to characterize the variably mantled epikarst of the Arbuckle-Simpson in terms of its thickness, and the hydraulic properties of hydraulic conductivity and storativity. The sediment cores were analyzed for porosity, moisture content, and particle size distribution. Hydraulic conductivity was calculated for the sediment core material using the particle size distribution and porosity data. The electrical and hydraulic properties of the epikarst were also compared to determine any relationships.

Findings and Conclusions: The epikarst zone was found to be approximately nine times larger than the soil zone thickness at the study sites. The averaged epikarst zone was found to range in thickness from approximately 9 to 60 feet, but much deeper epikarst zones can be expected. The hydraulic conductivity results correlated well to NRCS Soil Survey data. The storage potential of the mantled epikarst was estimated as on the same order of magnitude as the saturated thickness of the aquifer. No clear overall relationship was found between the electrical and hydraulic properties of the epikarst. A direct relationship between the electrical resistivity and hydraulic conductivity data was found when clay content was significant.

ADVISER'S APPROVAL: Todd Halihan